Annexure -VIII

UNIVERSITY GRANTS COMMISSION
BAHADUR SHAH ZAFAR MARG
NEW DELHI – 110 002

Final Report of the work done on the Major Research Project.

1. Project report No. 1st /2nd /3rd/Final: **Final**
2. UGC Reference No.F. **41-603/2012(SR)** dated **16.07.2012**
3. Period of report: From **01.07.2012** To **31.12.2015**
4. Title of research project: **Development of Compressed Sensing Based Image Reconstruction Techniques for Medical Imaging Applications.**
5. (a) Name of the Principal Investigator: **Dr. Bhabesh Deka**

   (b) Deptt.: **Electronics and Communication Engineering**

   (c) University/College where work has progressed: **Tezpur University**
6. Effective date of starting of the project: **05.09.2012**
7. Grant approved and expenditure incurred during the period of the report:

   a. Total amount approved Rs. **12,25,800.00**

   b. Total expenditure Rs. **10,22,532.00**

c. Report of the work done: (Please attach a separate sheet)

i. Brief objective of the project: **Please see p. 4, Annexure-1**

ii. Work done so far and results achieved and publications, if any, resulting from the work (Give details of the papers and names of the journals in which it has been published or accepted for publication): **Please see Annexure-1 (For publication details see p.63)**

iii. Has the progress been according to original plan of work and towards achieving the objective? if not, state reasons : **Yes**

iv. Please indicate the difficulties, if any, experienced in implementing the Project:

- **In medical imaging applications, the collection of good quality image data is very important because results are highly data dependent. So, we requested experts who are already quite into this field for sharing MRI data. They agreed after we assured them that it was meant only for the research purpose. This not only helped us in availing the data but also significant while reproducing their works for comparisons. This in no doubt consists of some procedural delay due to medical ethics of data distribution and other institutional level formalities. So, initially, the project implementation part went a bit slow.**

- **As compressed sensing MR image reconstruction is relatively new research requiring sound knowledge of convex optimization. Due to this fact, first one year is fully was mostly devoted on learning required theoretical background and most of the works are done in the second and third year only.**

Bhabesh Deka

- **During implementation of the project we also experienced that for smooth running of fast reconstruction algorithms requires a work station equipped with high capacity of RAM (at least 8 GB or higher) and 64 bit operating system (OS). Because, for processing of 2D multi-slice and 3D MRI data required sufficient memory capacity. However, we managed with general purpose PC having 2GB RAM and 32 bit OS by scaling down our implementations.**

- **For practical implementation of compressed sensing MR image reconstruction required high speed parallel processing hardware. We have implemented only in software. However practical implementation is beyond the scope of this project.**

v. If project has not been completed, please indicate the approximate time by which it is likely to be completed. A summary of the work done for the period (Annual basis) may please be sent to the Commission on a separate sheet.

NA

vi. If the project has been completed, please enclose a summary of the findings of the study. One bound copy of the final report of work done may also be sent to University Grants Commission.:

A bound copy of the project completion report is attached. Please see Annexure-I.

vii. Any other information which would help in evaluation of work done on the project. At the completion of the project, the first report should indicate the output, such as (a) Manpower trained (b) Ph. D. awarded (c) Publication of results (d) other impact, if any

We have successfully completed the project with national and international publications in journal/conference (Please see Annexure-I). To explore the findings of the Project further, the Project Fellow employed with this project has currently enrolled in the Ph.D. programme of the Department with same area of research as that of the project.

a) **Manpower trained : No. of M. Tech. students who completed their final year projects: 05**
   1. **Mr. Sumit Datta (EDO12009)**
   2. **Mr. Manir Ahmed (EDO12010)**
   3. **Mr. Sanjib Kalita (ELD13008)**
   4. **Mr. Md. Abdul Kayom Khairuzzaman (EDO13004)**
   5. **Ms. Silpi Sikha Lahon (ELD14020).**

b) **No. of Ph.D. awarded/ongoing : one (Mr. Sumit Datta (ELP15004) enrolled in spring 2015)**

c) **Publication of results : Please see p. 63, Annexure-1**

04.07.2016

PRINCIPAL INVESTIGATOR
(SIGNATURE WITH SEAL)

Associate Professor
Department Of Electronics & Comm.Engg.
Tezpur University

04/7/16

REGISTRAR
(SIGNATURE WITH SEAL)

कुलसचिव
तेजपुर विश्वविद्यालय
Registrar
Tezpur University

Annexure – IX

UNIVERSITY GRANTS COMMISSION
BAHADUR SHAH ZAFAR MARG
NEW DELHI – 110 002

PROFORMA FOR SUBMISSION OF INFORMATION AT THE TIME OF SENDING THE FINAL REPORT OF THE WORK DONE ON THE PROJECT

1. TITLE OF THE PROJECT: **Development of Compressed Sensing Based Image Reconstruction Techniques for Medical Imaging Applications.**
2. NAME AND ADDRESS OF THE PRINCIPAL INVESTIGATOR : **Dr. BhabeshDeka, Associate Professor, Dept. of Electronics and Communication Engineering, Tezpur University, Tezpur, Assam-784028**
3. NAME AND ADDRESS OF THE INSTITUTION: **Tezpur University, Napaam, Tezpur, Assam-784028**
4. UGC APPROVAL LETTER NO. AND DATE: **F. No.41-603/2012(SR) and 16.07.2012**
5. DATE OF IMPLEMENTATION **: 05-09-2012**
6. TENURE OF THE PROJECT : **3 Years**
7. TOTAL GRANT ALLOCATED: **Rs.12,25,800.00**
8. TOTAL GRANT RECEIVED : **Rs.10,38,154.00**
9. FINAL EXPENDITURE : **Rs.10,22,532.00**
10. TITLE OF THE PROJECT : **Development of Compressed Sensing Based Image Reconstruction Techniques for Medical Imaging Applications**
11. OBJECTIVES OF THE PROJECT

    a) To study the state-of-the-art compressed sensing based MR image reconstruction algorithms in the literature.
    b) To implement CS-MRI reconstruction algorithms in the MATLAB environment.
    c) To develop a faster and improved CS-MRI reconstruction algorithm for practical implementations.

12. WHETHER OBJECTIVES WERE ACHIEVED: **Yes. Please see Annexure-1**

OBJECTIVE 1: To study the state-of-the-art compressed sensing based MR image reconstruction algorithms in the literature.

We have studied various types of existing techniques for compressed sensing MR image reconstruction based on convex optimization. A comprehensive literature survey is done on various data acquisition techniques in compressed sensing MRI. (Please see Chapters 1 and 2 in Annexure-1)

BhabeshDeka

OBJECTIVE 2: To implement CS-MRI reconstruction algorithms in the MATLAB environment.

Different convex optimization based compressed sensing MR image reconstruction algorithms are implemented in MATLAB environment and evaluated their performances. (Please see Chapter 4 in Annexure-1)

OBJECTIVE 3: To develop a faster and improved CS-MRI reconstruction algorithm for practical implementations.

i. **We have proposed an efficient k-space under-sampling pattern namely the 'variable density Poisson disk under-sampling pattern' to efficiently acquire k-space data in MRI. Reconstructed results using the proposed undersampling pattern are compared to some other well known undersampling patterns and it has been seen that the proposed under-sampling pattern gives better results compared to others in terms of MSE, PSNR, and MSSIM. (Please see Chapter 3 in Annexure-1)**

ii. **Proposed a high throughput MR image reconstruction algorithm. The performance of the proposed Algorithm is compared with state-of-the-art L1-minimization algorithms. From the results we observed that the proposed algorithm gives better results in terms of CPU time and quality of reconstructed MR images in terms of PSNR and MSSIM. (Please see Chapter 4 in Annexure-1)**

iii. **Proposed the Wavelet tree sparsity based compressed sensing MR image reconstruction algorithm for 2D multi-slice MRI. (Please see Chapter 5 in Annexure-1)**

iv. **A fast interpolation technique is proposed for compressed sensing 2D multi-slice MR image reconstruction from highly undersampled measurements. Results show that the proposed interpolation technique is more than twenty times faster than the state-of-the-art. (Please see Chapter 6 in Annexure-1)**

13. ACHIEVEMENTS FROM THE PROJECT:

a) Manpower trained : No. of M. Tech. students who completed their final year projects: 05
   1. Mr. Sumit Datta (EDO12009)
   2. Mr. Manir Ahmed (EDO12010)
   3. Mr. Sanjib Kalita (ELD13008)
   4. Mr. Md. Abdul Kayom Khairuzzaman (EDO13004)
   5. Ms. Silpi Sikha Lahon (ELD14020).

b) No. of Ph.D. awarded/ongoing : one
   (Mr. Sumit Datta (ELP15004) enrolled in spring 2015)

Bhabesh Deka

c) Publication of results : **Please see p. 63, Annexure-1**

14. SUMMARY OF THE FINDINGS: **Please see Annexure-2**
(IN 500 WORDS)

15. CONTRIBUTION TO THE SOCIETY :
Application of compressed sensing in MRI significantly reduces the data acquisition time. In traditional MRI radiologists frequently use anaesthesia for paediatric patients to prevent motion artifacts. In some clinical tests, one need to breath-hold 20-30 seconds to avoid degradation of images due to organ motion. This is very difficult for patients having diseases of heart and lungs and also for children. Clinical implementation of compressed sensing MRI would improve patient care, especially the paediatric and aged patients, and certainly the healthcare economics.

16. WHETHER ANY PH.D. ENROLLED/PRODUCED OUT OF THE PROJECT

Yes. Mr. Sumit Datta joined this project on 2nd August, 2013 and continued till the completion of the project i.e. 31st December, 2015. While continuing the project work, he also got enrolled in the Ph.D. program of the Department of ECE in January, 2015. His area of research is "Compressed Sensing MRI". He is expected to complete his Ph.D. by 2018.

17. NO. OF PUBLICATIONS OUT OF THE PROJECT: **Please see p. 63, Annexure-1**
(PLEASE ATTACH)

Bhabesh Deka 04.07.2016
(PRINCIPAL INVESTIGATOR)

(REGISTRAR/ PRINCIPAL)
(Seal)
कुलसचिव
तेजपुर विश्वविद्यालय
Registrar
Tezpur University

(Not Applicable)
(CO-INVESTIGATOR)

Annexure-1

PROJECT COMPLETION REPORT

PROJECT TITLE

Development of Compressed Sensing Based Image Reconstruction Techniques for Medical Imaging Applications

SUBMITTED BY

Dr. BHABESH DEKA
Associate professor
Department of Electronics and Communication Engineering
Tezpur University, Napaam, Tezpur
Assam, India-784028,

DATE OF SUBMISSION

April, 2016

UGC Reference No: F. No. 41-603/2012 (SR) dated 16.07.2012

Project Duration: From **01.07.2012 to 31.12.2015**

ACKNOWLEDGEMENTS

I extend my heartily gratitude to the **University Grants Commission (UGC), New Delhi, India** for selecting our project proposal and providing the required financial support to carry out the project work.

I am highly indebted to the **Department of Electronics & Communication Engineering, Tezpur University** for giving the opportunity and necessary infrastructures to carry out the project work in the Department.

Contents

List of Figures

List of Tables

List of Symbols

$\mathbf{A}$	Measurement matrix
$\boldsymbol{\alpha}$	Sparse coefficient vector
α	Step size
β	Constant
D_x , D_y	Finite difference operators on the x and y -axis
∇	Gradient
ε	Error constant
$f(.)$	Function
F_u	Fourier undersampling operator
$\varphi(.)$	Logarithmic barrier function
$\boldsymbol{\Phi}$	Sensing matrix
$\mathbf{g}$	Gradient
$\mathbf{H}$	Hessian
$\|\|.\|\|_0$	L_0-norm
$\|\|.\|\|_1$	L_1-norm
$\|\|.\|\|_2$	L_2-norm
$\|\|.\|\|_{TV}$	TV-norm
λ	Lagrangian multiplier
$\lambda_1, \lambda_2, \lambda_3$	Regularization constants
$\boldsymbol{\lambda}$	Dual variable
m	Data size
μ	Mutual coherence
n	Data size
ν	Dual variable
$\mathbf{P}$	Pre-conditioner
$\mathbf{r}$	Residual
$\mathbb{R}$	Real number
$\boldsymbol{\Psi}$	Representation bases
$\mathbf{x}$	Signal /Image as a $n \times 1$ column vector
$\mathbf{y}$	Measured k-space data

Chapter 1
Introduction

Compressed sensing or compressive sampling (CS) is a signal processing or image processing technique for efficiently acquiring and reconstructing a signal or image from a few samples or measurements by solving an underdetermined system. According to the CS theory, one can reconstruct certain signals and images from very less number of samples or measurements than traditional methods would require by the Nyquist rate [1]. To make it happen, it relies on two principles: sparsity and incoherence, meaning the signal is either sparse or compressible in some transform domain and that it should be acquired or sensed with a set of bases that are completely different with those required for its representation.

The fundamental idea of CS is to recover a sparse signal from a few linear measurements by Convex Optimization or Greedy Algorithms. There are some extremely common cases where data collection is a major problem for a variety of reasons. Like, the number of sensors may be limited or the measurements may be extremely expensive or the sensing process may be too slow. Therefore, one can collect only a few samples in a limited period of time like in the Magnetic Resonance Imaging (MRI).

The CS theory can be implemented in many applications such as- single pixel camera, MRI image reconstruction, channel estimation in wireless communication, radar imaging.

Magnetic Resonance Imaging (MRI) is an essential medical imaging tool for soft tissue imaging. It has the ability to create an image without the use of ionizing radiations. Images may be acquired in multiple planes (Axial, Sagittal, Coronal, or Oblique) without repositioning the patient [2].

Traditionally, the MRI data acquisition process is designed to meet the Nyquist criterion, which depends on the resolution and field of view (FOV). For high resolution we require more number of samples. If the Nyquist criterion is violated, artefacts due the linear reconstruction may exist. Typically, getting a single MR image involves collection of a series of data frames. To meet these requirements, we need a large amount of data and whole data acquisition process becomes a time consuming process. It is also not possible to increase the speed of data acquisition arbitrarily due to some instrumental and physiological constraints. In addition, movement of body parts during lengthy signal acquisition would cause unrecoverable artifacts in the reconstructed images. The only way to reduce the time of whole data acquisition is to acquire fewer amounts of data and reconstruct the MR image from the limited data without degrading the image quality.

In MRI, data acquisition process is done in the k-space or frequency domain. These images are also compressible in some transform domain. Due to linear combination of acquired data in frequency domain and transform sparsity of MR images, MRI naturally fits to the two key requirements imposed by the compressed sensing reconstruction of MRI.

Compressed sensing research was initiated in 2006 by two scientists, namely by Donoho [3] and by Candes [1]. Within a decade, it has become the most attractive research area in astronomy, radar imaging, signal processing, and medical imaging and so on. To define the CS problem, consider $\mathbf{x}$ be a sparse signal of length n which is under sampled by a measurement matrix $\mathbf{A}$ and $\mathbf{y}$ indicate the observed data, where $\mathbf{x} \in \mathbb{R}^n$, $\mathbf{A} \in \mathbb{R}^{n \times m}$, $\mathbf{y} \in \mathbb{R}^m$ and $m \ll n$. Based on the knowledge of measurement matrix $\mathbf{A}$ and measured signal $\mathbf{y}$ we have to recover the sparse signal $\mathbf{x}$. This problem can be solved by L_0-norm minimization i.e.

$$\begin{aligned} &\text{minimize} \quad \| \mathbf{x} \|_0 \\ &\text{subject to} \quad \mathbf{y} - \mathbf{A}\mathbf{x} \leq \varepsilon \end{aligned} \tag{1.1}$$

where ε is the error term and $\|.\|_0$ counts the number of nonzero elements.

Solving the above problem is impractical as it is an NP-hard problem. One way to solve this problem approximately is by using the L_1-norm instead of the L_0-norm. Thus the above problem can be represented as-

$$\begin{aligned} &\text{minimize} \| \mathbf{x} \|_1 \\ &\text{subject to} \quad \mathbf{y} - \mathbf{A}\mathbf{x} \leq \varepsilon \end{aligned} \tag{1.2}$$

where $\| \mathbf{x} \|_1 = |.| + |.| + \ldots$ .The solution of L_1-norm problem gives the exact original signal when $\mathbf{x}$ is sufficiently sparse. Problem (1.1) can also be solved by using greedy techniques, like the matching pursuit (MP) [11], the orthogonal matching pursuit (OMP) [12], etc.

1.1. CS-MRI Problem Formulation

CS problem for compressible signals:

Suppose a signal $\mathbf{x} \in \mathbb{R}^n$ is dense in time domain but it has a sparse representation when it is expressed with a proper basis $\mathbf{\Psi} \in \mathbb{R}^{n \times n}$. And $\mathbf{y} \in \mathbb{R}^m$ is the measured signal by a sensing waveform matrix $\mathbf{\Phi} \in \mathbb{R}^{m \times n}$, where $m \ll n$ [9, 10].

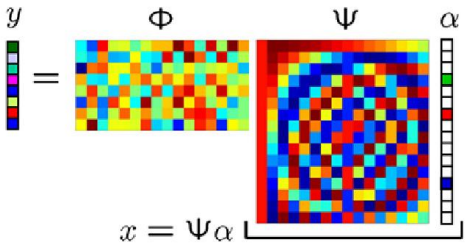

Fig. 1.1: Matrix representation of compressed sensing

For the accurate reconstruction of the signal $\mathbf{x}$, the representation basis $\mathbf{\Psi}$ and measurement matrix $\mathbf{\Phi}$ must be incoherent as much as possible. Then the problem can be represented as-

$$\begin{aligned} &\text{minimize} \quad \| \mathbf{\Psi x} \|_1 \\ &\text{subject to} \quad \mathbf{y} - \mathbf{\Phi \Psi \alpha} \leq \varepsilon \end{aligned} \tag{1.3}$$

where ε is some error constant.

CS-MRI with greedy approximation:

Problem (1.3) can also be written as-

$$\begin{aligned} &\text{minimize} \quad \| \mathbf{y} - \mathbf{\Phi\Psi\alpha} \|_2^2 \\ &\text{subject to} \quad \| \mathbf{\Psi x} \|_0 \leq L \end{aligned} \tag{1.4}$$

where L indicates the number of columns in the $m \times n$ matrix $\mathbf{\Phi\Psi}$ to be used to represent the sparse coefficient vector $\boldsymbol{\alpha}$. Generally, MR image is sparse in transform domain like the DCT, the wavelet, etc. For CSMRI the above problem can be rewritten as-

$$\begin{aligned} &\text{minimize} \quad \| \mathbf{y} - \mathbf{F}_u \mathbf{x} \|_2^2 \\ &\text{subject to} \quad \| \mathbf{\Psi x} \|_0 \leq L \end{aligned} \tag{1.5}$$

where $\mathbf{x}$ is the MR image, $\mathbf{y}$ is the corresponding measured k-space data, $\mathbf{\Psi x}$ are wavelet coefficients, and $\mathbf{F_u}$ is the $m \times n$ undersampled Fourier Transform matrix. To solve the above problem Mallat and Zhang have proposed a greedy algorithm known as the Matching Pursuit (MP) algorithm [11]. The algorithm iteratively selects a set of atoms from a dictionary for best sparse representation of the given signal. Pati *et al.* proposed an extension of MP algorithm known as the Orthogonal Matching Pursuit (OMP) algorithm [11]. The main difference is that in the OMP algorithm in each iteration coefficients are updated by orthogonal projection of the signal on the selected atoms of the dictionary.

CS-MRI with L_1-norm minimization:

In case of CSMRI, MR images have sparse representation in transform domains like the DCT, the wavelet transform, etc. Here, the problem can be represented as-

$$\begin{aligned} &\text{minimize} \quad \| \mathbf{\Psi x} \|_1 \\ &\text{subject to} \quad \mathbf{y} - \mathbf{F_u x} \leq \varepsilon \end{aligned} \tag{1.6}$$

This problem can be solved by different L1-minimization algorithms. A few important landmark works in the CSMRI are cited below.

The Primal Dual Interior Point Method (PDIPM) is the classical method for the solution of the L_1-minimization problem. But the number of computation is too high in PDIPM. In the work of Daubechies [4], the author has introduced an iteratively shrinkage algorithm known as the *Iterative Shrinkage Thresholding* (IST) to solve the L_1- minimization problem. At each iteration, the objective function is shrunk by a thresholding function. Michael Lustig *et al.* [6] tried to efficiently under-sample the MRI data and reconstruct the MR image from under-sampled data. They have designed an efficient under-sampling pattern based on estimated PDF. Finally, for reconstruction, the *Nonlinear Conjugate Gradient* (NCG) algorithm is used for simplicity. Koh *et al.* [5] has solved the L_1-minimization problem using the *Truncated Newton Interior Point Method* (TNIPM). The TNIPM is much faster than the PDIPM, because in TNIPM a pre-conditioner is used which approximates the $\mathbf{A}^T\mathbf{A}$ by $\tau\mathbf{I}$ where $\mathbf{I}$ is

the identity matrix and τ is a constant term which simplifies the problem and hence reduces the number of computations. Mario A.T. Figgueiredo *et al.* [7] have proposed a new gradient projection algorithm known as the *Gradient Projection for Sparse Reconstruction* (GPSR) to solve the compressed sensing and other inversion problem. The GPSR is relatively faster algorithm than the previous algorithms.

CS-MRI field has mainly two research directions. One is how efficiently MRI data can be acquired and other is how fast reconstruction can be done without compromising the image quality.

1.2. Objectives

The various objectives that were achieved during the implementation of the project are:

I. Study of the state-of-the-art CSMRI algorithms to explore new algorithms that could establish trade-off between faster convergence and computational complexity.

II. Development of High Throughput CS-MRI Reconstruction Techniques.

III. Development of efficient Multi-slice MR image reconstruction algorithms using combination of interpolation and compressed sensing.

1.3. Scope of the Work

Today MRI is an essential medical imaging tool burdened by an inherently slow data acquisition process. It is recommended because MRI does not use any ionizing radiation. In case of dynamic MRI a small amount of measurements can be possible within a short period of time. The slow imaging speed in MRI is a challenge for dynamic MRI like cardiac imaging in which a small number of samples is recoded per heart beat. Thus to reduce the scan time, we have to highly undersample the MRI data (k-space) and reconstruct the MR image without degrading the image quality from few undersampled data. The application of compressed sensing (CS) to MRI has the potential for significant scan time reduction which will improve patient care and reduce costs.

1.4. Organisation of the Report

The rest of the report is organized into six chapters, each of them giving a detailed description about various ingredients of the project.

Chapter-2 discusses about working process of MRI. This chapter is about the data acquisition technique i.e. different types of RF pulse sequences for various imaging technique.

Chapter-3 mainly deals with the concept of compressed sensing, its application in magnetic resonance image acquisition and the detailed description about the proposed random variable density undersampling pattern.

Chapter-4 discusses about the L1-minimization algorithms, their application in MR image reconstruction and the detailed description about the proposed high throughput MR image reconstruction method.

Chapter-5 is about the wavelet tree structure and implementation of group sparsity of wavelet coefficient as a regularization term with TV-L1-L2 model of CSMRI.

Chapter-6 discusses about the interpolated compressed sensing theory and the detailed description about the proposed efficient interpolation based 2D multi-slice MR image reconstruction technique.

Chapter 7 is the concluding chapter of the report that deals with success and the future prospects that can be made in this area.

References:

[1] E.J. Candμes, J. K. Romberg, and T. Tao, "Robust uncertainty principles: exact signal reconstruction from highly incomplete frequency information," *IEEE Transactions on Information Theory*, vol. 52, no. 2, pp. 489-509, 2006.

[2] J.T. Bushberg, A. J. Seibert, E. M. Leidholdt, and J. M. Boone, *The essential physics of medical imagin*g, Lippincott Williams & Wilkins, Philadelphia, PA, 3rd Edition, 2012.

[3] D. Donoho, "Compressed sensing," *IEEE Transactions on Information Theory*, vol. 52, no. 4, pp. 1289-1306, 2006.

[4] I. Daubechies, M. Defrise and C. D. Mol, "An iterative thresholding algorithm for linear inverse problems with a sparsity constraint," *Communications on Pure and Applied Mathematics*, vol. 57, no. 11, pp. 1413-1457, 2004.

[5] K. Koh, S. jean Kim, S. Boyd, and Y. Lin, "An interior-point method for large scale l1-regularized logistic regression," *Journal of Machine Learning Research*, vol. 8, pp.1519-1555, 2007

[6] M. Lustig, D. Donoho, and J. M. Pauly, "Sparse MRI: The application of compressed sensing for rapid MR imaging," *Magnetic Resonance in Medicine*, vol. 58, pp. 1182-1195, 2007.

[7] M. Figueiredo, R. D. Nowak, and S. J. Wright, "Gradient projection for sparse reconstruction: Application to compressed sensing and other inverse problems," *IEEE Journal of Selected Topics in Signal Processing*, vol.1, no. 4, pp. 586-597, 2007.

[8] J.M. Bioucas-Dias, M. Jose, and M. A. T. Figueiredo, "A new TwIST: Two-step iterative shrinkage/ thresholding algorithms for image restoration," *IEEE Transactions on Image Processing,* vol.16, no.12, pp. 2992-3004, 2007.

[9] E. Candes and M. Wakin, "An introduction to compressive sampling," *IEEE Signal Processing Magazine*, vol. 25, no. 2, pp. 21-30, 2008.

[10] S. Boyd, and L. Vandenberghe, *Convex Optimization*, Cambridge University Press, New York, NY, USA, 1st Edition, 2004.

[11] S.G. Mallat and Z. Zhang, "Matching Pursuits with Time-frequency Dictionaries," *IEEE Transactions on Signal Processing*, vol. 41, no. 12, pp. 3397-3415, 1993.

[12] Y.C. Pati, R. Rezaiifar, and P. S. Krishnaprasad, "Orthogonal Matching Pursuit: Recursive Function Approximation with Applications to Wavelet Decomposition," *Proc. of the 27th Annual Asilomar Conference on Signals, Systems, and Computers*, pp. 40-44, 1993.

Chapter 2

Magnetic Resonance Imaging

2.1. Introduction

Magnetic resonance imaging (MRI), nuclear magnetic resonance imaging (NMRI), or magnetic resonance tomography (MRT) is a medical imaging technique. MRI uses non-ionizing radiation to generate image. In MRI, the scanner forms a strong magnetic field around the area to be imaged and apply RF pulses when the RF pulse is switched off the body emits back the energy which it absorbs from the RF pulse. This radiation is picked up by a receiver coil, which is then used to construct the image.

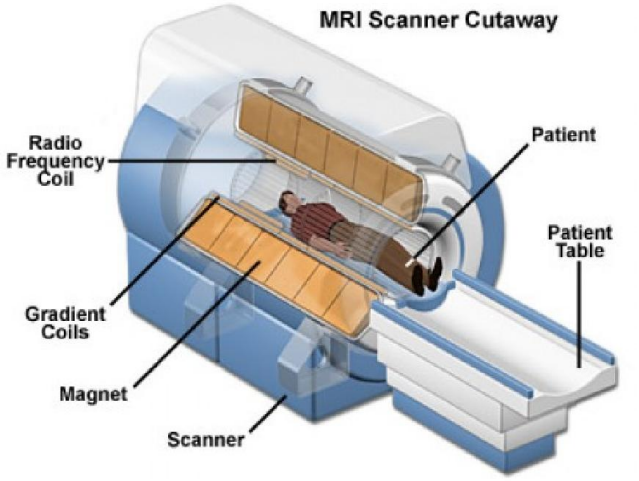

Fig.2.1. MRI Scanner

A large proportion of our body is made up of water molecule which contains Hydrogen atoms. The nuclei of Hydrogen atoms have only one proton and they behave like little bar magnets because they are charged and spin about themselves. When these little bar magnets are placed in a strong magnetic field they align with it and rotate around the axis of the field in a movement which is known as precession or precession frequency. The stronger the magnetic field higher the precession frequency. If we send a RF pulse at the range of precession frequency then they can absorb this radiation and pick up energy and go from a lower to a higher energy level, which is said to be at resonance. When the RF pulse is turned off this energy is just handed over to their surroundings by emitting back the radiation. They re-emit radiation at a different rate because each tissue of the body has different chemical composition and physical state. MRI uses this signal from the nuclei of hydrogen atoms for image generation [Chapter 14-15, 1], [2].

2.2. How does MRI work?

The patient is placed in a static magnetic field. Hydrogen protons within the patient's body align to the magnetic field. A Radio Frequency (RF) pulse is emitted from the scanner, of a specific range of frequencies. If the emitted frequencies are in the range of procession frequency of Hydrogen protons then Hydrogen protons absorb the energy from the RF pulse. Generally RF pulses are applied for a small duration in the range of millisecond. When RF pulses are turned off the Hydrogen protons re-emits the energy according to their surrounding environments. Receiver coil receives this re-emitted signal and corresponding MR image is generated.

Suppose we want to make cross-sectional images of the human body. The excitation pulse is therefore delivered only to the frequency of that slice which we want to image and not to the whole body. For this region three different gradients are used namely, Slice Selection Gradient, Frequency Encode Gradient and Phase Encode Gradient. Gradients are additional magnetic fields that are generated by gradient coils and add to or subtract from the main magnetic field. Depending on their position along the gradient, protons are temporarily exposed to magnetic fields of different strength and hence differ in their precessional frequencies [2].

2.2.1. **Different Gradients**

The Slice Selection Gradient (SSG) determines the slice of tissue to be imaged in the body together with RF excitation pulse. To do this the Slice Selection Gradient (GSS) is applied perpendicular to the desired slice plane. This is added to B0, and the protons present a resonance frequency variation proportionate to GSS. An RF wave is simultaneously applied, with the same frequency as that of the protons in the desired slice plane. This causes a shift in the magnetization of only the protons on this plane. As none of the hydrogen nuclei located outside the slice plane are excited, they will not emit a signal.

The Frequency Encode Gradient (FEG), also known as the readout gradient, is applied in a direction perpendicular to the Slice Selection Gradient. Once the signal from the slice has been isolated, the remaining two in-plane dimensions need to be encoded (in this case the 'x' and 'y' directions). One of the directions (say 'y' direction) is encoded by changes of frequency.

Suppose a gradient is applied in the y-direction to change frequency. However, this would not be sufficient to uniquely describe frequency to each column and row of pixels. For the last dimension the signal is encoded in terms of phase. It is applied before the frequency encode gradient and after the slice encode gradient, along the third perpendicular axis [2].

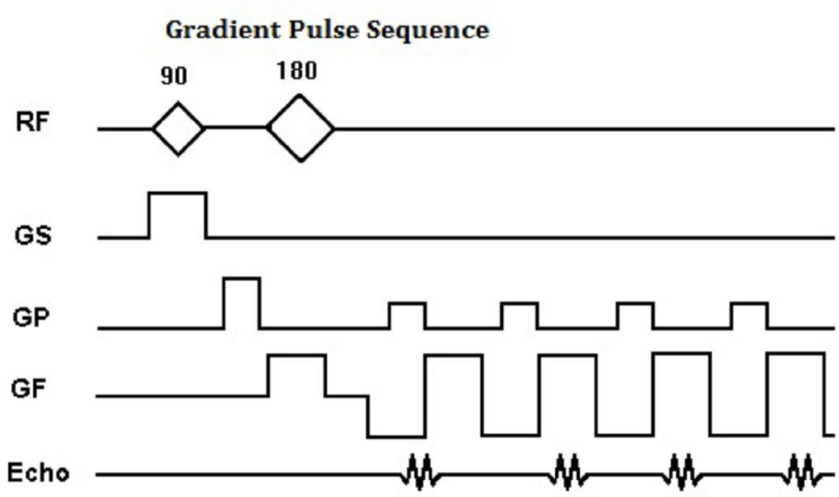

Fig.2.2: Gradient Pulse sequences in MRI

2.3. k-Space

Data from the signals is stored in a mathematical area known as k-space which is equivalent to a Fourier plane. k-space has two axis with the horizontal axis (k_x) representing the frequency information and the vertical axis (k_y) the phase information. To get the MR image from a k-space data requires a 2D inverse Fourier Transform. The general way to fill the k-space is to use a line-by-line rectilinear trajectory. One line of k-space is fully acquired at each excitation. Between each repetition, there is a change in phase-encoding-gradient strength, corresponding to a change in k_y-coordinate. This allows filling of all the lines of k-space from top to bottom. Centre region of the k-space contain structural information of the image and periphery contain the information about the resolution of the image.

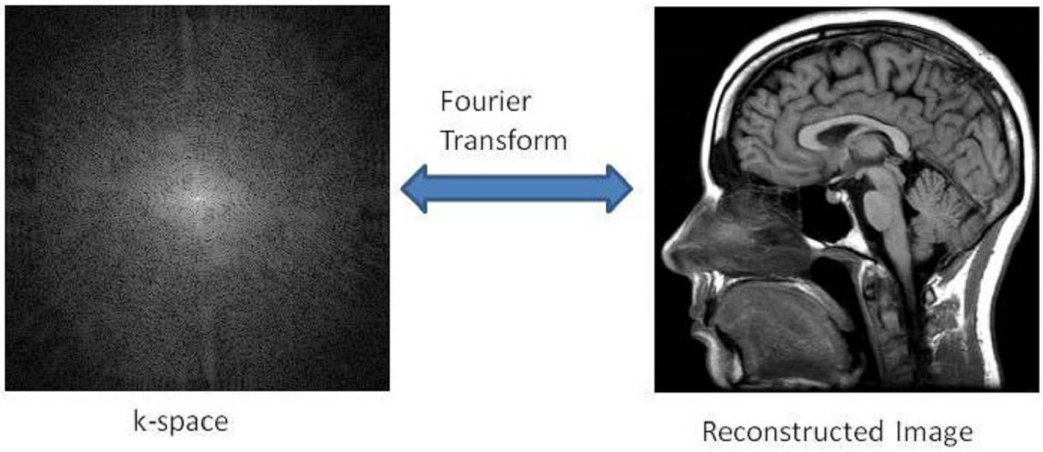

Fig. 2.3: A typical k-space and its corresponding MR Image

2.4. Imaging Parameters

2.4.1. Relaxation Time

The term relaxation means that the spins are relaxing back into their lowest energy state or back to their equilibrium state. Once the radio frequency (RF) pulse is turned off, the protons will have to realign with the axis of the B_0 magnetic field and give up all their excess energy [2].

T1 Relaxation Time:

T1 is called the longitudinal relaxation time because it refers to the time it takes for the spins to realign along the longitudinal axis. T1 is also called the spin-lattice relaxation time because it refers to the time taken for the spins to give the energy they obtained from the RF pulse back to the surrounding lattice in order to go back to their equilibrium state i.e. recovery of longitudinal orientation. T1 Relaxation Time refers to interval where 63 % of longitudinal magnetization is recovered.

T2 Relaxation Time:

T2 relaxation time refers to the progressive dephasing of spinning dipoles following the 90^0 pulse as seen in a spin-echo sequence due to tissue-particular characteristics. This is alternatively known as spin-spin relaxation i.e. loss of transverse magnetization. T2 Relaxation Time refers to interval where only 37% of original transverse magnetization is present.

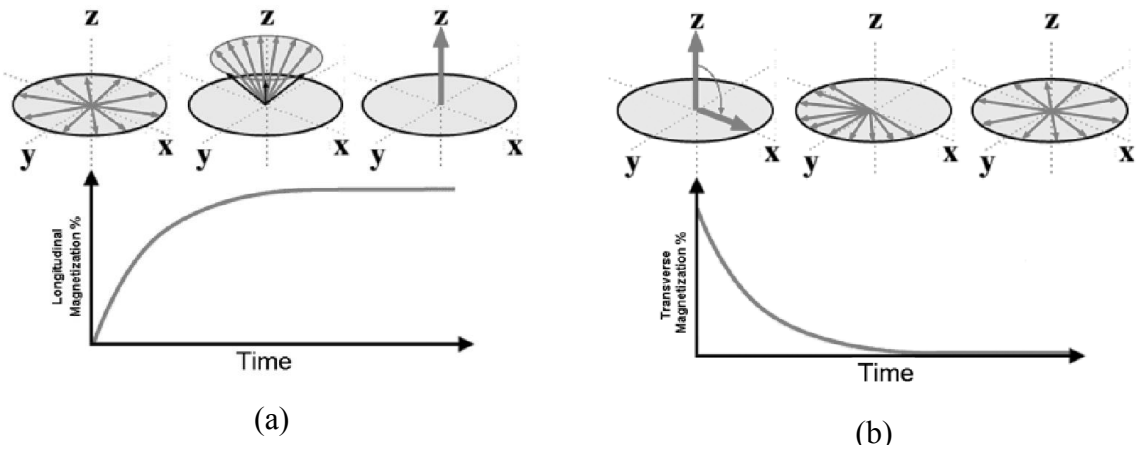

Fig. 2.4: (a) Recovery of longitudinal magnetization, and (b) loss of transverse magnetization

2.4.2. Repetitions Time

The repetition time or (TR) is the time from the application of an excitation pulse to the next pulse. It determines how much longitudinal magnetization recovers between each pulse. It is measured in milliseconds.

2.4.3. Echo Time

The echo time or TE refers to time between the application of radiofrequency excitation pulse and the peak of the signal induced in the coil. It is measured in milliseconds.

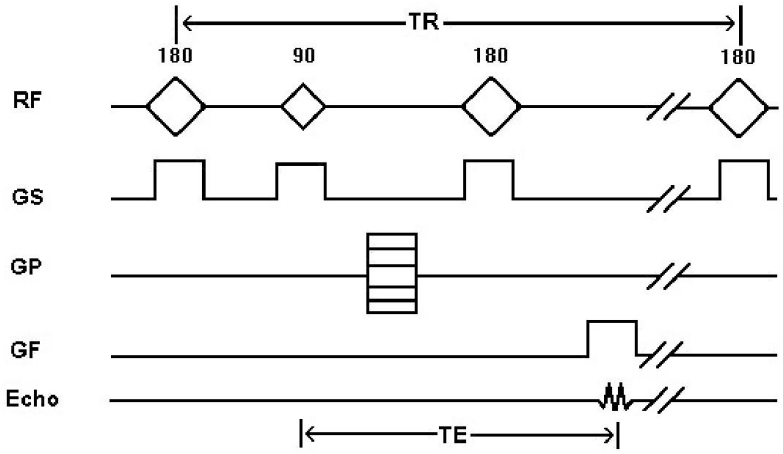

Fig. 2.5: Repetition time and Echo Time

2.5. Image Contrast

2.5.1. T1-weighted

Images with contrast that is mainly determined by T1 are called T1-weighted images. Tissues with a short T1 appear bright because they regain most of their longitudinal magnetization during the TR interval and thus produce a stronger MR signal. Tissues with a long T1 appear dark because they do not regain much of their longitudinal magnetization during the TR interval and thus produces a weaker MR signal.

2.5.2. T2-weighted

Images with contrast that is mainly determined by T2 are called T2-weighted images. Tissues with a short T2 appear dark on T2-weighted images and tissues with a longT2 appear bright on T2-weighted images. Table 2.1 shows different types of tissue brightness in T1 and T2-weighted images.

2.5.3. PD-weighted

A proton density or PD -weighted image depends on the number of precessing hydrogen protons. A very long TR is selected to give neither a T1 nor T2-weighted image. The difference in the signals received from different tissues depends only on the number, or density, of hydrogen atoms. Fig. 2.1 shows different brain MR images with T1, T2 and PD.

Table 2.1: Signal Intensities of Different Tissues on T1-and T2-weighted

Tissue	**T1-weighted image**	**T2-weighted image**
Fat	Bright	Bright
Tumour	Dark	Bright
Inflammatory tissue	Dark	Bright
Muscle	Dark	Dark
Compact bone	Dark	Dark
Connective tissue	Dark	Dark
Aqueous liquid	Dark	Bright
Hyaline cartilage	Bright	Bright
Fibrous cartilage	Dark	Dark

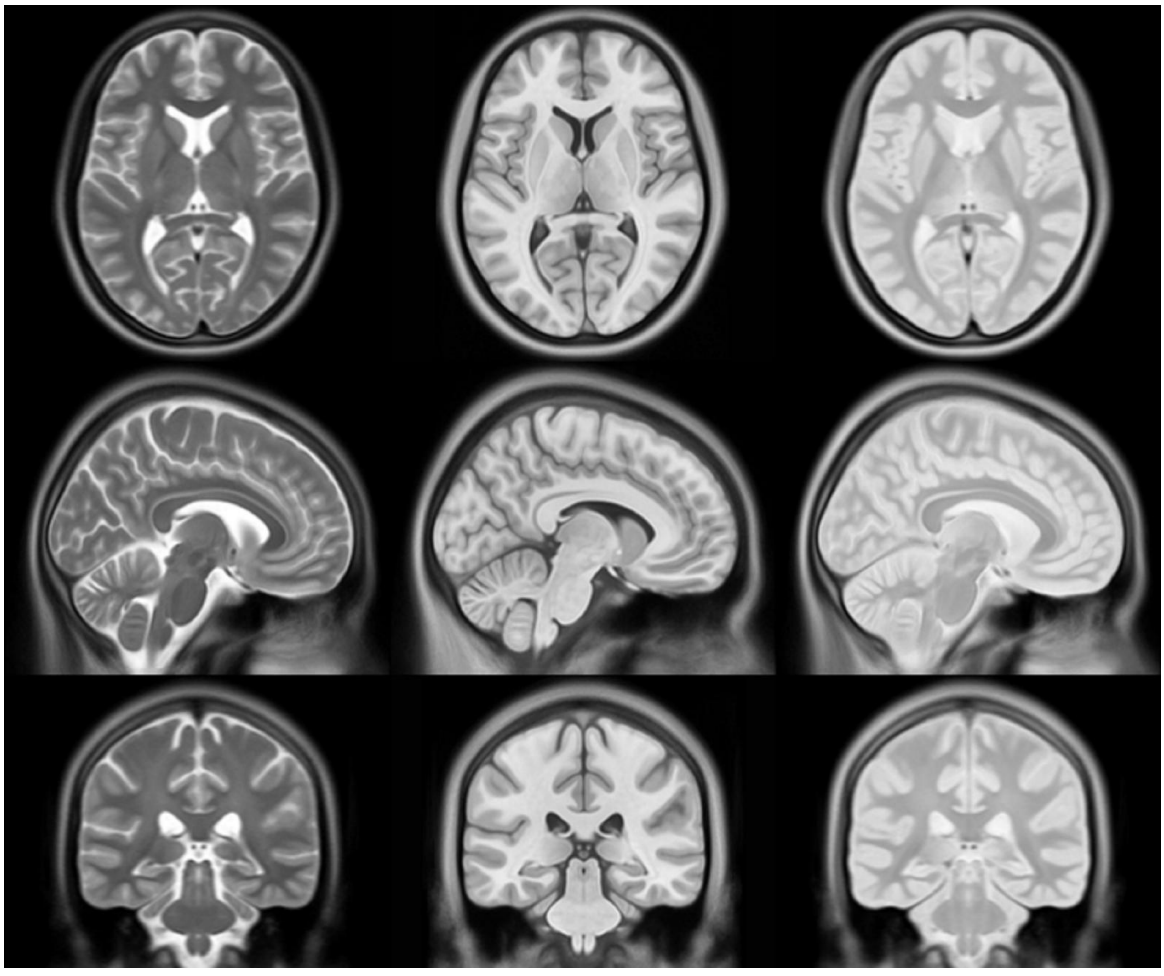

Fig. 2.6: Different types of MR images. From left to right T1, T2 and PD-weighted MR images.

References:

[1] J. T. Bushberg, A. J. Seibert, E. M. Leidholdt, and J. M. Boone, *The essential physics of medical imaging*, Lippincott Williams & Wilkins, Philadelphia, PA, 3rd Edition, 2012.

[2] D. W. McRobbie, E. A. Moore, M. J. Graves, and M. R. Prince, *MRI from Picture to Proton*, Cambridge University Press, Cambridge, UK, 1st Edition, 2006.

Chapter 3

Basics of CSMRI and Design of a Practical Undersampling Pattern

3.1. Introduction

Sensing and compression of data are the two very common processes in modern day life. According to the Nyquist criterion, a signal is sampled /sensed at least at a rate equal to twice the maximum frequency of the signal for accurate reconstruction [1]. This results in a huge amount of data which makes it difficult for further processing, memory shortage for data storage, bandwidth problem for data transmission, and so on.

The solution of this problem is data compression. It is found that most of the natural signals and images can be represented in some transform domain where it is sparse or compressible. It means that in the transform domain only a few coefficients are significantly large in magnitude and contain the most of the information and remaining coefficients contain less or no information. By keeping only those few large coefficients, we can reconstruct the original signal /image without significant loss of information. Data compression is very common in image, audio, video compressions; mobile, radar communications, etc. Compression solves the problem of data storage and data transmission but still we have to acquire a large amount of data.

Few years ago, researchers in the signal/image processing community found that data compression can be directly performed during data acquisition process itself. This new data acquisition paradigm is known as the *compressed sensing*. The compressed sensing is the combination of two steps i.e. data acquisition and encoding of the data in a single step. Using compressed sensing the number of samples needed for accurate reconstruction of signal/ image is much smaller than the traditional Nyquist sampling criterion. Thus, it also reduces the time required for whole data acquisition process. It is very much helpful in those cases where data acquisition is the major problem like in the Magnetic Resonance Imaging (MRI) [1, 2].

3.2. Requirements for the CS

The two main requirements for the application of compressed sensing is -

1. The signal or image must be sparse or has a sparse representation in some transform domain i.e. the signal/ image must be compressible.

2. Aliasing artefacts due to under sampling must be incoherent with the sparse representation domain.

3.2.1. Sparsity

For the application of compressed sensing signal must be either sparse or compressible in a transform domain. Generally, natural signals / images are not sparse. But they have a sparse

representation in some transform domain having a basis set $\boldsymbol{\Psi}$ i.e. suppose $\mathbf{x}$ is an image which is dense in the spatial domain and but has a sparse representation when projected on to $\boldsymbol{\Psi}$ (like the DCT, the wavelet, etc.), i.e. $\boldsymbol{\alpha} = \boldsymbol{\Psi}^T \mathbf{x}$, where $\mathbf{x} \in \mathbb{R}^n$, $\boldsymbol{\Psi} \in \mathbb{R}^{n \times n}$ and $\boldsymbol{\alpha} \in \mathbb{R}^n$ [3].

3.2.2. Incoherence

For accurate reconstruction of the signal or image from compressively sensed data, the data acquisition or sensing bases $\boldsymbol{\Phi}$ must be incoherent with the sparse representation bases $\boldsymbol{\Psi}$.

Suppose a signal or image $\mathbf{y} \in \mathbb{R}^m$ is acquired with $\boldsymbol{\Phi} \in \mathbb{R}^{m \times n}$, i.e. $\mathbf{y} = \boldsymbol{\Phi}\mathbf{x}$. Then for accurate reconstruction of $\mathbf{x}$ from the undersampled data $\mathbf{y}$, $\boldsymbol{\Phi}$ must be incoherent with $\boldsymbol{\Psi}$. The mutual coherence between $\boldsymbol{\Phi}$ and $\boldsymbol{\Psi}$ can be measured as-

$$\mu(\boldsymbol{\Phi}, \boldsymbol{\Psi}) = \sqrt{n} \max_{1 \le k, j \le n} |\langle \phi_k, \psi_j \rangle| \tag{3.1}$$

According to the linear algebra $\mu(\boldsymbol{\Phi}, \boldsymbol{\Psi}) \in [1, \sqrt{n}]$. If $\boldsymbol{\Phi}$ and $\boldsymbol{\Psi}$ contain correlated elements then incoherence is small. For accurate compressed sensing reconstruction with less aliasing artifacts incoherency between $\boldsymbol{\Phi}$and $\boldsymbol{\Psi}$ should large be as much as possible [3].

3.2.3. Restricted Isometry Property (RIP)

The main task in the compressed sensing is to transform the $(n \times 1)$-signal $\mathbf{x}$ to the $(m \times 1)$-measurement $\mathbf{y}$ by using proper measurement matrix $\boldsymbol{\Phi}$. Candès and Tao proposed a condition for the measurement matrix, $\mathbf{A} = \boldsymbol{\Phi}\boldsymbol{\Psi}$ known as the restricted isometry property (RIP). Assuming that $\mathbf{x}$ is s-sparse, i.e. $\mathbf{x} = \boldsymbol{\Psi}\boldsymbol{\alpha}$ then $\mathbf{A}$ guarantees reconstruction or satisfies the RIP of order s, where $s < n$, if their exists an isometry constant $0 < \delta_s < 1$, such that for all s-sparse vector $\boldsymbol{\alpha}$-

$$(1 - \delta_s) \| \boldsymbol{\alpha} \|_2^2 \le \| \mathbf{A}\boldsymbol{\alpha} \|_2^2 \le (1 + \delta_s) \| \boldsymbol{\alpha} \|_2^2 \tag{3.2}$$

δ_s is the smallest number that satisfies the equation (3.2). Orthogonal matrix has $\delta_s = 0$ for all s. $\delta_s < 1$ allows for reconstruction of any signal $\mathbf{x}$. If $\delta_s << 1$ the sampling matrix $\boldsymbol{\Phi}$ has a large probability to accurately reconstruct the signal $\mathbf{x}$. The isometry constant δ_s of a given matrix is hard to find, but there are some known bounds for δ_s of random matrix [3].

3.3. Goal of compressed sensing

Consider a finite length, one-dimensional, discrete time signal $\mathbf{x} \in \mathbb{R}^n$. Compressed sensing claims that from m random measurements where $m \ll n$ one can perfectly reconstruct the original signal $\mathbf{x}$, i.e. if the measured signal $\mathbf{y} = \mathbf{\Phi x}$, then one can reconstruct the approximation of the original signal $\mathbf{x}$ from the knowledge of $\mathbf{y}$ and $\mathbf{\Phi}$. In general $\mathbf{x}$ is dense in time domain but sparse in some transform domain with proper basis $\mathbf{\Psi}$ i.e. $\mathbf{x} = \mathbf{\Psi \alpha}$, where $\mathbf{\Psi} \in \mathbb{R}^{n \times n}$, $\boldsymbol{\alpha} \in \mathbb{R}^n$ and $\boldsymbol{\alpha}$ is sparse. Then the measured signal $\mathbf{y}$ can be represented as - $\mathbf{y} = \mathbf{\Phi x} = \mathbf{\Phi \Psi \alpha}$ [3].

3.4. Compressed Sensing in MRI

In MRI data acquisition presses is very slow which is mainly limited by some physical (gradient amplitude, slew rate) and physiological (nerve stimulation) constraints. The goal of compressed sensing MRI research is to reduce the amount of acquired data without much degradation in the quality of image reconstruction.

Image reconstruction with compressed sensing is a technique in which less amount of data are acquired to reconstruct the image without significant loss of image quality.

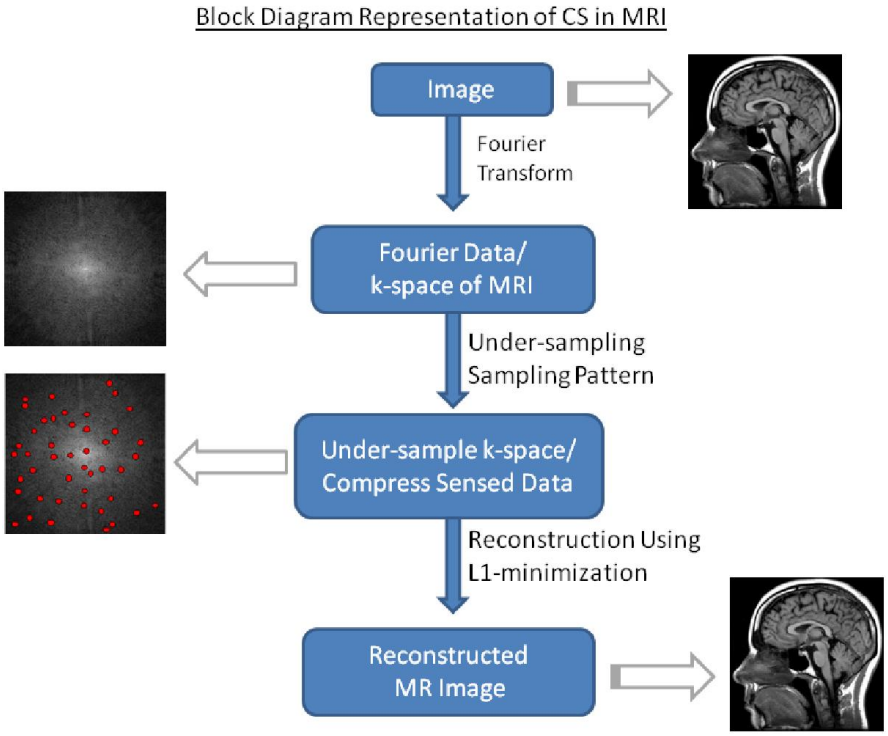

Fig. 3.1: Block diagram representation of CS in MRI

3.4.1. The Natural Fit between CS and MRI

MRI fulfils the key requirements of compressed sensing. At first, the sparsity of the image, most of the MR images are approximately sparse in transform domain. As shown in Fig. 3.2(c), wavelet coefficients of MR image are approximately sparse. The wavelet transform is a multi scale representation of the original image. Coarse-scale coefficients of the wavelet represent the low resolution image elements and fine-scale coefficients represent the high resolution elements. Secondly, the sensing basis must be incoherent with respect to the sparse representation basis. In MRI data acquisition is performed in k-space (shown in Fig. 3.2(b)) which is nothing but the Fourier transform of the MR image. Now, a strong incoherence also exists between the Fourier transform and the wavelet transform. Thus, MRI is naturally fit for the application of compressed sensing. Fig. 3.3, demonstrates an example how the CS-MRI reconstruction produces undersampling artifacts which are totally incoherent to the wavelet transform coefficient.

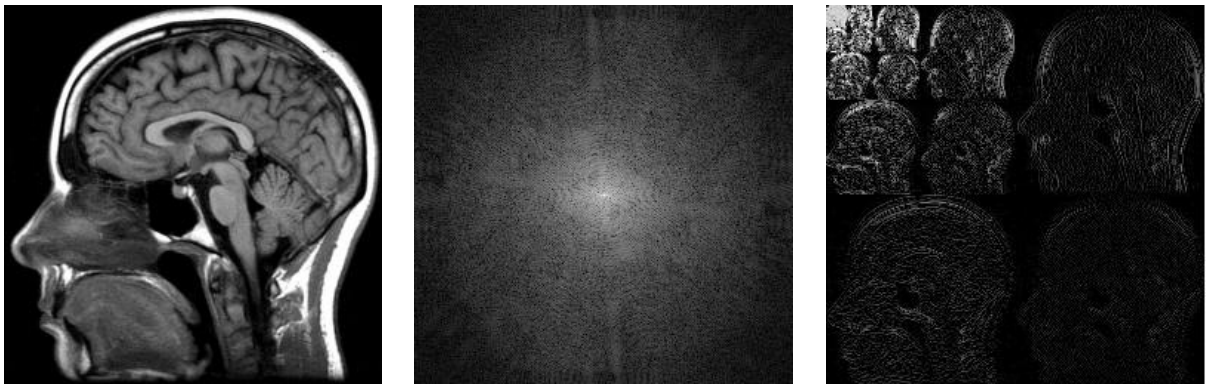

(a) (b) (c)

Fig. 3.2: (a) Original MR image (256x256), (b)k-space of the corresponding MR Image, and (c) Wavelet representation of the original MR image.

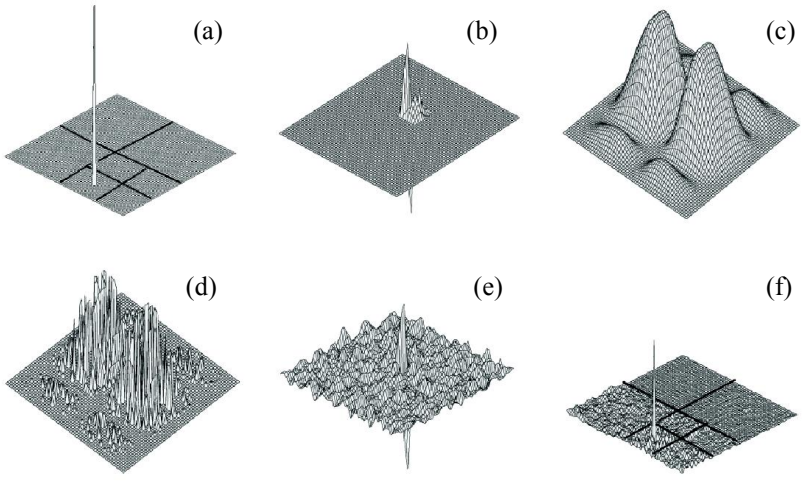

Fig. 3.3: (a) A single point in the wavelet domain, (b) the corresponding image domain representation, (c) the k-space representation of the image point, (d) the undersampled k-space representation, (e) the corresponding image and wavelet domain representations of (d), respectively.

3.4.2. Undersampling in k-space

The data acquisition is the most important part in compressed sensing MRI. The main target is how efficiently one can acquire only a few samples for reconstruction of the MR image without compromising with the quality of the image.

An incoherent aliasing artifact, as explained above, is an important criterion for CS reconstruction. Equispaced k-space undersampling creates coherent aliasing artifacts. In Fig.3.4, it is clear that uniform k-space sampling produces coherent aliasing artifacts; here it is not possible to distinguish between original and its replicas because all are similar.

But in case of random under-sampling, situation is different. Here the reconstructed image contains artifacts but they are incoherent. This type of artifacts can be easily distinguished because these are like additive random noise. They appear in the MR Image due to the leakage of energy because of undersampling and can be easily removed during the reconstruction process by thresholding.

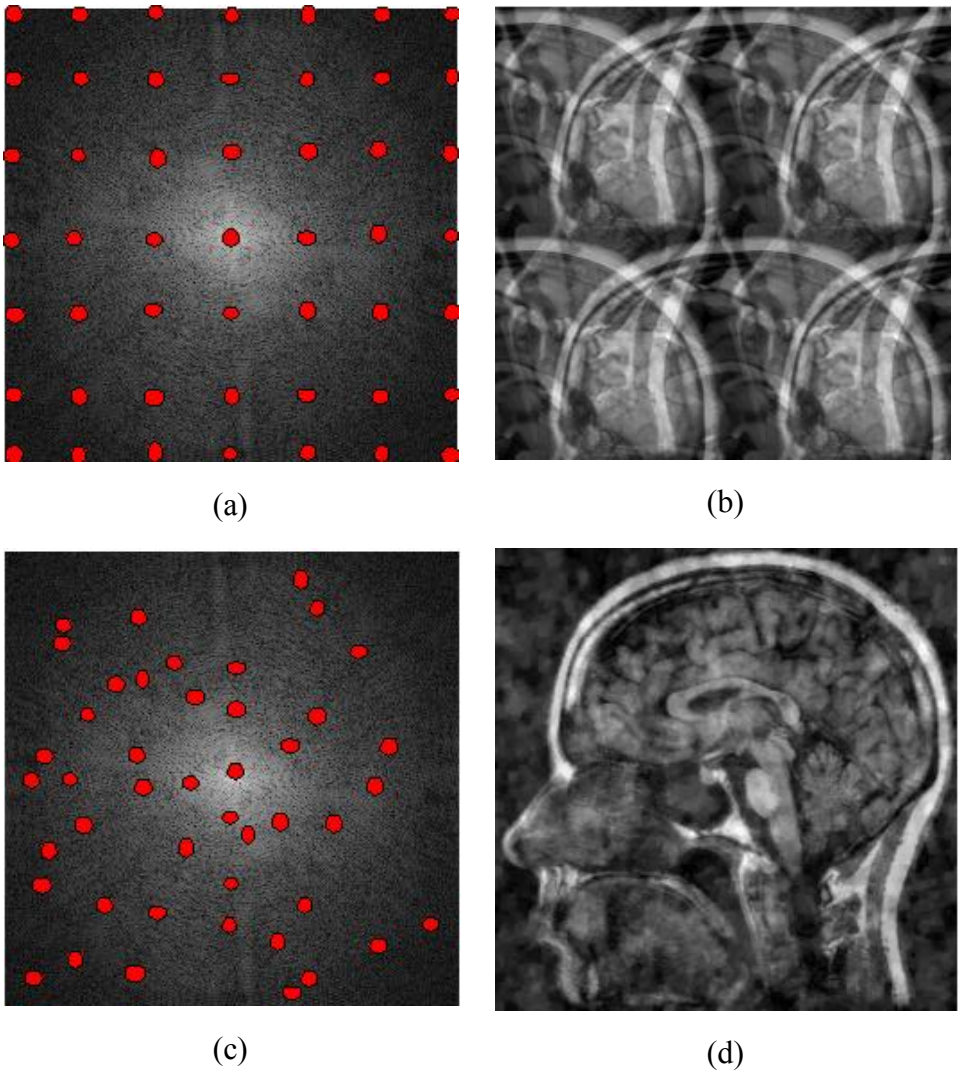

Fig. 3.4: (a) Uniform k-space sampling, (b) MR image from the uniform k-space sampling data, (c) Random k-space sampling, and (d) MR Image from the random k-space sampling data

In MRI, data acquisition process is performed in k-space. Centre region of the k-space contains information about gross structure and contrast of the original MR Image, most of the information required to produce the MR image. Accordingly, the peripheral region contains the spatial resolution information of MR image. Therefore, if the total numbers of samples are limited then we have to acquire more samples from the centre region and relatively less sample from the periphery. In Fig.3.5 it is clearly shown that the centre region of the k-space contains the main information about the corresponding MR image. Therefore, we apply the variable density undersampling where more samples are collected near the centre region and accordingly fewer samples from the periphery region [1].

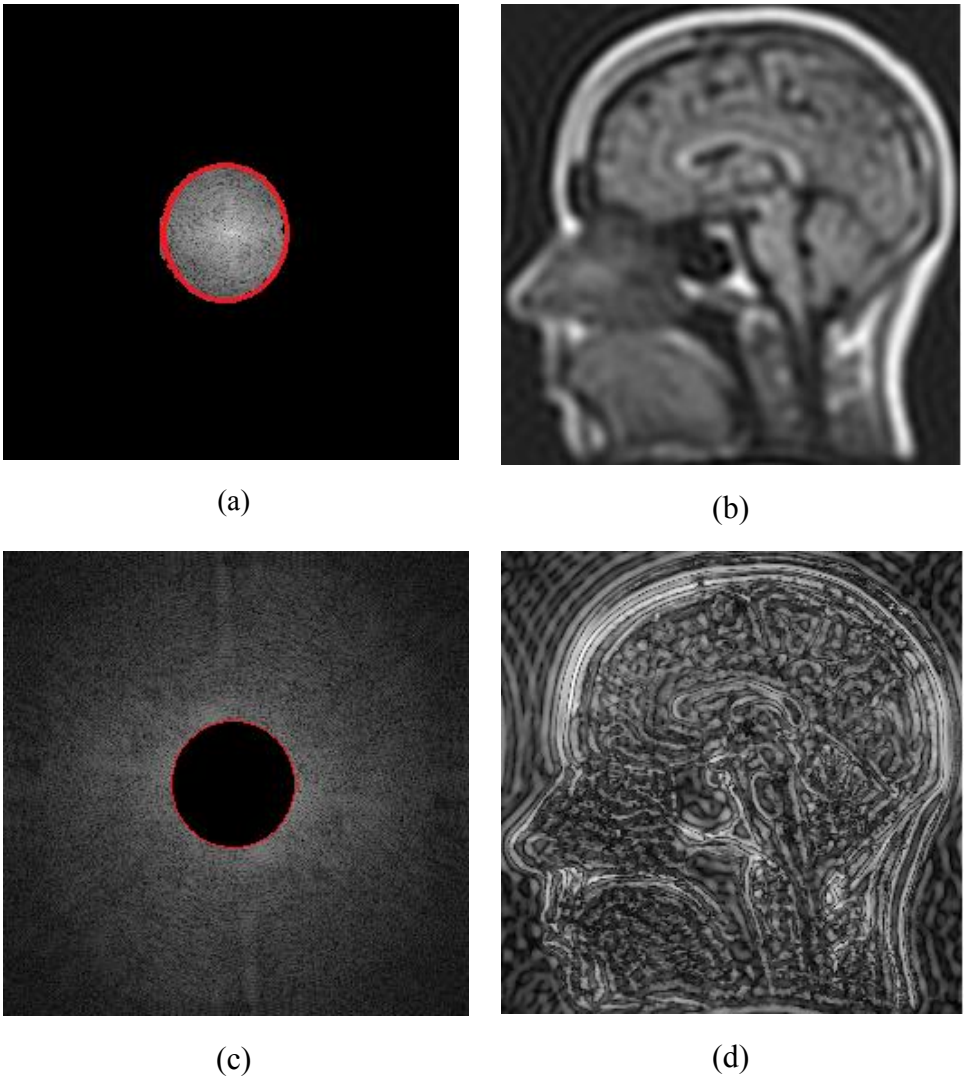

Fig. 3.5: (a) Centre region of a typical k-space, (b) Corresponding MR image from centre region of k-space. (c) Peripheral region of a typical k-space, and (d) Corresponding MR image from peripheral region of k-space

Variable density undersampling Pattern:

The main aim of the variable undersampling pattern is to collect more samples from the centre region of k-space. Many variable density undersampling patterns are proposed based on different estimation techniques, like the Monte Carlo estimation of PDF [1], the variable density radial lines, the variable-density Poisson-disc sampling pattern [5], etc. Fig.3.6 shows some well known variable density sampling patterns.

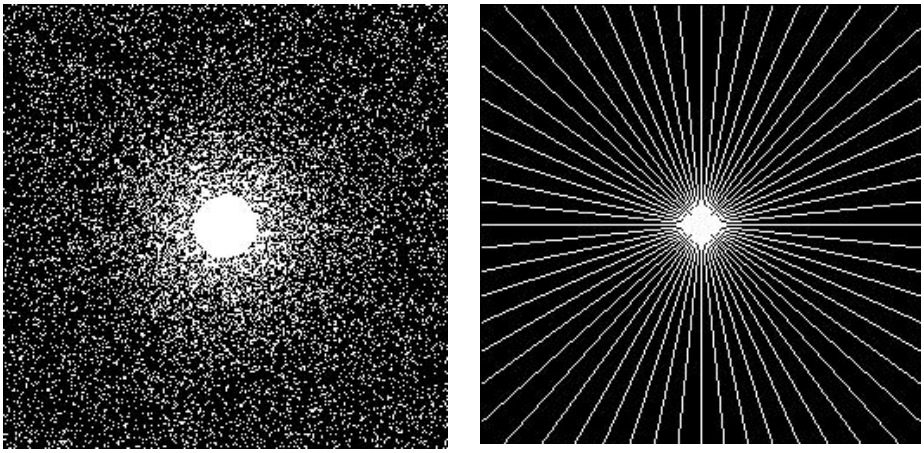

(a) (b)

(c)

Fig. 3.6: (a) Variable density undersampling pattern based on the estimated probability density function, (b) Radial type variable density undersampling pattern, and (c) variable-density Poisson-disc undersampling pattern [5].

3.5. Proposed variable density undersampling pattern

The proposed variable density sampling pattern known as the variable density Poisson disk sampling pattern mainly consists of several Poisson Disks arranged concentrically.

The Poisson disk generates random points which have following properties-

1. They are tightly packed together.

2. They maintain a specified minimum distance between two neighbouring points as shown in Fig.3.7(c)

In Poisson disk, at first a grid is generated such that every cell contains at most one sampling point. If points are at least distance r from each other, then cell size must be $r/2$. Therefore no two neighbouring points are too close.

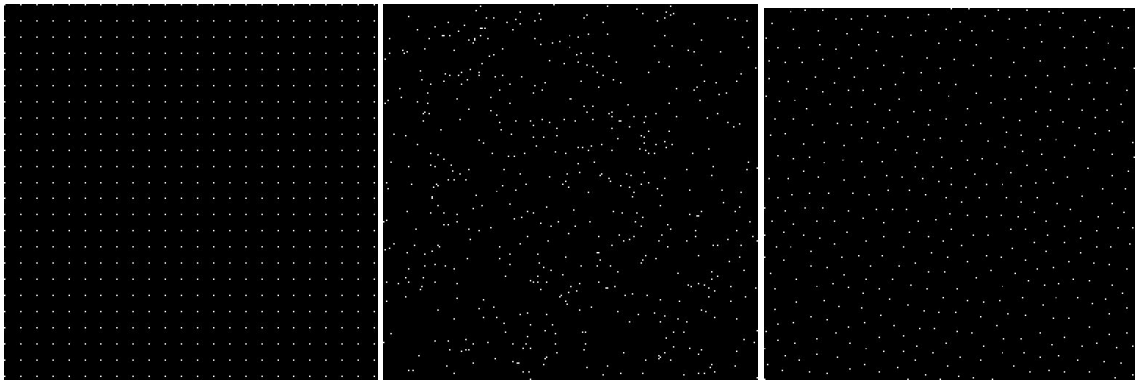

(a) (b) (c)

Fig.3.7: (a) Uniform sampling pattern, (b) Random sampling pattern, and (c) Poisson Disk sampling pattern

In Fig. 3.8, it is clear that points in the Poisson Disk sampling pattern are purely random in nature i.e. they contain the randomness property but also keep a minimum distance between two neighbouring points

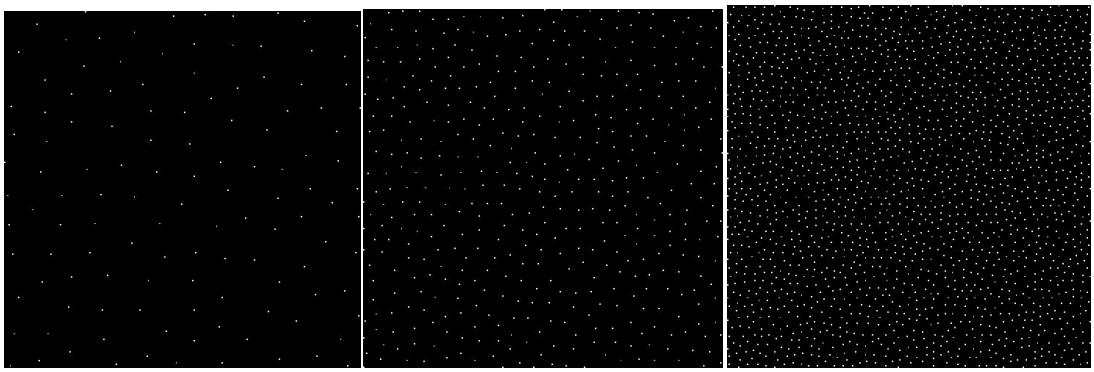

(a) (b) (c)

Fig. 3.8: (a), (b), and (c) are the Poisson disks with decreasing minimum distance

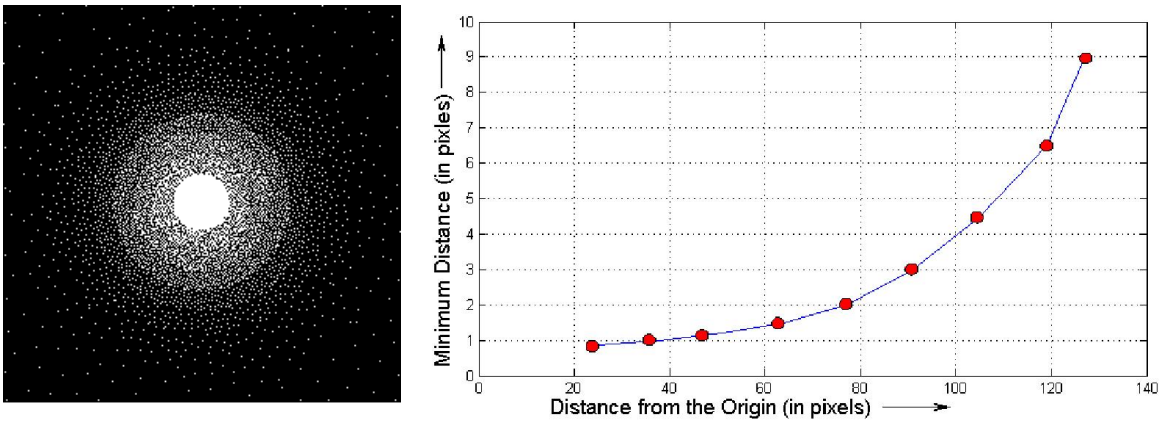

(a) (b)

Fig. 3.9: (a) The proposed variable density Poisson disk undersampling pattern, and (b) the variation of the minimum distance of each Poisson disk with respect to distance from centre

But for efficiently sampling the k-space data we need variable density sampling pattern. Fig. Fig. 3.9 (a) shows a special variable density sampling pattern sampling pattern, namely, the variable density Poisson disk sampling pattern, which contains several Poisson disks. The disk near to the centre region contains relatively smaller minimum distance and accordingly disk in the periphery contain relatively larger minimum distance. The variation of minimum-distance from centre to periphery is approximately exponential type. In the proposed variable density Poisson disk undersampling pattern, N random points are generated in such a way that two neighbouring points are not too close i.e. always maintains a minimum distance (MD) between them. To implement variable density sampling, ensembles of concentric Poisson disks with varying MD are considered. A Poisson disk at the centre would have the smallest MD which may be fixed as follows. The variation of MD from the centre to the periphery is approximately exponential as shown in Fig.3.9 (b).

For comparisons, design of another two variable density sampling patterns are shown in the same way as followed for the variable density Poisson disk sampling pattern, namely, the variable density random sampling pattern and the variable density Gaussian sampling pattern shown in Fig.3.10.

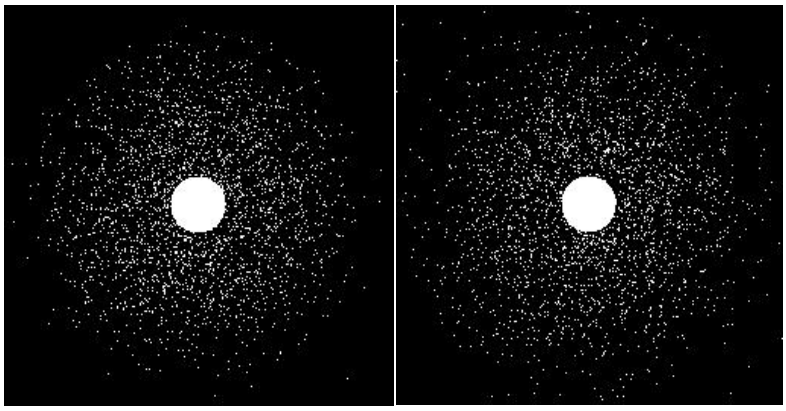

(a) (b)

Fig.3.10: (a) The variable density Gaussian undersampling pattern, and (b) the variable density random undersampling pattern

3.6. Experimental results

Experimental setup:
Numerous experiments have been conducted to show the superiority of the proposed undersampling pattern in CSMRI. All experiments are performed on a PC with 3.4GHz Intel core i7 CPU with 2GB RAM and MATLAB (2012b). We have collected 2D single slice brain MR data from the "MRI of Trinidad & Tobago Limited" (http://mritnt.com/education-centre/common-uses/mri-of-the-brain/).

We have simulated different types of k-space trajectories to evaluate the gradient variation. For practical applications, an undersampling pattern should have small gradient variations in a given k-space trajectory. For comparison of gradient variations, we compute *gradient loads* for different types of undersampling patterns in different k-space trajectories, namely, the Line Trajectory, the Spiral Trajectory, and the Zigzag Trajectory as shown in Fig.3.11 [6].

Computation of gradient load:
The gradient load E is the normalized vector sum of the applied gradients G^x and G^y, in x and y directions, respectively in an MRI data acquisition system. It is defined by:

$$E = \frac{1}{NG_o^2}\sum_{I=1}^{N}[(G_I^x)^2 + (G_I^y)^2]$$

where G_o is the magnitude of gradient step and N is the number of selected samples in k-space [7].

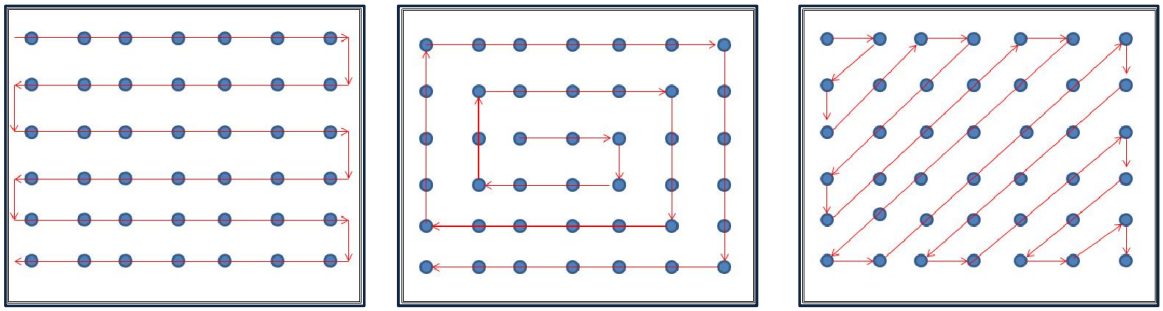

(a) (b) (c)

Fig.3.11: Different k-space Trajectories. (a) The Line trajectory, (b) the Spiral trajectory, and (c) the Zigzag trajectory

For CS reconstruction of the MR image from undersampled data we used the nonlinear conjugate gradient (NCG) algorithm [1]. NCG algorithm minimizes the sum of L_1 and TV-norms with the data fidelity term. We have taken TV and L_1-norm regularization parameters as 0.35 and 0.01, respectively for our simulation. For convergence, we set a common stopping criterion i.e. the relative change of the objective function is less than 10^{-4}. It takes

on average 40 iterations for convergence with the given stopping criterion which is just about 2 minutes for a simulation platform as mentioned above.

We have also evaluated performance of the proposed sampling pattern for CS reconstruction using 20% sampling ratio in terms of mean squared error (MSE), peak signal-to-noise ratio (PSNR) and mean structural similarity index (MSSIM).

Results and discussions:

From the Fig. 3.12 we have observed that the VD Poisson disk under sampling pattern have the least gradient load in all trajectories compared to other undersampling schemes. It is also observed that the proposed undersampling pattern gives almost the same gradient variation in both trajectories, namely, the line trajectory and zigzag trajectory. But in spiral trajectory, it gives slightly higher gradient variation. So, the proposed undersampling pattern is suitable with either line trajectory or zigzag trajectory.

From the plot shown in Fig. 3.13, it is clear that the proposed sampling pattern produce the least MSE for different sampling ratios. Similarly, Fig. 3.14 shows that the proposed sampling pattern gives the best PSNR in different sampling ratios. We also compute MSSIM for measuring structural similarities between two images. It is designed to improve on traditional methods for the measurement of the quality of reconstructed images like PSNR and MSE, which have been proven to be inconsistent with human eye perception. The maximum value of MSSIM is one when both images are same. Fig. 3.15 shows the proposed sampling pattern has the best MSSIM compared to other sampling patterns for different sampling ratios.

Finally, reconstructed MR images using different undersampling scheme are shown in Fig. 3.16. From the results, we observe that the proposed undersampling scheme gives significant improvements in terms of higher contrast and better preservation of edges over other undersampling schemes.

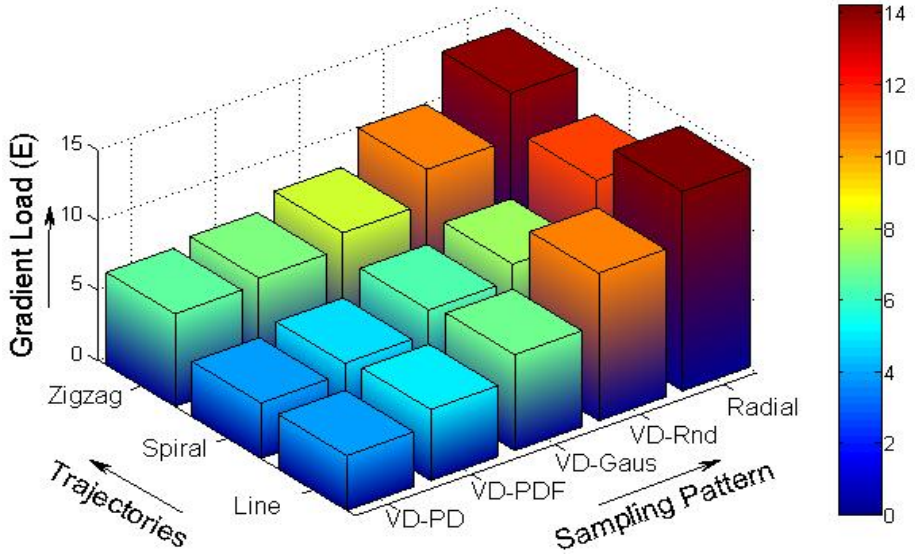

Fig.3.12: Variation of gradient load of various undersampling methods in different trajectories

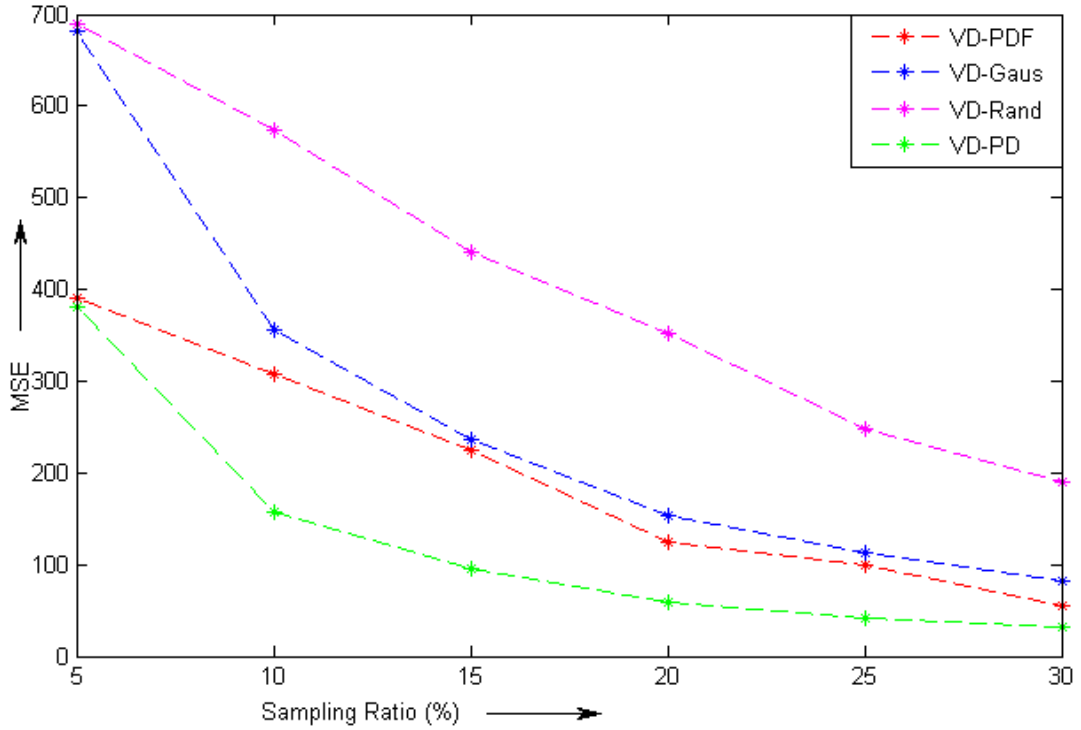

Fig. 3.13: Variation of MSE with increasing sampling ratio for different types of undersampling patterns

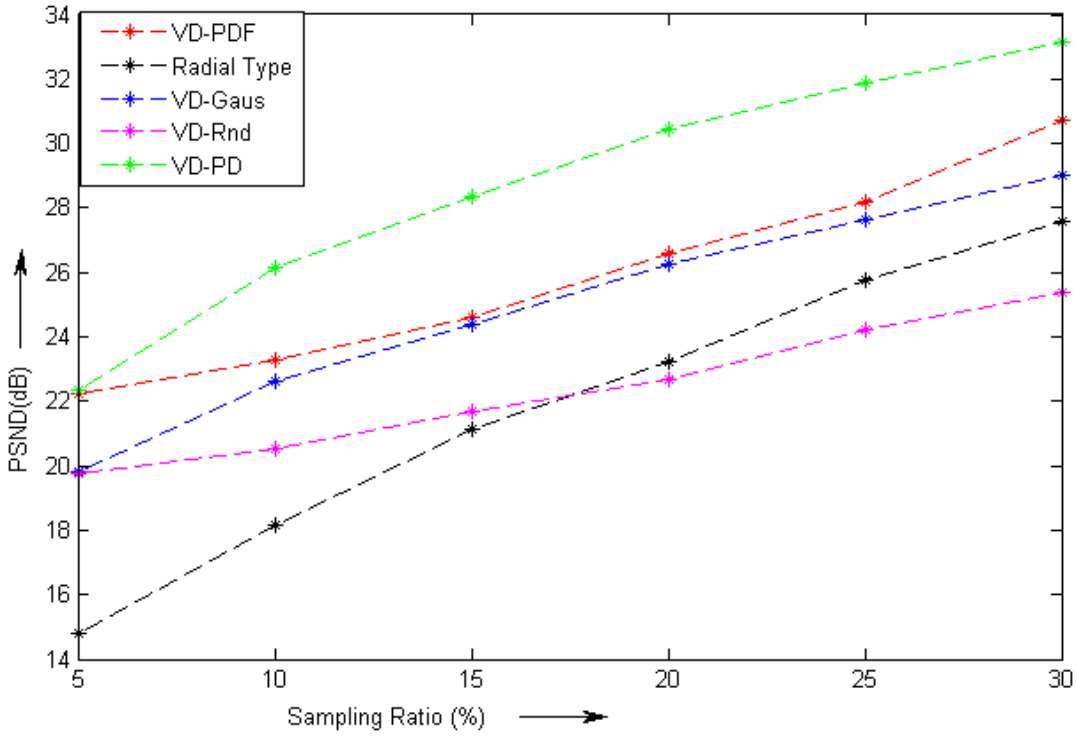

Fig. 3.14: Variation of PSNR (in dB) with increasing sampling ratio for different types of undersampling patterns

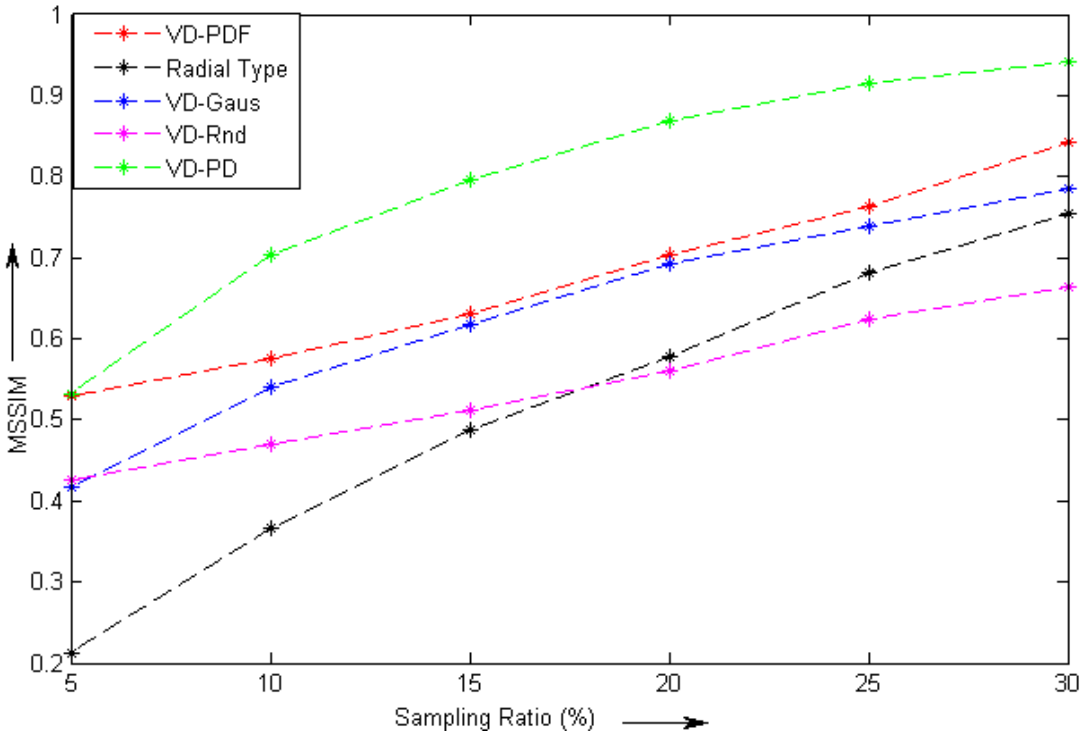

Fig. 3.15: Variation of MSSIM with increasing sampling ratio for different types of undersampling patterns

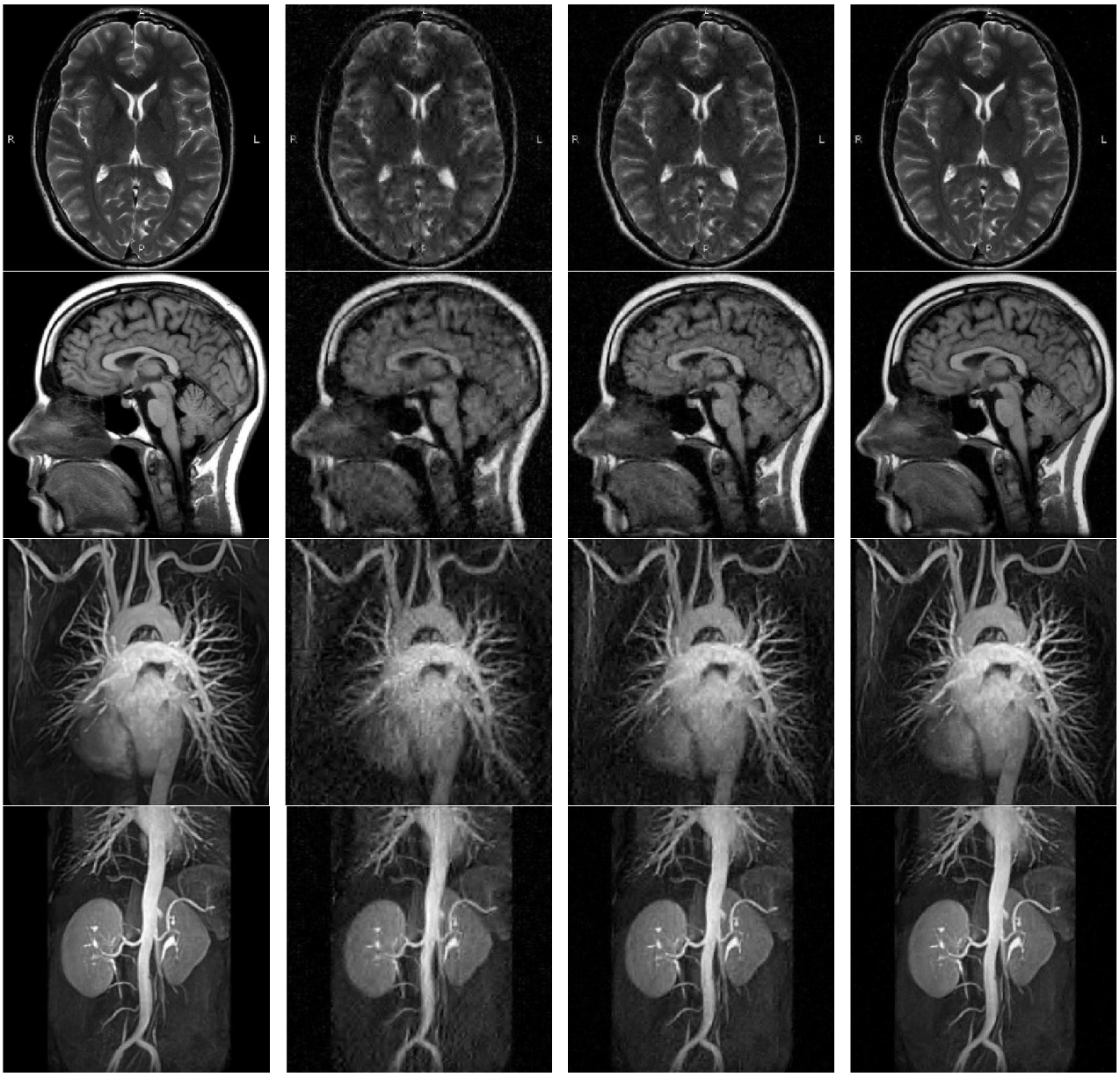

Fig. 3.16: **First column**: Original MR images of axial Brain, sagittal Brain, Chest and Renal arteries. **Columns 2-4**: Reconstructed images for different methods using the radial, the estimated PDF, and the variable density Poisson disk undersampling patterns.

3.7. Conclusions

We propose a variable density random undersampling pattern based on Poisson disk for efficiently acquiring k-space data. Proposed undersampling pattern is not only able to show significant improvements in terms of gradient load, MSE, PSNR and MSSIM but in terms of visual quality of reconstructed images too it has definite advantage over the state-of-the-art.

References:

[1] M. Lustig, D. Donoho, and J. M. Pauly, "Sparse MRI: The application of compressed sensing for rapid MR imaging," *Magnetic Resonance in Medicine*, vol. 58, pp. 1182-1195, 2007.

[2] M. Figueiredo, R. D. Nowak, and S. J. Wright, "Gradient projection for sparse reconstruction: Application to compressed sensing and other inverse problems," *IEEE Journal of Selected Topics in Signal Processing*, vol. 1, no. 4, pp. 586-597, 2007.

[3] E. Candes and M. Wakin, "An introduction to compressive sampling," *IEEE Signal Processing Magazine*, vol. 25, no. 2, pp. 21-30, 2008.

[4] M. Lustig, D. Donoho, J. Santos, and J. Pauly, "Compressed sensing MRI,"*IEEE Signal Processing Magazine,* vol. 25 , no. 2, pp.72-82, 2008.

[5] S. S. Vasanawala, M. J. Murphy, M. T. Alley, P. Lai, K. Keutzer, J. M. Pauly, and M. Lustig, "Practical parallel imaging compressed sensing MRI: Summary of two years of experience in accelerating body MRI of pediatric patients", *in Proc. of the IEEE International Symposium on Biomedical Imaging: From Nano to Macro*, pp. 1039-1043, 2011.

[6] K. S. Nayak and D. G. Nishimura, "Randomized trajectories for reduced aliasing artifact,'' *in Proc. of the scientific meeting and exhibition of ISMRM*, Sydney, Australia, pp.670, 1998.

[7] I. Sersa and S. Macura, "Excitation of Arbitrary Shapes by Gradient Optimized Random Walk in Discrete k-Space," *Magnetic Resonance in Medicine*, vol. 37, pp. 920-931,1997.

Chapter 4

Reconstruction Based on L_1-Norm Minimization

4.1. Introduction

In this chapter, we will present an overview of existing algorithms to reconstruct $\mathbf{x}$ from the measured signal $\mathbf{y} = \mathbf{A}\mathbf{x}$. More specifically, suppose $\mathbf{x}$ is a sparse signal of length n which is undersampled by a measurement matrix $\mathbf{A}$ and $\mathbf{y}$ is the observed data, where $\mathbf{x} \in \mathbb{R}^n$, $\mathbf{A} \in \mathbb{R}^{n \times m}$, $\mathbf{y} \in \mathbb{R}^m$ and $m \ll n$. Based on the knowledge of the measurement matrix $\mathbf{A}$ and measured signal $\mathbf{y}$, we have to recover the sparse signal $\mathbf{x}$. According to linear algebra, this problem can be solved by L_0-norm minimization i.e.

$$\begin{aligned} &\text{minimize} \quad \| \mathbf{x} \|_0 \\ &\text{subject to} \quad \mathbf{y} - \mathbf{A}\mathbf{x} \leq \varepsilon \end{aligned} \tag{4.1}$$

where ε is the error term and $\|.\|_0$ counts the number of non-zero elements.

Problem (4.1) is impractical to solve as it is combinatorial in nature. This problem can be solved by replacing the L_0-norm with the L_1-norm. The modified problem is a convex optimization problem and can be represented as-

$$\begin{aligned} &\text{minimize} \| \mathbf{x} \|_1 \\ &\text{subject to} \quad \mathbf{y} - \mathbf{A}\mathbf{x} \leq \varepsilon \end{aligned} \tag{4.2}$$

where $\| \mathbf{x} \|_1 = |.| + |.| + \ldots$. The solution of this L_1-norm problem gives the exact original signal when $\mathbf{x}$ is sufficiently sparse.

To solve the above L_1-norm minimization, different relevant works on convex optimization are studied for implementation on CSMRI, viz. the Primal-Dual Interior Point Method (PDIPM), the Truncated Newton Interior-Point Method (TNIPM), the Gradient Projection (GP) Method, the Iterative Shrinkage Thresholding Algorithm (ISTA), the Fast Iterative Shrinkage Thresholding Algorithm (FISTA), the Two-Step IST (TWIST), the Sparse Reconstruction by separable Approximation (SpaRSA), the Total Variation (TV) based algorithms, the Projections Over Convex Set (POCS), the Gradient Projection for Sparse Reconstruction (GPSR), the Split Bregman Method, the Alternating Direction Method (ADM), the Split Augmented Lagrangian Shrinkage Algorithm (SALSA), the Total Variation L_1 Compressed Sensing (TVCMRI), the Reconstruction from Partial Fourier data (RecPF) and the Fast Composite Splitting Algorithm (FCSA).

4.2. Primal-Dual Interior Point Method (PDIPM)

The Primal-Dual Interior Point Method is the classical method for the solution to the L_1-minimization problem [9].Consider a squandered convex optimization problems that include both equality and inequality constraints,

$$\begin{aligned} &\text{minimize} && f_o(\mathbf{x}) \\ &\text{subject to} && f_i(\mathbf{x}) \le 0, \quad i = 1, ..., m \\ & && \mathbf{Ax} = \mathbf{y} \end{aligned} \tag{4.3}$$

where, $f_0, ...f_m : \mathbb{R}^n \to \mathbb{R}$ are convex and twice continuously differentiable, and $\mathbf{A} \in \mathbb{R}^{m \times n}$. We assume that the problem is solvable, an optimal $\mathbf{x}^*$ exists and the optimal value of $f_o(\mathbf{x}^*)$ is p^*.

We also assume that there exists a dual optimal $\boldsymbol{\lambda}^*$ and $\mathbf{v}^*$, which together with $\mathbf{x}^*$ satisfy the KKT conditions

$$\mathbf{Ax}^* = \mathbf{y}, \tag{4.4}$$

$$f_i(\mathbf{x}^*) \le 0, \quad i = 1, ..., m; \quad \boldsymbol{\lambda}^* \ge 0 \tag{4.5}$$

$$\nabla f_o(\mathbf{x}^*) + \sum_{i=1}^{m} \boldsymbol{\lambda}_i^* \nabla f_i(\mathbf{x}^*) + \mathbf{A}^T \mathbf{v}^* = 0 \tag{4.6}$$

$$-\boldsymbol{\lambda}_i^* \nabla f_i(\mathbf{x}^*) = 0, \quad i = 1, ..., m \tag{4.7}$$

Interior-point methods solve the problem (4.3) or the KKT conditions (4.4 – 4.7) by applying Newton's method to a sequence of equality constrained problems, or to a sequence of modified versions of the KKT conditions.

The only difference between the KKT conditions (4.4 - 4.7) and the modified KKT conditions (4.8 – 4.10) is that the complementarity condition $-\boldsymbol{\lambda}_i^* \nabla f_i(\mathbf{x}^*) = 0$ is replaced by the condition $-\boldsymbol{\lambda}_i^* \nabla f_i(\mathbf{x}^*) = 1/t$. Then the modified KKT equations are given as-

$$\mathbf{Ax}^* = \mathbf{y}, \tag{4.8}$$

$$\nabla f_o(\mathbf{x}^*) + \sum_{i=1}^{m} \boldsymbol{\lambda}_i^* \nabla f_i(\mathbf{x}^*) + \mathbf{A}^T \mathbf{v}^* = 0 \tag{4.9}$$

$$-\boldsymbol{\lambda}_i^* \nabla f_i(\mathbf{x}^*) = 1/t, \quad i = 1, ..., m \tag{4.10}$$

From the modified KKT conditions, we can write the residual $\mathbf{r}_t(\mathbf{x},\boldsymbol{\lambda},\mathbf{v})=0$, where we can define

$$\mathbf{r}_t(\mathbf{x},\boldsymbol{\lambda},\mathbf{v})=\begin{pmatrix}\nabla f_o(\mathbf{x})+\mathbf{D}f_i(\mathbf{x})^T\boldsymbol{\lambda}+\mathbf{A}^T\mathbf{v}\\ -diag(\boldsymbol{\lambda})f(\mathbf{x})-\dfrac{1}{t}\\ \mathbf{A}\mathbf{x}-\mathbf{y}\end{pmatrix} \tag{4.11}$$

where, $t>0$ and

$$f(\mathbf{x})=\begin{pmatrix}f_1(\mathbf{x})\\ \vdots\\ \vdots\\ f_m(\mathbf{x})\end{pmatrix},\quad \mathbf{D}f(\mathbf{x})=\begin{pmatrix}\nabla f_1(\mathbf{x})^T\\ \vdots\\ \vdots\\ \nabla f_m(\mathbf{x})^T\end{pmatrix}$$

If $\mathbf{x},\boldsymbol{\lambda},\mathbf{v}$ satisfy $\mathbf{r}_t(\mathbf{x},\boldsymbol{\lambda},\mathbf{v})=0$, then $\mathbf{x}=\mathbf{x}^*(t)$, $\boldsymbol{\lambda}=\boldsymbol{\lambda}^*(t)$ and $\mathbf{v}=\mathbf{v}^*(t)$. Here $\mathbf{x}$ is primal feasible, and $\boldsymbol{\lambda},\mathbf{v}$ are dual feasible, with duality gap m/t. The first block component of $\mathbf{r}_t$,

$$\mathbf{r}_{dual}=\nabla f_o(\mathbf{x})+\mathbf{D}f_i(\mathbf{x})^T\boldsymbol{\lambda}+\mathbf{A}^T\mathbf{v} \tag{4.12}$$

is called the dual residual, and the middle block

$$\mathbf{r}_{cent}=-diag(\boldsymbol{\lambda})f(\mathbf{x})-\frac{1}{t} \tag{4.13}$$

is the centrality residual. The last block component $\mathbf{r}_{pri}=\mathbf{A}\mathbf{x}-\mathbf{y}$ is called the primal residual.

By Newton method we can solve the nonlinear equation $\mathbf{r}_t(\mathbf{x},\boldsymbol{\lambda},\mathbf{v})=0$. The current point and Newton step can be denote as

$$\mathbf{y}=(\mathbf{x},\boldsymbol{\lambda},\mathbf{v}),\quad \Delta\mathbf{y}=(\Delta\mathbf{x},\Delta\boldsymbol{\lambda},\Delta\mathbf{v}), \tag{4.14}$$

respectively. The Newton step is characterized by the linear equations

$$\mathbf{r}_t(\mathbf{y}+\Delta\mathbf{y}) \approx \mathbf{r}_t(\mathbf{y}) + \mathbf{D}\mathbf{r}_t(\mathbf{y})\Delta\mathbf{y} = 0 \tag{4.15}$$

i.e., $\Delta\mathbf{y} = -\mathbf{D}\mathbf{r}_t(\mathbf{y})^{-1}\mathbf{r}_t(\mathbf{y})$. In terms of $\mathbf{x}, \boldsymbol{\lambda}, \mathbf{v}$ we can write-

$$\begin{pmatrix} \nabla^2 f_o(\mathbf{x}) + \sum_{i=1}^{m} \boldsymbol{\lambda}_i \nabla^2 f_i(\mathbf{x}) & \mathbf{D}f_i(\mathbf{x})^T & \mathbf{A}^T \\ -diag(\boldsymbol{\lambda}) f(\mathbf{x}) & -diag(f(\mathbf{x})) & 0 \\ \mathbf{A} & 0 & 0 \end{pmatrix} \begin{pmatrix} \Delta\mathbf{x} \\ \Delta\boldsymbol{\lambda} \\ \Delta\mathbf{v} \end{pmatrix} = \begin{pmatrix} \mathbf{r}_{dual} \\ \mathbf{r}_{cent} \\ \mathbf{r}_{pri} \end{pmatrix} \tag{4.16}$$

From the solution of (4.16) we get the primal-dual search $\Delta\mathbf{y}_{pd} = (\Delta\mathbf{x}_{pd}, \Delta\boldsymbol{\lambda}_{pd}, \Delta\mathbf{v}_{pd})$.

4.3. Truncated Newton Interior-Point Method (TNIPM)

Using a Lagrangian formulation, the problem (4.2) can be rewritten as an unconstrained optimization problem:

$$\mathbf{x}^* = \arg\min_{\mathbf{x}} F(\mathbf{x}) = \arg\min_{\mathbf{x}} \frac{1}{2} \| \mathbf{A}\mathbf{x} - \mathbf{y} \|_2^2 + \lambda \| \mathbf{x} \|_1 \tag{4.17}$$

where λ is the Lagrangian multiplier [4].

Now the problem (4.17) can be rewritten as a quadratic program but with inequality constraints:

$$\begin{aligned} &\min \frac{1}{2} \| \mathbf{A}\mathbf{x} - \mathbf{y} \|_2^2 + \lambda \sum_{i=1}^{n} u_i \\ &\text{subject to } -u_i \le x_i \le u_i, \quad i = 1, ..., n \end{aligned} \tag{4.18}$$

Then the logarithmic barrier function for the constraints $-u_i \le x_i \le u_i$ is constructed as follows:

$$\varphi(\mathbf{x}, \mathbf{u}) = -\sum_i \log(u_i + x_i) - \sum_i \log(u_i - x_i) \tag{4.19}$$

Over the domain of $(\mathbf{x}, \mathbf{u})$, the central path consists of the unique minimiser $\left(\mathbf{x}^*(t), \mathbf{u}^*(t)\right)$ of the convex function:

$$F_t(\mathbf{x}, \mathbf{u}) = t\left(\frac{1}{2} \| \mathbf{A}\mathbf{x} - \mathbf{y} \|_2^2 + \lambda \sum_{i=1}^{n} u_i\right) + \varphi(\mathbf{x}, \mathbf{u}) \tag{4.20}$$

where the parameter $t \in [0, \infty)$.

For (4.20) the optimal search direction using Newton's method is computed by-

$$\mathbf{H}\begin{pmatrix} \Delta\mathbf{x} \\ \Delta\mathbf{u} \end{pmatrix} = -\mathbf{g} \tag{4.21}$$

where $\mathbf{H} = \nabla^2 F_t(\mathbf{x}, \mathbf{u})$ is the Hessian and $\mathbf{g} = \nabla F_t(\mathbf{x}, \mathbf{u})$ is the gradient at the current iterate $(\mathbf{x}, \mathbf{u})$.

For a large scale, solving the Newton system (4.21) exactly is not computationally efficient. We need to find a search direction which gives a good trade-off between computational effort and the convergence rate it provides. In this method the search direction is computed as an approximate solution to the Newton system (4.21), using Preconditioned Conjugate Gradient (PCG) method.

Search Direction via PCGs:
The Hessian can be representations as-

$$\begin{aligned} \mathrm{H} &= t\nabla^2 \,||\, \mathbf{Ax} - \mathbf{y} \,||_2^2 + \nabla^2 \varphi(\mathbf{x}, \mathbf{u}) \\ &= \begin{pmatrix} 2t\mathbf{A}^T\mathbf{A} + \mathbf{D}_1 & \mathbf{D}_2 \\ \mathbf{D}_2 & \mathbf{D}_1 \end{pmatrix} \end{aligned} \tag{4.22}$$

where

$$\mathbf{D}_1 = diag\left(\frac{2\left(u_1^2 + x_1^2\right)^2}{\left(u_1^2 - x_1^2\right)^2}, \ldots\ldots\ldots, \frac{2\left(u_n^2 + x_n^2\right)^2}{\left(u_n^2 - x_n^2\right)^2} \right) \in \mathbb{R}^n$$

$$\mathbf{D}_2 = diag\left(\frac{-4u_1x_1}{\left(u_1^2 - x_1^2\right)^2}, \ldots\ldots\ldots, \frac{-4u_nx_n}{\left(u_n^2 - x_n^2\right)^2} \right) \in \mathbb{R}^n$$

The Hessian $\mathbf{H}$ is symmetric and positive definite. The gradient can be representations as-

$$\mathbf{g} = \begin{pmatrix} \mathbf{g}_1 \\ \mathbf{g}_2 \end{pmatrix} \in \mathbb{R}^n \tag{4.23}$$

where

$$\mathbf{g}_1 = \nabla_{\mathbf{x}} \varphi(\mathbf{x},\mathbf{u}) = 2t\mathbf{A}^T(\mathbf{A}\mathbf{x}-\mathbf{y}) + \begin{pmatrix} \frac{2x_1}{\left(u_1^2 - x_1^2\right)} \\ \vdots \\ \frac{2x_n}{\left(u_n^2 - x_n^2\right)} \end{pmatrix} \in \mathbb{R}^n$$

$$\mathbf{g}_2 = \nabla_u \varphi(\mathbf{x},\mathbf{u}) = t\lambda\mathbf{I} + \begin{pmatrix} \frac{2u_1}{\left(u_1^2 - x_1^2\right)} \\ \vdots \\ \frac{2u_n}{\left(u_n^2 - x_n^2\right)} \end{pmatrix} \in \mathbb{R}^n$$

Here we calculate the search direction approximately, applying the PCG algorithm. The PCG algorithm uses a pre-conditioner $\mathbf{P}$, which approximate the Hessian of $t\|\mathbf{y}-\mathbf{A}\mathbf{x}\|_2^2$ with diagonal entries. The pre-conditioner $\mathbf{P}$ is written as-

$$\mathbf{P} = \begin{pmatrix} 2t\,diag\left(\mathbf{A}^T\mathbf{A}\right) & 0 \\ 0 & 0 \end{pmatrix} + \begin{pmatrix} \mathbf{D}_1 & \mathbf{D}_2 \\ \mathbf{D}_2 & \mathbf{D}_1 \end{pmatrix} \tag{4.24}$$

The cost of computing the diagonal entries of $\mathbf{A}^T\mathbf{A}$ is still expensive; we can approximate the diagonal matrix $diag\left(\mathbf{A}^T\mathbf{A}\right)$ with a scaled identity matrix $\tau\mathbf{I}$ to obtain the pre-conditioner

$$\mathbf{P} = \begin{pmatrix} 2\tau t\mathbf{I} & 0 \\ 0 & 0 \end{pmatrix} + \begin{pmatrix} \mathbf{D}_1 & \mathbf{D}_2 \\ \mathbf{D}_2 & \mathbf{D}_1 \end{pmatrix} \tag{4.25}$$

where τ is a positive constant. This pre-conditioner performs well especially when the diagonal elements of $\mathbf{A}^T\mathbf{A}$ show relatively small variations.

4.4. Nonlinear Conjugate Gradient (NCG)

The nonlinear conjugate gradient method (NCG) is also known as the conjugate gradient (CG) method in nonlinear optimization [1, 11]. For a quadratic function:

$$f(\mathbf{x}) = \|\mathbf{A}\mathbf{x}-\mathbf{y}\|_2^2 \tag{4.26}$$

The minimum of f is obtained when the gradient is 0 i.e.

$$\nabla_{\mathbf{x}} f = 2\mathbf{A}^T(\mathbf{A}\mathbf{x}-\mathbf{y}) = 0 \tag{4.27}$$

The nonlinear conjugate gradient method is generally used to find the local minimum of a nonlinear function using its gradient $\nabla_{\mathbf{x}} f$ alone. It works when the function is approximately quadratic near the minimum, which is the case when the function is twice differentiable at the minimum.

Given a function $f(\mathbf{x})$ of n variables to minimize, its gradient $\nabla_{\mathbf{x}} f$ indicates the direction of maximum increase. One simply starts in the opposite (steepest descent) direction:

$$\Delta \mathbf{x}_0 = -\nabla_{\mathbf{x}} f(\mathbf{x}_0) \tag{4.28}$$

with an adjustable step length $\boldsymbol{\alpha}$ and performs a line search in this direction until it reaches the minimum of f :

$$\begin{aligned} \alpha_0 &= \arg\min_{\alpha} f(\mathbf{x}_0 + \boldsymbol{\alpha} \Delta \mathbf{x}_0) \\ \mathbf{x}_1 &= \mathbf{x}_0 + \alpha_0 \Delta \mathbf{x}_0 \end{aligned} \tag{4.29}$$

After this first iteration in the steepest direction $\Delta \mathbf{x}_0$ the following steps constitute one iteration of moving along a subsequent conjugate direction s_n, where $s_0 = \Delta \mathbf{x}_0$.

4.5. Iterative Shrinkage-Thresholding (IST)

Iterative Shrinkage-Thresholding (IST) method mainly involves operations such as vector-addition and matrix-vector multiplications [3, 5].

The problem (4.2) can be rewritten as-

$$\min_x F(\mathbf{x}) = f(\mathbf{x}) + \lambda g(\mathbf{x}) \tag{4.30}$$

where $f(\mathbf{x}) = \frac{1}{2} \| \mathbf{y} - \mathbf{A}\mathbf{x} \|_2^2$ and $g(\mathbf{x}) = \| \mathbf{x} \|_1$.

The update rule to minimize (4.30) is computed using a second-order approximation of f :

$$\mathbf{x}^{(k+1)} = \arg\min_{\mathbf{x}} \{ f(\mathbf{x}^k) + (\mathbf{x} - \mathbf{x}^k)^T \nabla f(\mathbf{x}^k) + \frac{1}{2} \| \mathbf{x} - \mathbf{x}^k \|_2^2 . \nabla^2 f(\mathbf{x}^k) + \lambda g(\mathbf{x}) \} \tag{4.31}$$

$$\mathbf{x}^{(k+1)} \approx \arg\min_{\mathbf{x}} \{ (\mathbf{x} - \mathbf{x}^k)^T \nabla f(\mathbf{x}^k) + \frac{\alpha^k}{2} \| \mathbf{x} - \mathbf{x}^k \|_2^2 . \nabla^2 f(\mathbf{x}^k) + \lambda g(\mathbf{x}) \} \tag{4.32}$$

$$\mathbf{x}^{(k+1)} \approx \arg\min_{\mathbf{x}} \{ \frac{1}{2} \| \mathbf{x} - \mathbf{u}^k \|_2^2 + \frac{\lambda}{\alpha^k} g(\mathbf{x}) \} \tag{4.33}$$

$$\mathbf{x}^{(k+1)} \approx G_{\alpha}(\mathbf{x}^k) \tag{4.34}$$

where $\mathbf{u}^k = \mathbf{x}^k - \frac{1}{\alpha^k} \nabla f(\mathbf{x}^k)$

In (4.33), the Hessian $\nabla^2 f(\mathbf{x}^k)$ is approximated by a diagonal matrix $\alpha^k \mathbf{I}$. Then the closed-form solution of (4.34) is given as-

$$\mathbf{x}^{(k+1)} = \arg\min_{\mathbf{x}} \left\{ \frac{(\mathbf{x}_i - \mathbf{u}_i^k)^2}{2} + \frac{\lambda \mid \mathbf{x}_i \mid}{\alpha^k} \right\} \tag{4.35}$$

$$\mathbf{x}^{(k+1)} = soft\left(\mathbf{u}_i^k, \frac{\lambda}{\alpha^k} \right) \tag{4.36}$$

where,

$$\begin{aligned} soft(u, a) &= sign(u) \max\{|u| - a, 0\} \\ &= \begin{cases} sign(u)(|u| - a) & \text{if } |u| > a \\ 0 & \text{otherwise} \end{cases} \end{aligned}$$

is the soft-thresholding or shrinkage function.

The parameter α approximate the Hassian Matrix $\nabla^2 f(x^k)$ as-

$$\alpha^{(k+1)} = \frac{(\mathbf{x}^k - \mathbf{x}^{k-1})^T (\nabla f(\mathbf{x}^k) - \nabla f(\mathbf{x}^{k-1})}{(\mathbf{x}^k - \mathbf{x}^{k-1})^T (\mathbf{x}^k - \mathbf{x}^{k-1})} \tag{4.37}$$

This is known as the Barzilai-Borwein equation.

4.6. Two-stepIterative Shrinkage-Thresholding (TwIST)

Algorithms in this class have a two-step IST (TwIST) structure, i.e., each iterate depends on the two previous iterates, rather than only on the previous one [10].

The solution of the IST algorithm can be rewrite as-

$$\mathbf{x}_{t+1} = (1 - \beta)\mathbf{x}_t + \beta \Psi_\lambda \left(\mathbf{x}_t + \mathbf{A}^T \left(\mathbf{A}\mathbf{x}_t - \mathbf{y} \right) \right) \tag{4.38}$$

where $\beta > 0$ and Ψ_λ is a Thresholding operator. In the original IST algorithm, $\beta = 1$.

Each iteration of the IST algorithm only involves some addition, matrix-vector product by $\mathbf{A}$ and $\mathbf{A}^T$, and the application of the Thresholding operation.

Consider the linear system $\mathbf{A}\mathbf{x} = \mathbf{y}$, with $\mathbf{A}$ positive definite; define a so-called splitting of $\mathbf{A}$ as $\mathbf{A} = \mathbf{C} - \mathbf{R}$, such that $\mathbf{C}$ is positive definite and easy to invert (e.g. a diagonal matrix). *A* stationary two-step iterative method for solving $\mathbf{A}\mathbf{x} = \mathbf{y}$, is defined as-

$$\mathbf{x}_1 = \mathbf{x}_0 + \beta_0 \mathbf{C}^{-1}\left(\mathbf{A}\mathbf{x}_0 - \mathbf{y}\right) \tag{4.39}$$

$$\mathbf{x}_{t+1} = (1-\alpha)\mathbf{x}_{t-1} + \alpha\mathbf{x}_t + \beta\mathbf{C}^{-1}\left(\mathbf{A}\mathbf{x}_0 - \mathbf{y}\right) \tag{4.40}$$

for $t \geq 1$,where $\mathbf{x}_0$ is the initial vector and α, β, β_0 are the parameters of the algorithm . The designation "two-step" stems from the fact that $\mathbf{x}_{t+1}$ depends on both $\mathbf{x}_t$ and $\mathbf{x}_{t-1}$, rather than only on $\mathbf{x}_t$.

From recent studies on CSMRI, it is seen that the TV-L1-L2 model for MR image reconstruction from random undersampled data gives better results [5, 6, 7, 2, 8]. The model is defined as follows:

$$\mathbf{x}^* = \arg\min_{\mathbf{x}} \left\{ \tfrac{1}{2}\left\|\mathbf{F}_u\mathbf{x} - \mathbf{y}\right\|_2^2 + \lambda_1 \left\|\mathbf{\Psi}\mathbf{x}\right\|_1 + \lambda_2 \left\|\mathbf{x}\right\|_{TV} \right\} \tag{4.41}$$

where $\mathbf{x}$ is the MR image, $\mathbf{y}$ is the measured Fourier data and $\mathbf{F}_u$ is the undersampling Fourier operator. Assume that $\mathbf{x}$ has a sparse representation in the wavelet domain ($\mathbf{\Psi}$). Some of the well known TV-L1-L2 model based CS reconstruction algorithms for MR image reconstruction are-

- Total Variation L1 Compressed Sensing (TVCMRI), 2008.
- Reconstruction from Partial Fourier data (RecPF), 2010.
- Fast Composite Splitting Algorithm (FCSA), 2011.

4.7. Proposed High Throughput Reconstruction Technique for CS based MRI

We have developed a novel high throughput MR image reconstruction algorithm based on the TV-L1-L2 model without compromising the quality. The experimental results show that the proposed method is quite efficient compared to the state-of-the-art MR image reconstruction techniques in terms of the CPU time and the quality of the reconstructed MR images. The average CPU time required for the proposed method is approximately 2-3 seconds per image for 20% sampling ratio when implemented in a PC equipped with Intel i7 processor with 2 GB RAM.

Consider $\mathbf{x}$ is an MR image of size $(\sqrt{N} \times \sqrt{N})$ ordered lexicographically into a column vector of dimension $(N \times 1)$. $\mathbf{F}_\mathrm{u}$ is a partial Fourier operator and $\mathbf{y}$ is the measured undersampled k-space data of size $(M \times 1)$ such that as $\mathbf{y} = \mathbf{F}_u\mathbf{x}$, where $M << N$. Now the CSMRI problem is to reconstruct the MR image $\mathbf{x}$ from the measured data $\mathbf{y}$ and sensing matrix $\mathbf{F}_\mathrm{u}$. We assume that $\mathbf{x}$ has a sparse representation in some transform domain ($\mathbf{\Psi}$). Now invoking the TV-L1-L2 model as defined above, we get

$$\mathbf{x}^* = \arg\min_{\mathbf{x}} \left\{ \frac{1}{2} \| \mathbf{F}_u\mathbf{x} - \mathbf{y} \|_2^2 + \lambda_1 \| \mathbf{\Psi}\mathbf{x} \|_1 + \lambda_2 \| \mathbf{x} \|_{TV} \right\} \tag{4.42}$$

where λ_1 and λ_2 are two positive parameters and $\mathbf{\Psi}$ is the wavelet transform matrix. The total variation or TV- norm may be defined as

$$\| \mathbf{x} \|_{\mathrm{TV}} = \sum_{ij} \left(\left(\mathbf{D}_x \, x_{ij} \right)^2 + \left(\mathbf{D}_y \, x_{ij} \right)^2 \right), \tag{4.43}$$

where $\mathbf{D}_x$ and $\mathbf{D}_y$ denote the finite difference operators on the x and y -axis respectively. The terms $\| \mathbf{F}_u \mathbf{x} - \mathbf{y} \|_2^2$ and $\| \mathbf{\Psi x} \|_1$ denote the L_2-norm of error and the L_1-norm of a sparse vector, respectively. If we consider only first and second terms then it is a general L_1-minimization problem. But, here the TV-term is added to preserve edges in the CS reconstructed image. However, the addition of this non-smooth TV-term makes this problem very difficult to solve.

To solve this problem we first decompose the above problem into two subproblems- one is the total variation regularization and other is the L_1-norm regularization. The target solution is obtained by the linear combination of the two subproblem solutions. We solve these two subproblems independently in each iteration by using the augmented Lagrangian multiplier method (ALM). In order to solve the TV subproblem, it is first converted into its dual form followed by the ALM steps. The solutions of both the subproblems are then linearly combined to get the final solution.

The algorithmic steps of the proposed algorithm is summarized in **Algorithm 1**, where λ_1 and λ_2 are two regularization parameters and $\mathbf{\Psi}$ is the sparse representation basis set (i.e. wavelets). The $\mathbf{u}_1$ is the solution of the L_1- regularized sub problem and the $\mathbf{u}_2$ gives the solution of the TV regularized sub problem. After combining solutions of both the sub problems, the overall algorithm is accelerated using the steps of the ALM. Finally, $\mathbf{x}^*$ gives the reconstructed MR image.

Algorithm 1: Proposed Algorithm

Input : $\mathbf{y}, \mathbf{F_u}, \tau, \rho, \lambda_1, \lambda_2$ and $\mathbf{\Psi}$

1. **While** not converged $(k = 1, 2, ..)$
2. $t_1 \leftarrow 1, \mathbf{z}_l \leftarrow \mathbf{x}_k, \mathbf{u}_l \leftarrow \mathbf{x}_k$
3. **While** not converged $(l = 1, 2, ..)$
4. $\mathbf{g} \leftarrow \mathbf{z}_l - \frac{1}{\tau}\mathbf{F}_u^T\left(\mathbf{F}_u\mathbf{z}_l - \mathbf{y} - \frac{1}{\lambda_k}\mathbf{p}_k\right)$
5. $\mathbf{u}_1 \leftarrow \text{prox}_\rho\left(2\lambda_1 \| \mathbf{\Psi x} \|_1\right)(\mathbf{g})$
6. $\mathbf{u}_2 \leftarrow \text{prox}_\rho\left(2\lambda_2 \| \mathbf{x} \|_{TV}\right)(\mathbf{g})$
7. $\mathbf{u}_{l+1} \leftarrow \frac{1}{2}\left(\mathbf{u}_1 + \mathbf{u}_2\right)$
8. $\mathbf{u}_{l+1} \leftarrow \text{project}(\mathbf{u}_{l+1}, [k_1, k_2])$
9. $t_{l+1} \leftarrow \frac{1}{2}\left(1 + \sqrt{1 + 4t_l^2}\right)$
10. $\mathbf{z}_{l+1} \leftarrow \mathbf{u}_{l+1} + \frac{t_l - 1}{t_{l+1}}\left(\mathbf{u}_{l+1} - \mathbf{u}_l\right)$
10. end **While**
11. $\mathbf{x}_{k+1} \leftarrow \mathbf{u}_{l+1}$
12. $\mathbf{p}_{k+1} \leftarrow \mathbf{p}_k + \mu_k(\mathbf{y} - \mathbf{F_u}\mathbf{x}_{k+1})$
13. $\mu_{k+1} \leftarrow \rho.\mu_k$
14. end **While**

Output : $\mathbf{x}^* \leftarrow \mathbf{x}_{k+1}$

4.8. Simulation results

4.8.1. Prior Art

We have implemented L1-normminimization based CS-MRI reconstruction algorithms like-

- Primal-Dual Interior Point Methods (PDIPM), 1997.
- Iterative Shrinkage Thresholding Methods (IST), 2004.
- Two-Step IST (TWIST), 2007.
- Truncated Newton Interior-Point Method (TNIPM), 2007.
- Gradient Projection for Sparse Reconstruction (GPSR), 2008.
- Proximal Gradient Methods (FISTA), 2009.
- Sparse Reconstruction by separable Approximation (SpaRSA), 2009.
- Split Augmented Lagrangian Shrinkage Algorithm (SALSA), 2010

The PDIPM solves the L1-minimization problem in a classical way. Experimental result shows the PDIM requires CPU time in order of thousand which is much higher than other algorithms. But in the TNIPM method a pre-conditioner is used to reduce the number of operations. Required CPU time for different L1-norm minimization problem are shown in Fig.4.1. From the figure, we say that the required CPU time for the TNIPM and the IST are required higher CPU time compare to other methods. On the other hand, in case of SALSA algorithm the required least CPU time compare to other methods.

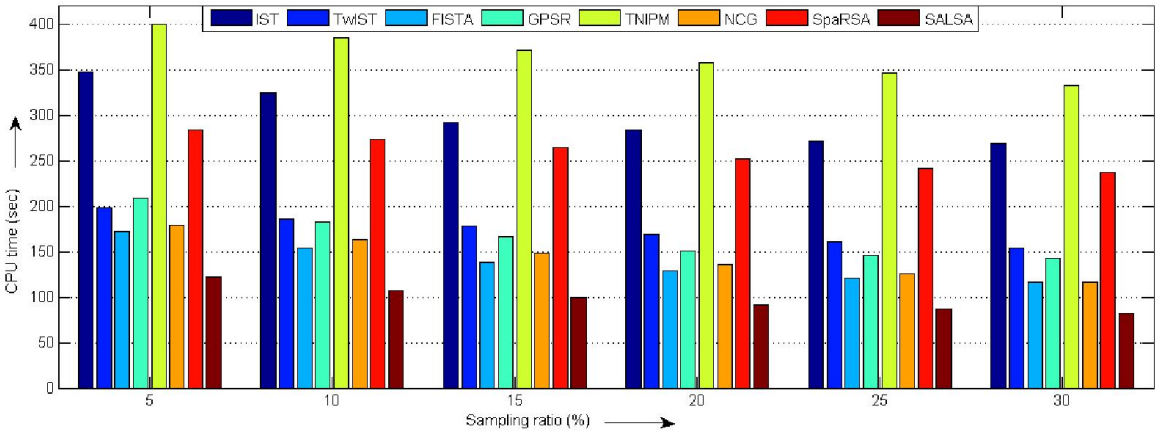

Fig. 4.1: Comparison of CPU-Time requirements of different CS-MRI reconstruction algorithms with changing sampling ratio

4.8.2. The proposed method

Experimental setup:

Numerous experiments have been conducted to show the superiority of the proposed algorithm on CSMRI. All experiments are on a PC with 3.4GHz Intel core i7 CPU with 2GB RAM and MATLAB (2012b).

We have collected MRI data set from GNRC Hospital, Guwahati, India (http://www.gnrchospitals.com). We have collected 2D single slice Sag T2 TOP L. S. Spine MRI data and 3-pl $T2^*$ FGRE orbit MRI data. The L. S. Spine MRI data were acquired from a GE 1.5T signa HDxt scanner with following parameters: TR/TE: 3520/111.044 ms, slice thickness: 4 mm, spacing between scans: 5 mm, sampling (%): 100, and Flip angle: 90deg. The orbit MRI data were acquired from a GE 1.5T signa HDxt scanner with following parameters: TR/TE: 5.536/1.692 ms, slice thickness: 5 mm, spacing between scans: 4 mm, sampling (%): 100, and Flip angle: 30deg.

We have also collected 2D single slice brain MR data from the "MRI of Trinidad &Tobago Limited" (http://mritnt.com/education-centre/common-uses/mri-of-the-brain/).

For CS reconstruction of the MR image using different algorithms we have taken $\lambda_1 = 0.01$ and $\lambda_2 = 0.35$. We have set a common stopping criterion i.e. the relative change of the objective function is less than or equal to 10^{-4} for the convergence. For our simulations on

CS reconstructions the sampling pattern is the estimated PDF undersampling pattern in [1] at 20% sampling ratio.

To evaluate the performance of the proposed algorithm we compare CS reconstruction results with those of the state-of-the-art. We compute the CPU time, peak signal-to-noise ratio (PSNR) and mean structural similarity index (MSSIM). MSSIM measures the image quality based on structural similarity whose value ranges between 0 and 1. Two very similar images will have MSSIM value very close to 1.

Results and discussions:

PSNRs of the CS reconstructed brain MR images with different techniques are shown in Fig. 4.2. It is clearly observed the proposed method gives higher PSNR values for different sampling ratios compared to other methods. Similarly, Fig. 4.3 shows that the proposed technique has the best MSSIM value compared to other reconstruction methods for different sampling ratios. This shows that the proposed method is able to preserve various details present in the image better than other methods.

CPU time is used to investigate the time complexity of the proposed method compared to other methods. It indicates how quickly the particular algorithm reaches the convergence. Fig.4.4 shows that the NCG method requires the highest amount of computational time to perform its complex operations among all other CSMRI reconstruction methods. On the other hand, the proposed method requires the least computational time in any sampling ratio because in each iteration it moves a substantial amount towards the convergence due to the acceleration scheme of the ALM.

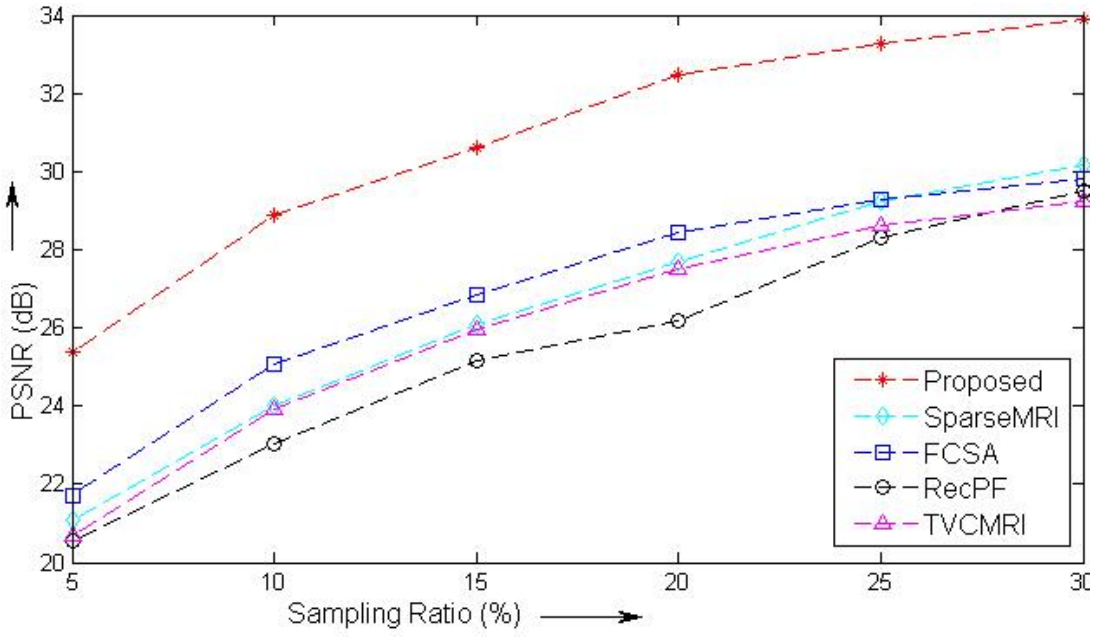

Fig.4.2: Variation of PSNR (in dB) with increasing sampling ratios for various algorithms

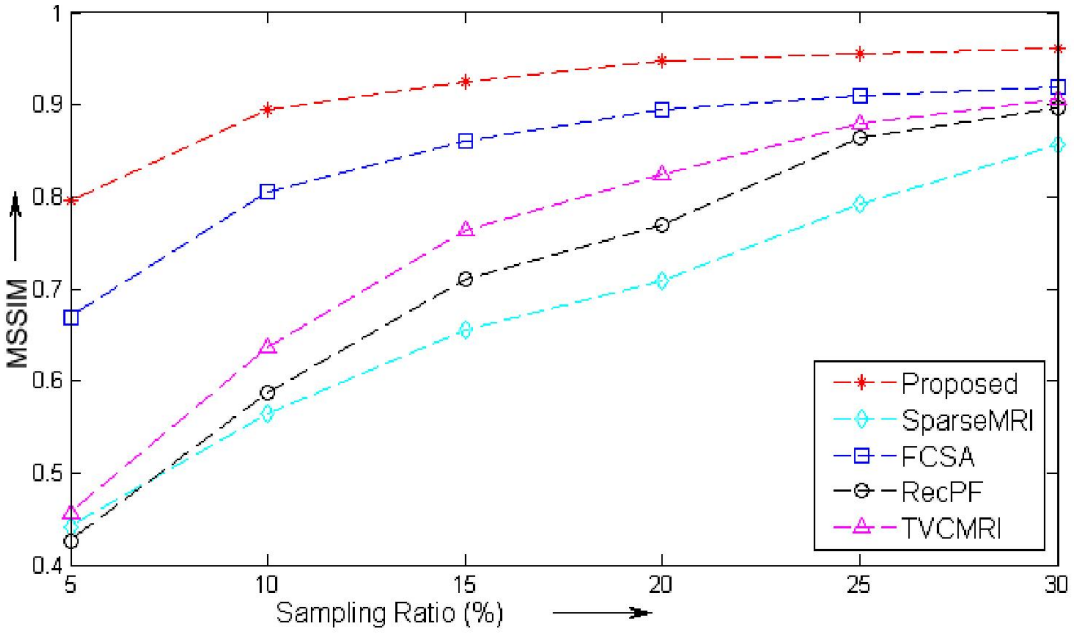

Fig.4.3: Variation of MSSIM values with increasing sampling ratios for various algorithms

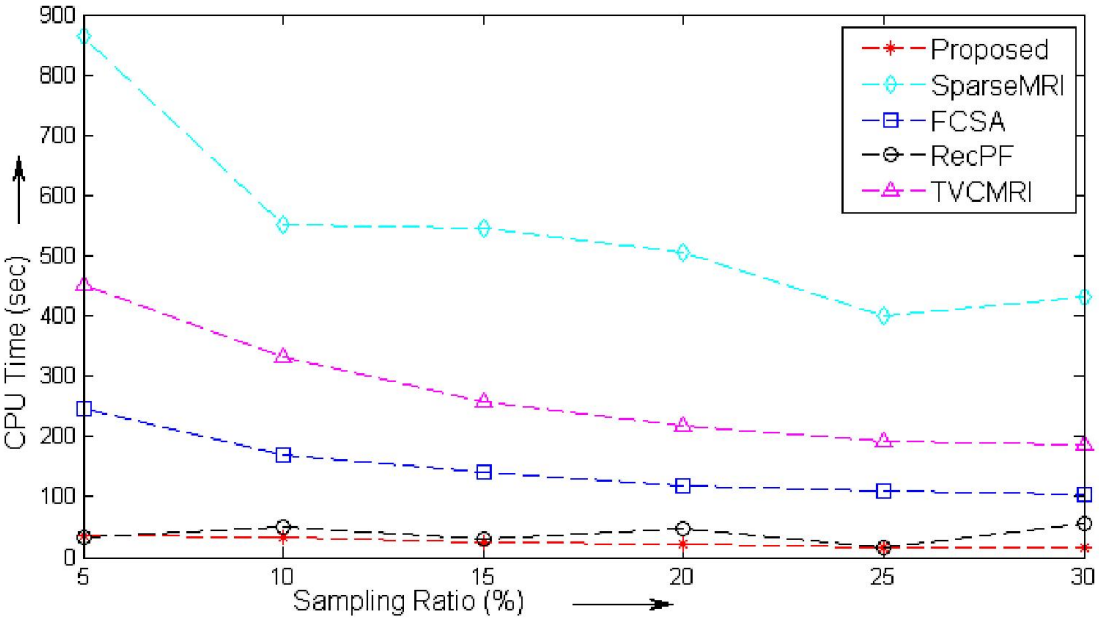

Fig. 4.4: Variation of CPU-time with increasing sampling ratios for various algorithms

The corresponding CS reconstructed MR images of brain and L.S. spine using different algorithms are shown in Figs. 4.5 and 4.6, respectively. From reconstructed images, it is seen that the proposed technique gives better reconstruction in terms of higher contrast and better preservation of edges. From Fig. 4.5, it is clearly observed that the proposed method gives almost negligible visual aliasing artifacts compared those in the RecPF, the TVCMRI, and the FCSA methods.

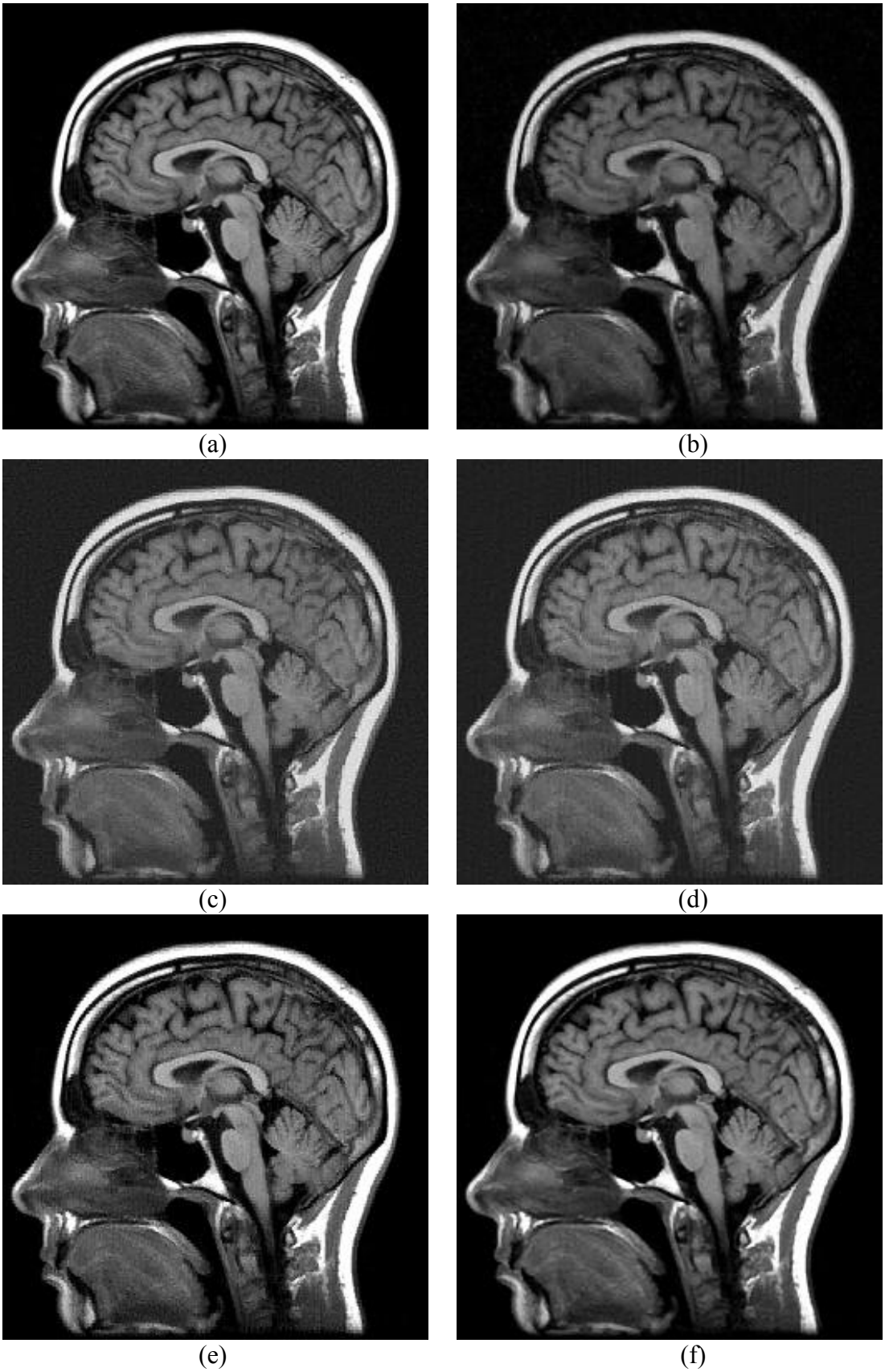

Fig. 4.5: (a) Original brain MR image and (b) to (f) are the reconstructed images by the NCG, the RecPF, the TVCMRI, the FCSA and the proposed algorithm, respectively with 20% sampling ratio

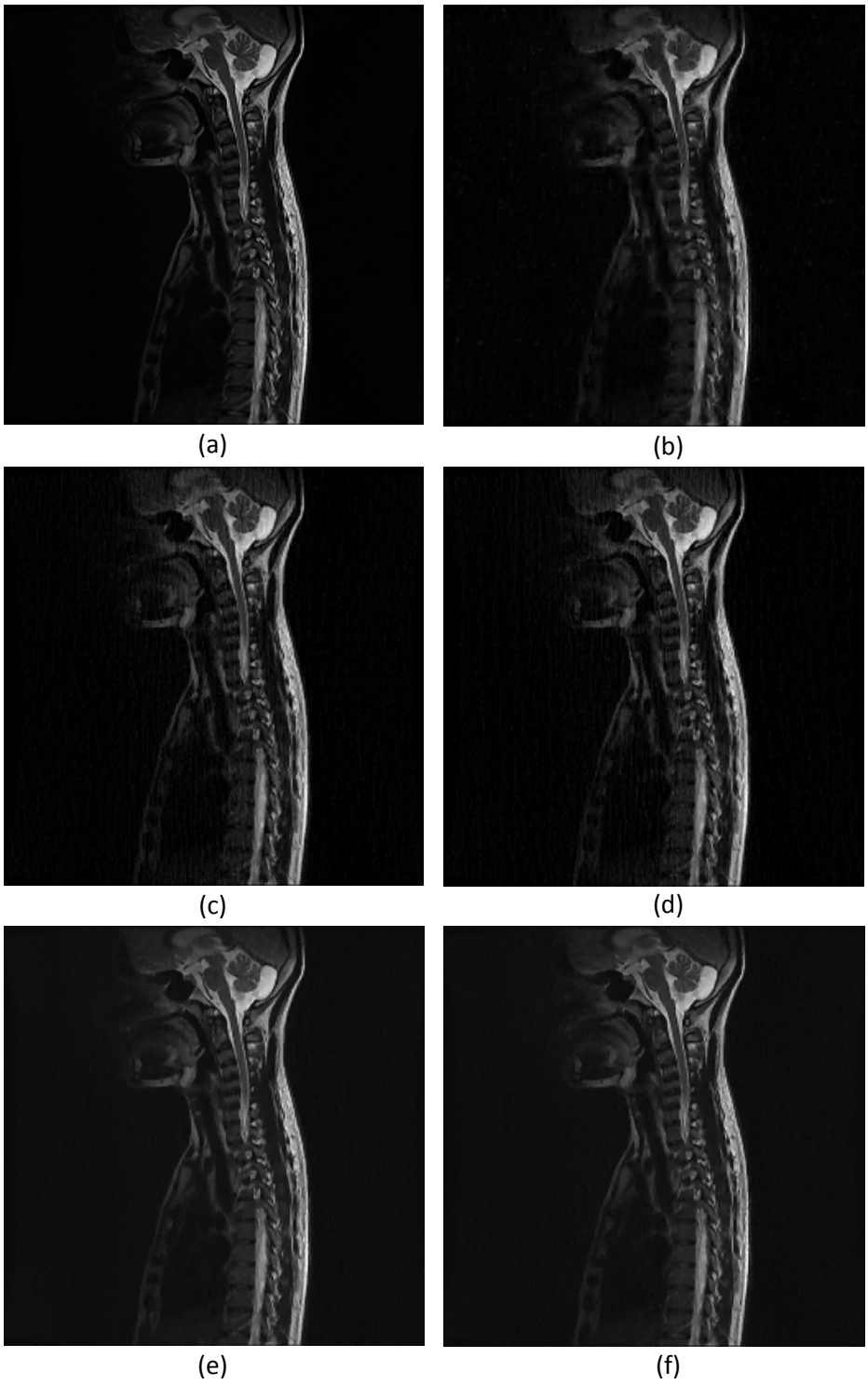

Fig. 4.6: (a) Original LS Spine MR image and (b) to (f) are the reconstructed images by the NCG, the RecPF, the TVCMRI, the FCSA and the proposed algorithm, respectively with 20% sampling ratio

4.9. Conclusions

We have proposed a TV-L1-L2 based high throughput MR image reconstruction algorithm using the acceleration scheme of the ALM. Reconstruction results on two *in vivo* MR images show significant improvements in terms of CPU time, PSNR, and MSSIM over the state-of-the-art. From different reconstructed images we observe that the proposed method gives better reconstruction results in terms of higher contrast and better preservation of edges with very less visual aliasing artifacts.

References:

[1] M. Lustig, D. Donoho, and J. M. Pauly, "Sparse MRI: The application of compressed sensing for rapid MR imaging," *Magnetic Resonance in Medicine*, vol. 58, pp.1182-1195, 2007.

[2] J. Yang, Y. Zhang, W. Yin, "A fast alternating direction method for TVL1-L2 signal reconstruction from partial Fourier data," *IEEE Journal of Selected Topics in Signal Processing*, vol.4 no.2, pp.288-297, 2010.

[3] I. Daubechies, M. Defrise, C. De Mol, "An iterative thresholding algorithm for linear inverse problems with a sparsity constraint," *Communications on Pure and Applied Mathematics,* vol. 57 , no.11, pp. 1413-1457, 2004.

[4] S. Kim, K. Koh, M. Lustig, S. Boyd, D. Gorinevsky, "An interior-point method for large-scale L1-regularized least squares," *IEEE Journal of Selected Topics in Signal Processing*, vol. 1, no. 4, pp. 606-617, 2008.

[5] A. Beck, M. Teboulle, "A fast iterative shrinkage-thresholding algorithm for linear inverse problems," *SIAM Journal on Imaging Sciences*, vol. 2, no.1, pp.183-202, 2009.

[6] L.I. Rudin, S. Osher, E. Fatemi, "Nonlinear total variation based noise removal algorithms," *Physica D,* vol. 60, pp. 259-268, 1992.

[7] J. Huang, S. Zhang, D. N. Metaxas, "Efficient MR image reconstruction for compressed MR imaging," *Medical Image Analysis*, vol. 15, no. 5, pp. 670-679, 2011.

[8] S. Ma, W. Yin, Y. Zhang, A. Chakraborty, "An efficient algorithm for compressed MR imaging using total variation and wavelets," *in Proc. of the IEEE Conference on Computer Vision and Pattern Recognition*, pp. 1-8, 2008.

[9] S. Boyd, L. Vandenberghe, *Convex Optimization*, Cambridge University Press, 1st Ed., New York, NY, USA, 2004.

[10] J. M. Bioucas-Dias, M. Jose, and M. A. T. Figueiredo, "A new TwIST: Two-step iterative shrinkage/thresholding algorithms for image restoration," *IEEE Transactions on Image Processing*, vol. 16, no.12, pp. 2992-3004, 2007.

[11] D. Bertsekas, *Constrained Optimization and Lagrange Multiplier Methods*, Athena scientific series in optimization and neural computation, Athena Scientific, 1st Edition, 1996.

Chapter 5

Wavelet Tree Sparsity

5.1. Introduction

The discrete wavelet transform (DWT) is quite well known in image processing. In two-dimensional images, wavelet filters are normally applied in both vertical and horizontal directions to produce four subbands, namely, the Low-Low (LL), the Low-High (LH), the High-Low (HL) and the High-High (HH) bands. Then only the LL band is iteratively decomposed to obtain the coarsest approximation band and a series of detail subbands at different resolutions. Since each subband represents a filtered and a subsampled version of the underlying image, coefficients of each subband are related to the original image. The relationship is illustrated below, showing the situation for HL bands i.e. those that have been high-pass filtered horizontally and low-pass filtered vertically.

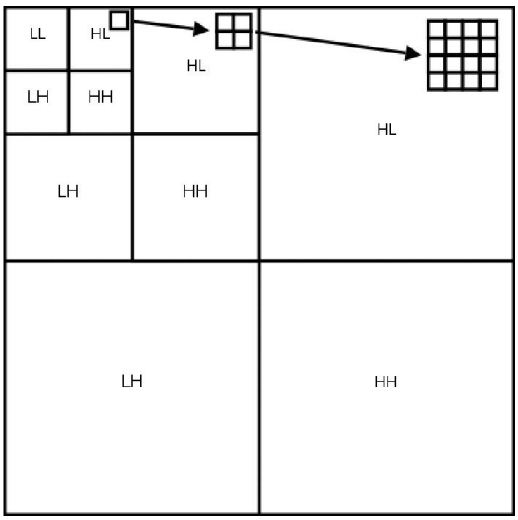

Fig. 5.1: Parent-child relationships between subband coefficients

From the above figure, we see that the subsampling structure means that a coefficient (the parent) in the highest level HL band corresponds spatially to a 2×2 block of coefficients (the children) in the immediately lower HL band, each coefficient of which itself has a 2×2 block of child coefficients in the next lower level HL band, and so on. 1. This is called the *quadtree* structure distribution of wavelet coefficients in various subbands. Here, the coefficients in the highest scale can be seen as the root nodes and the coefficients in the lowest scale are the leaf nodes. Each coefficient (non leaf) has four children in the next lower scale below it. If a parent coefficient has a large/small value, its children also tend to be large/small. Besides the sparsity of wavelet coefficients, this tree structure also provides another good prior for compressive sensing recovery [6, 7]. According to structured sparsity theory, the minimum required number of measurements for compressed sensing reconstruction can be reduced to by using structural sparsity as a prior term rather than

$O(K + K \log n)$ for standard K-sparse signal [6]. The improvement by exploiting tree structure can be significant when n is large.

5.2. Related work

It has been observed that sparse signal can be exactly reconstructed from highly undersampled linear measurements. In compressed sensing MRI, we can reconstruct good quality MR image with a small number of measurements because MR images are sparse in transform domain like wavelet. From recent studies it has been observed that the wavelet coefficient follow a quadtree structure for 2D image. In wavelet domain the children coefficient follows the property of the parent coefficients. By utilizing this structural property of wavelet coefficients the quality of CSMRI reconstruction can be improved further [6, 7].

5.3. Enhancing the sparsity of MR image by wavelet tree structure

Chen and Huang [6] proposed a new model, which combines wavelet sparsity, gradient sparsity and tree structure of wavelet as regularization terms with data fidelity term. In tree structure model, each pair of parent child wavelet coefficients is kept in one group, which forces them either to be zeros or non-zeros. They first decompose this composite regularization problem i.e. wavelet tree sparsity based TV-L1-L2 model into three simpler subproblems. One is the L_1-norm regularization subproblem, the second is the TV regularization subproblem, and the third is the wavelet tree sparsity subproblem. The L_1-norm subproblem is directly solved by the FISTA [8]. The TV-subproblem is first converted to a dual problem then the dual is solved by using the FISTA [9]. Finally, the tree sparsity subproblem is solved by using a group Thresholding operator. Then solutions of the three subproblems are linearly combined to get the actual solution. They conduct extensive experiments to compare the algorithm with other state-of-the-art CSMRI reconstruction algorithms. The new TV-L1-L2 model with tree sparsity of wavelet coefficients is

$$\hat{\mathbf{x}} = \underset{\mathbf{x}}{\operatorname{argmin}} \tfrac{1}{2} \| \mathbf{F}_u \mathbf{x} - \mathbf{y} \|_2^2 + \lambda_1 \| \mathbf{x} \|_{TV} + \lambda_2 \| \boldsymbol{\Psi}^T \mathbf{x} \|_1 + \lambda_3 \| \boldsymbol{\Psi}^T \mathbf{x} \|_{tree} \tag{5.1}$$

$$\text{or, } \hat{\mathbf{x}} = \underset{\mathbf{x}}{\operatorname{argmin}} \tfrac{1}{2} \| \mathbf{F}_u \mathbf{x} - \mathbf{y} \|_2^2 + \lambda_1 \| \mathbf{x} \|_{TV} + \lambda_2 \| \boldsymbol{\Psi}^T \mathbf{x} \|_1 + \lambda_3 \sum_{\mathbf{g} \in \mathbf{G}} \| \boldsymbol{\Psi}^T \mathbf{x}_{\mathbf{g}} \|_2 \tag{5.2}$$

where $\mathbf{x}$ and $\mathbf{y}$ represents the MR image and the measured k-space data, respectively, of a particular slice and $\mathbf{G}$ is a binary matrix, represent the grouping index. To solve this problem efficiently a new variable $\mathbf{z}$ is introduced as given below:

$$\hat{\mathbf{x}} = \underset{\mathbf{x}}{\operatorname{argmin}} \tfrac{1}{2} \| \mathbf{F}_u \mathbf{x} - \mathbf{y} \|_2^2 + \lambda_1 \| \mathbf{x} \|_{TV} + \lambda_2 \left(\| \boldsymbol{\Psi}^T \mathbf{x} \|_1 + \sum_{i=1}^{q} \| \mathbf{z}_{\mathbf{g}} \|_2 \right) \tag{5.3}$$

$$\text{subject to } \mathbf{z}_{\mathbf{g}} = \boldsymbol{\Psi}^T \mathbf{x}_{\mathbf{g}}$$

where q represent the total number of groups. According to the Lagrangian formulation the equivalent unconstraint problem can be written as:

$$\hat{\mathbf{x}} = \underset{\mathbf{x},\mathbf{z}}{\operatorname{argmin}} \tfrac{1}{2} \| \mathbf{F}_u \mathbf{x} - \mathbf{y} \|_2^2 + \lambda_1 \| \mathbf{x} \|_{TV} + \lambda_2 \left(\| \boldsymbol{\Psi}^T \mathbf{x} \|_1 + \sum_{i=1}^{q} \| \mathbf{z}_{\mathbf{g}} \|_2 + \tfrac{\beta}{2} \| \mathbf{z} - \mathbf{G}\boldsymbol{\Psi}^T \mathbf{x} \|_2^2 \right) \quad (5.4)$$

where β is a positive parameter. Algorithmic steps of the above problem are summarized in Algorithm-5.1, known as the wavelet tree sparsity MRI (WaTMRI) reconstruction algorithm. We have implemented above formulation for 2D multi-slice MR image reconstruction from highly undersampled measurements.

Algorithm 5.1 : WaTMRI algorithm

1.**Input** : $\mathbf{F}_u, \mathbf{y}, \boldsymbol{\Psi}, \lambda_1, \lambda_2$

2.**Initialization** : $t^{(1)} \leftarrow 1, \mathbf{x}^{(0)} \leftarrow \mathbf{F}_u^T \mathbf{y}, \mathbf{r}^{(1)} \leftarrow x^{(0)}, \rho \leftarrow L_h, k \leftarrow 0$

3.**While** not converged

4.$k \leftarrow k+1$

5.$\mathbf{z} \leftarrow \text{shrinkgroup}\left(\mathbf{G}\boldsymbol{\Psi}^T \mathbf{x}^{(k-1)}, \frac{\lambda}{\beta} \right)$

6.$\mathbf{x}_g \leftarrow \mathbf{r}^{(k)} - \frac{1}{\rho} \nabla h\left(\mathbf{r}^{(k)} \right)$

7.$\mathbf{x}_1 \leftarrow \text{prox}_{\frac{\lambda}{\rho}\|\Psi \mathbf{x}\|} (\mathbf{x}_g)$

8.$\mathbf{x}_2 \leftarrow \text{prox}_{\frac{\lambda}{\rho}\|\mathbf{x}\|_{TV}} (\mathbf{x}_g)$

9.$\mathbf{x}^{(k)} \leftarrow \dfrac{\left(\mathbf{x}_1 + \mathbf{x}_2 \right)}{2}$

10.$t^{(k+1)} \leftarrow \dfrac{\left(1+\sqrt{1+4(t)} \right)}{2}$

11.$\mathbf{r}^{(k+1)} \leftarrow \mathbf{x}^{(k)} + \dfrac{t^{(k)}-1}{t^{(k+1)}} \left(\mathbf{x}^{(k)} - \mathbf{x}^{(k-1)} \right)$

12. end **While**

13.**Output** : $\mathbf{x}^* \leftarrow \mathbf{x}^{(k)}$

5.4. Experimental Results

Experimental setup:
All experiments are performed on a PC with 3.4GHz Intel core i7 CPU with 2GB RAM and MATLAB (2012b). We have collected RF spoiled gradient echo (GE) abdomen MRI data available at (http://mridata.org/fullysampled/knees). These data were acquired from a 32-channel paediatric body MRI 3T scanner with following parameters, FOV: $260 \times 260\,\text{mm}^2$, TR/TE: 4.312/1.012 ms, ST: 1 mm, spacing between scans:-0.5 mm and matrix size: 192×256.

We have also collected a MRI data set from GNRC Hospital, Guwahati, India (http://www.gnrchospitals.com). We have collected a 2D multi-slice 3D BRAVO T1 HR brain MRI data. The data were acquired from a GE 1.5T signa HDxt scanner with following

parameters: TR/TE: 14.912/6.456 ms, slice thickness: 1.2 mm, spacing between scans: 1.2 mm, sampling (%): 100, and Flip angle: 15deg.

For CS reconstruction using different algorithms we have taken $\lambda_1 = 0.35$ and $\lambda_2 = 0.01$. We set a common stopping criterion i.e. the relative change of the objective function less than 10^{-4} for simulation of all algorithms.

We compute the peak signal-to-noise ratio (PSNR) and the mean structural similarity index (MSSIM) to evaluate the performance of the proposed multi-slice MR image reconstruction technique besides visual analysis of reconstructed images.

Results and discussions:

The WaTMRI takes on average 18 iterations whereas the FCSA and the NCG algorithms take on average 40 and 23 iterations, respectively for convergence at 20% sampling ratio. The corresponding CPU time required for the NCG, the FCSA and the WaTMRI are on average 130, 2 and 2.3sec./slice, respectively. Table 5.1 shows results for varying sampling ratios for different methods including the proposed method for an *in vivo* brain MR image. Results show that the proposed method takes almost similar time for reconstruction as taken by one of the fastest state-of-the-art algorithms, namely, the FCSA.

Table 5.1: PSNR, MSSIM and CPU time for different methods with varying sampling ratios

Sampling ratio (%)	PSNR (dB)			MSSIM			CPU time (sec.)		
	NCG	FCSA	WaTMRI	NCG	FCSA	WaTMRI	NCG	FCSA	WaTMRI
9%	21.42	23.07	24.48	0.6804	0.7143	0.7805	122.52	1.92	2.43
12%	24.78	26.16	27.11	0.7756	0.8185	0.8485	134.00	1.90	2.37
15%	26.97	28.81	29.68	0.8233	0.8635	0.8868	128.22	1.84	2.29
18%	28.17	29.94	31.14	0.8598	0.8804	0.9056	132.44	1.97	2.08
20%	29.88	31.45	32.53	0.8813	0.8967	0.9217	118.50	1.77	2.20

For quantitative evaluation of the proposed method we have computed PSNR and MSSIM values for the proposed method and two other TV-L1-L2 model based CSMRI algorithms, namely, the NCG [1] and the FCSA [3]. From Table 5.1, we have seen that the WaTMRI gives PSNR improvements on an average of 2.5 dB and 1dB than those of the NCG and the FCSA, respectively. Similarly, the WaTMRI gives MSSIM improvement on an average of 0.06 and 0.03 than those of the NCG and the FCSA, respectively. Therefore we can say that the WaTMRI gives better PSNR and MSSIM values than those of the NCG and the FCSA irrespective of sampling ratio.

Fig.5.2 shows the original abdomen MR image and the corresponding CS reconstructed images using different techniques. To compare the advantage of the proposed method over other methods, we have taken a small region of the reconstructed image and then zoomed it.

This may be observed at the bottom rightmost corner. From the highlighted results, it is seen that the WaTMRI gives better reconstruction in terms of higher contrast with better preservation of edges and less aliasing artifacts at just 20% undersampling ratio.

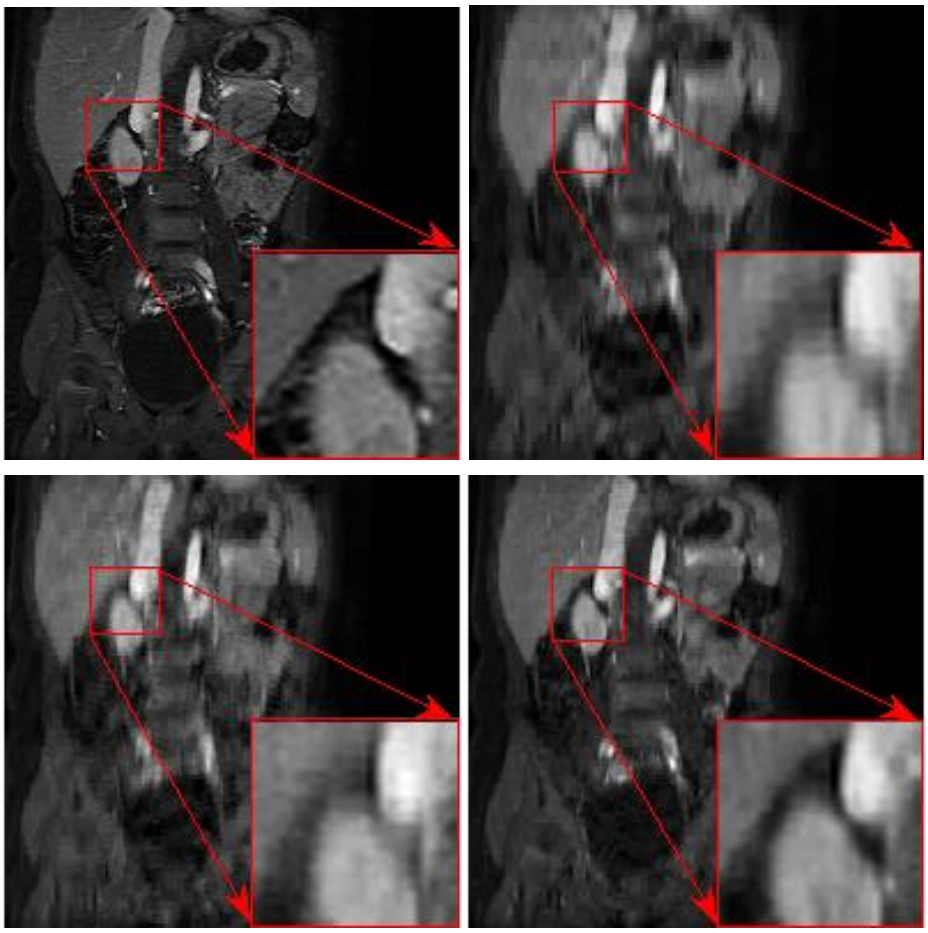

Fig. 5.2: First row left to right: Original abdomen MR image, reconstructed abdomen MR image using NCG method. Second row left to right: reconstructed abdomen MR image using FCSA methods and reconstructed abdomen MR image using WaTMRI

5.5. Conclusions

We have proposed a 2D multi-slice MR image reconstruction technique using the wavelet tree sparsity along with wavelet and gradient sparsities. We observe that reconstructions using the WaTMRI algorithm show significant improvements in terms of higher contrast and better preservation of edges over the state-of-the-art techniques.

References:

[1] M. Lustig, D. Donoho, and J. M. Pauly, "Sparse MRI: The application of compressed sensing for rapid MR imaging," *Magnetic Resonance in Medicine*, vol. 58, pp. 1182-1195, 2007.

[2] J. Yang, Y. Zhang, and W. Yin, "A fast alternating direction method for TVL1-L2 signal reconstruction from partial Fourier data," *IEEE Journal of Selected Topics in Signal Processing*, vol. 4, no. 2, pp.288-297, 2010.

[3] J. Huang, S. Zhang, and D. N. Metaxas, "Efficient MR image reconstruction for compressed MR imaging," *Medical Image Analysis*, vol. 15, no. 5, pp. 670-679, 2011.

[4] S. Ma, W. Yin, Y. Zhang, and A. Chakraborty, "An efficient algorithm for compressed MR imaging using total variation and wavelets," *in Proc. of the IEEE Conference on Computer Vision and Pattern Recognition*, pp. 1-8, 2008.

[5] A. Beck, and M. Teboulle, "A fast iterative shrinkage-thresholding algorithm for linear inverse problems," *SIAM Journal on Imaging Sciences*, vol. 2, no. 1, pp. 183-202, 2009.

[6] C. Chen and J. Huang, "Compressive sensing MRI with wavelet tree sparsity," *in Proc. of the Advances in Neural Information Processing Systems (NIPS) 25*, pp. 1115–112, 2012.

[7] C. Chen and J. Huang, "The benefit of tree sparsity in accelerated MRI," *Medical Image Analysis*, vol. 18, no. 6, pp. 834 - 842, 2014.

[8] A. Beck, M. Teboulle, "A fast iterative shrinkage-thresholding algorithm for linear inverse problems," *SIAM Journal on Imaging Sciences*, vol. 2, no.1, pp.183-202, 2009.

[9] A. Beck, M. Teboulle, "Fast Gradient-Based Algorithms for Constrained Total Variation Image Denoising and Deblurring Problems," *IEEE Transactions on Image Processing*, vol. 18, no. 11, pp. 2419-2434, 2009.

Chapter 6

Interpolated Compressed Sensing and Multi-slice MR image Reconstruction

6.1. Introduction

Multi-slice imaging is very common in clinical practice because it allows a volume of anatomy to be imaged. In spin echo imaging, TR is longer than TE, the scanner would be idle (not working) in most of the time, if a single slice is acquired. But in multiple slice imaging, adjacent slices are imaged while waiting for relaxation of the first slice towards equilibrium, resulting in decreased image acquisition time for the set of slices [9].

The slices are selected by applying RF pulses at different frequencies and detecting the signals from different slices at different times. When the slice selection gradient is turned on, each slice is tuned to a different resonant frequency. In particular, a specific slice can be selected for excitation by adjusting the RF pulse frequency to correspond to the resonant frequency of that slice. The process begins by applying an excitation pulse to one slice and collecting the echo signal. Then, while that slice is in longitudinal relaxation before the next cycle can begin, the excitation pulse frequency is shifted to excite another slice. This process is repeated to excite and collect signals from the entire set of slices at slightly different times within one TR interval [9], [Chapter 4, 10].

In many pulse sequences for MRI acquisition, there is a quite long delay between each excitation (repetition time) of a particular slice while the magnetization recovers. Because of the relatively long T1 relaxation time of tissues, a delay of up to three seconds may be necessary before repeating the excitation. To make the most efficient use of this time, we can excite a number of parallel slices in each interval, which is achieved by changing the frequency of the RF pulse. This procedure can be repeated to produce a series of slices as shown in Fig.6.1. The number of slices obtainable can be calculated by dividing the repetition time TR by the time required for each slice. For example, if TR = 400 ms and TE = 50 ms, the theoretically possible number of slices is eight (in practice seven, since each slice requires slightly more than TE) [9], [Chapter 15, 8].

The main advantage of multi-slice imaging is that a set of slices can be imaged in the same TR time. The main factor that limits the number of slices is the TR. The maximum number of slices is the TR value divided by the time required for each slice. This limitation is especially significant for T1-weighted images that use relatively short TR values. With selective excitation there is the possibility that when an RF excitation/saturation pulse is applied to one slice of tissue, it will also produce some effect in an adjacent slice. This is the reason for leaving gaps between slices during the acquisition.

However, additional slices may be acquired between two slices, which are otherwise interleaved, by interleave acquisition process. Here, we do not acquire adjacent slices

simultaneously. With multiple TR and RF pulses we can excite the desired slice locations. Consider a set of 3 mm slices placed one next to another so that 10 slices exactly span 30 mm. Then instead of sequential acquisition in the order (1, 2, 3, …, 10), we acquire interleaved slices means (for e.g. 1,4,7,10; 2,5,8; 3,6,9). Finally, we get all the 10 slices of 3mm width without any gap. Interleaved acquisitions are preferable because frequency range of RF pulses may not have sharp cut-offs and hence positioning of slices may not be very accurate [9].

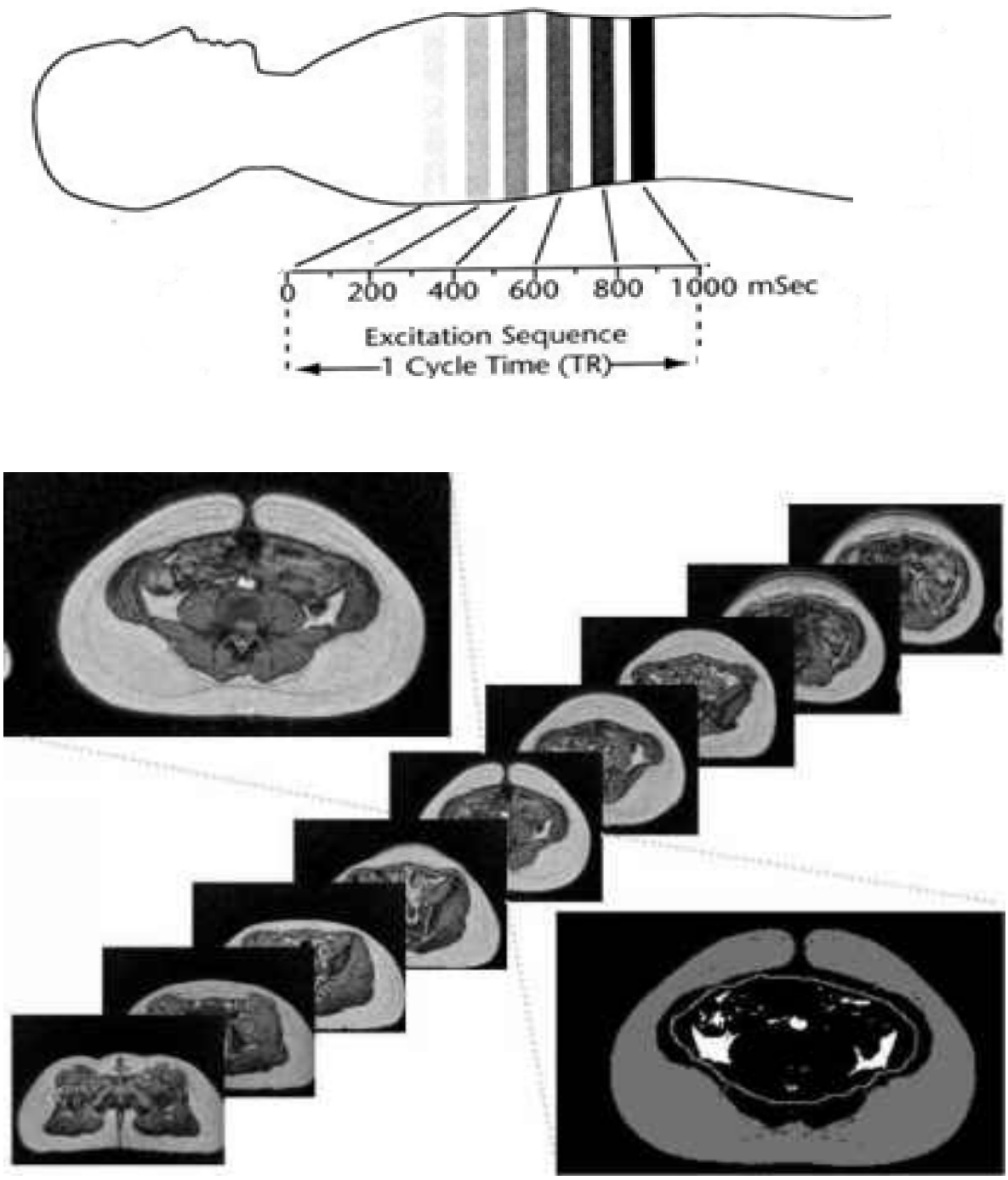

Fig. 6.1: 2D Multi-slice MR imaging

6.2. Interpolated Compressed sensing MRI

Recently the interpolated compressed sensing (iCS) MRI idea is proposed by Pang and Zhang [4, 5] and Pang *et al.* [6, 7]. They demonstrated a novel multi-slice acquisition technique for improving image quality and contrast by utilizing the inter-slice similarity. They estimated missing samples for some of the highly undersampled slices from their adjacent low undersampled counterparts using a novel strategy of combining an efficient interpolation technique with the existing CSMRI reconstruction techniques. They coined the term *interpolated compressed sensing* (iCS) to name their approach.

In multi-slice CS acquisition, some slices are highly undersampled (H-slice) and some slices are relatively low undersampled (L-slice). In case of H-slice the centre region of the *k*-space is acquired to obtain the low resolution image, on the other hand in case of L-slice more *k*-space data is acquired by using the incoherent undersampling strategy. The extra *k*-space data of the L-slice is used to estimate the high frequency information of H-slices. Using low resolution images of a pair of H-slice and L-slice a weighting function is obtained. This is then used to estimate the difference between the H-slice (or target slices) and L-slices by convolution with the low undersampled slice (L-slice). Finally, the CS reconstruction of each is carried out to generate a sequence of high resolution 2D multislice MRI sequence. The above process may be shown graphically as in Fig. 6.2. We summarize the Pang's method as follows:

Interpolation: First, the weighting function between the H-slice and the L-slice is generated by calculating ratio between corresponding two low resolution images. By taking Fourier Transform the weighting functions in *k*-space domain are obtained. Second, the estimated *k*-space data of the target H-slice are calculated by taking convolution of the weighting function and the undersampled *k*-space data of the L-slice. Third, combine these estimated data to the *k*-space of the originally acquired target slice.

CS Reconstruction: After interpolation all slices including L-slices are individually reconstructed by using nonlinear Conjugate Gradient (NCG) method [1].

6.3. Proposed multi-slice MR image reconstruction using interpolation and compressed sensing

3D MRI is the best way to analysis the 3D anatomical structure. But due to the slow imaging process the conventional 3D MRI usually leads to impractical scan time. Therefore, 2D multi-slice MRI is used instead. In 2D multi-slice MRI the anatomical variation in adjacent slices are vary less as they are highly correlated because a number of slices are acquired within a small volume. Therefore, we can estimate any intermediate slice from neighbouring slices. So, we can undersample adjacent slices non-uniformly and reconstruct good quality MR images by interpolating the missing samples from low undersampled slice to neighbouring highly undersampled slice.

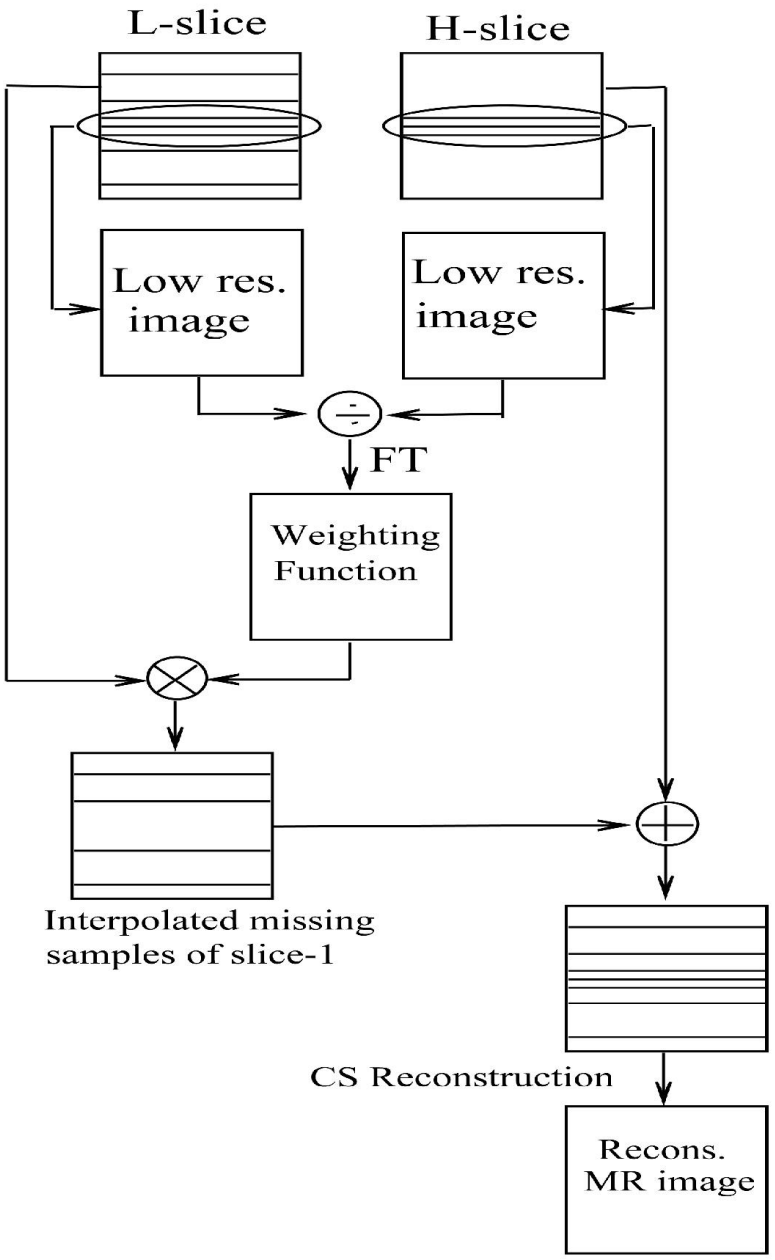

Fig. 6.2: Interpolated compressed sensing by Pang's method

This interpolation technique significantly reduces amount of total acquired data or measurements which in turn reduces the MRI scan time. We have proposed a fast 2D multi-slice interpolation technique to estimate the relative missing samples from a highly undersampled slice as shown in Fig.6.3. After interpolation each slice is individually reconstructed using the FCSA method.

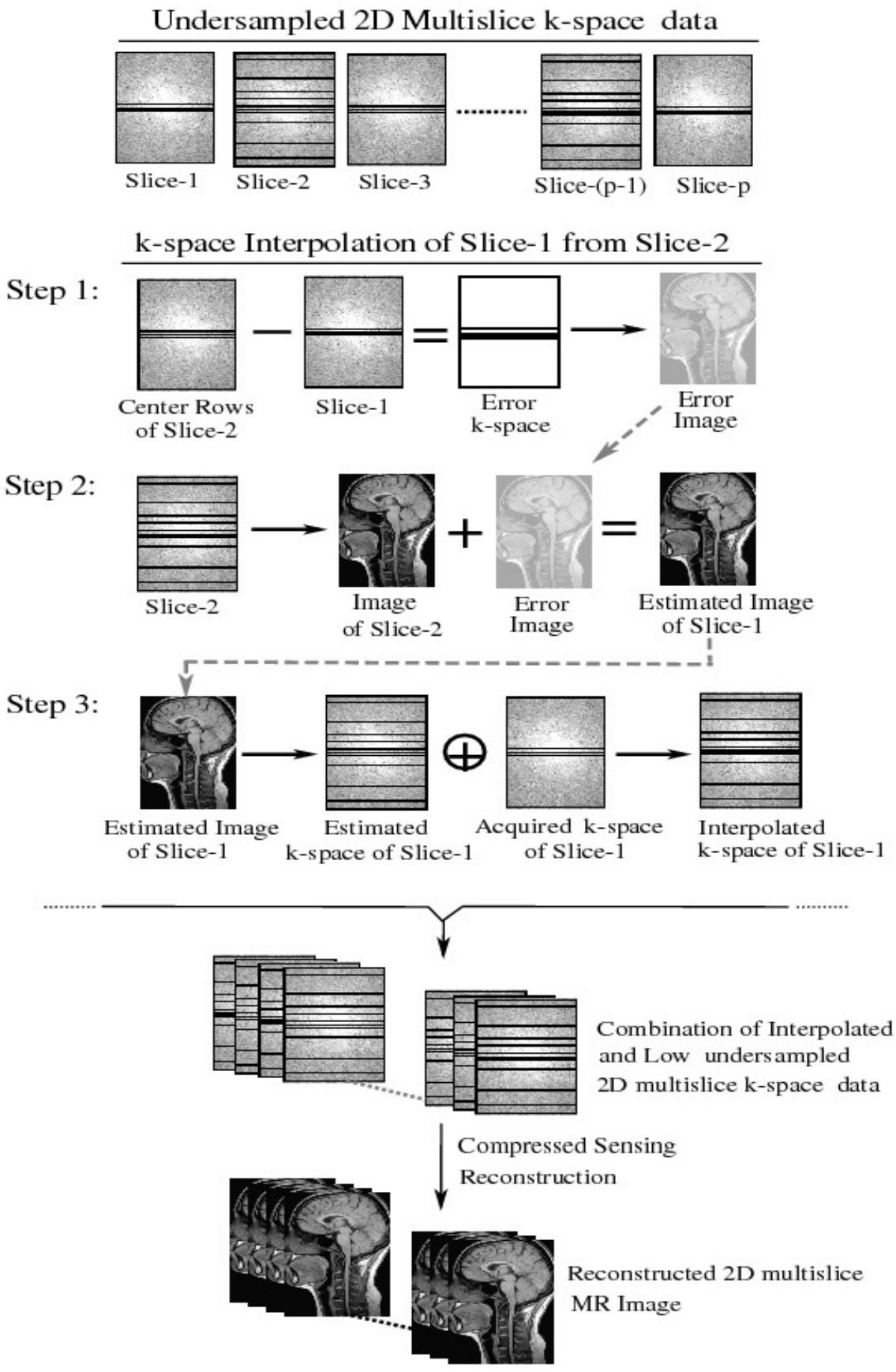

Fig. 6.3: Proposed interpolation based multi-slice MR image reconstruction

Algorithmic steps of the proposed technique are summarized in Algorithm-6.1. Suppose, $\mathcal{Y} = \left\{\mathbf{y}_h^1, \mathbf{y}_l^2, \mathbf{y}_h^3, ..., \mathbf{y}_h^p\right\}$ represents the ensemble of measured raw data corresponding to a set of 2D multi-slice images and $\mathcal{X} = \left\{\mathbf{x}^1, \mathbf{x}^2, \ldots, \mathbf{x}^p\right\}$ denotes the corresponding MR images. For example, $\mathbf{y}_h^1 = \mathbf{F}_h\,\mathbf{x}^1$ denotes the highly undersampled k-space data in slice-1 and $\mathbf{y}_l^2 = \mathbf{F}_l\,\mathbf{x}^2$ denotes the relatively low undersampled k-space data in slice-2, and so on. Here, $\mathbf{F}_h$ and $\mathbf{F}_l$ represent the Fourier operators for high and low undersampled slices, respectively. Here, first we estimate the highly undersampled slices using the proposed interpolation technique. Then each slice is individually reconstructed using the FCSA algorithm. $\mathbf{y}_h^{\text{target}}$ represents a highly undersampled target slice and $\mathbf{y}_h^c$ represents a hypothetical slice containing only a few lines of the low undersampled slice $\mathbf{y}_l$ from locations identical to those taken for $\mathbf{y}_h^{\text{target}}$.

Algorithm 6.1 : Proposed interpolated multi-slice MR Image Reconstruction Algorithm

---

1. **Input** : $\mathbf{F}_h, \mathbf{F}_l, \mathcal{Y} = \{\mathbf{y}_h^1, \mathbf{y}_l^2, \mathbf{y}_h^3, \ldots, \mathbf{y}_l^{p-1}, \mathbf{y}_h^p\}, \boldsymbol{\Psi}, \lambda_1, \lambda_2$
2. **While** repeat for all highly undersampled slices
3. $\quad \mathbf{E} \leftarrow \mathbf{y}_h^c - \mathbf{y}_h^{\text{target}}$
4. $\quad \mathbf{e} \leftarrow \mathbf{F}_h^{-1}\,\mathbf{E}$
5. $\quad \overline{\mathbf{x}} \leftarrow \mathbf{F}_l^{-1}\,\mathbf{y}_l$
6. $\quad \mathbf{x}_{\text{est}} \leftarrow \overline{\mathbf{x}} - \mathbf{e}$
7. $\quad \mathbf{y}_{\text{est}} \leftarrow \mathbf{F}_l\,\mathbf{x}_{\text{est}}$
8. $\quad \mathbf{y}_{\text{in}} \leftarrow \mathbf{y}_{est} \oplus \mathbf{y}_h^{\text{target}}$
9. end **While**
10. $\widehat{\mathcal{Y}} \leftarrow \mathbf{y}_{\text{in}}^1, \mathbf{y}_l^2, \mathbf{y}_{\text{in}}^3, \ldots, \mathbf{y}_l^{p-1}, \mathbf{y}_{\text{in}}^p$
11. **For** $k = 1 : p$
12. $\quad \hat{\mathbf{x}}^k \leftarrow \text{FCSA}\left(\mathbf{F}_l, \mathbf{y}^k, \Psi, \lambda_1, \lambda_2\right)$
13. end **For**
13. **Output** : $\widehat{\mathcal{X}} \leftarrow \left\{\hat{\mathbf{x}}^k\right\}_{k=1,\ldots,p}$

6.4. Experimental Results

Experimental setup:

Numerous experiments have been conducted to show the superiority of the proposed algorithm on CSMRI. All experiments are performed on a PC with 3.4GHz Intel core i7 CPU with 2GB RAM and MATLAB (2012b).We have collected 3D fast spin-echo (FSE) knee MRI data available at[1]. The knee MRI data were acquired from a GE HDx 3T scanner with

following parameters, field of view (FOV): $160\times160\,\text{mm}^2$, TR/TE: 1550/25.661 ms, slice thickness (ST): 0.6 mm, spacing between scans:0 mm and matrix size: 320×320.

We have also collected MRI data set from GNRC Hospital, Guwahati, India (http://www.gnrchospitals.com). We have collected 2D multi-slice 3D BRAVO T1 HR brain MRI data and 3D TOF- 1SLAB brain MRI data. The 3D BRAVO T1 HR brain MRI data were acquired from a GE 1.5T signa HDxt scanner with following parameters: TR/TE: 14.912/6.456 ms, slice thickness: 1.2 mm, spacing between scans: 1.2 mm, sampling (%): 100, and Flip angle: 15deg. The 3D TOF- 1SLAB brain MRI data were acquired from a GE 1.5T signa HDxt scanner with following parameters: TR/TE: 21/3.2 ms, slice thickness: 1.6 mm, spacing between scans: 0.8 mm, sampling (%): 100, and Flip angle: 20deg.

We have also simulated 2D multi-slice brain MR images using the BrainWeb simulator http://brainweb.bic.mni.mcgill.ca/brainweb with following parameters, pulse sequence: SFLASH, TR/TE: 18/10 ms, Flip angle: 30 deg, Image Type: magnitude, Noise level: 0 %, INU field: field A and INU level: 20 %.

For CS reconstruction of the MR image using different algorithm we have taken $\lambda_1 = 0.35$ and $\lambda_2 = 0.01$. For all algorithms we set a common stopping criterion i.e. the relative change of the objective function less than 10^{-4}. For convergence, CPU times required for the NCG and the FCSA algorithm are on average 130 and 2 secs. / slice, respectively. To evaluate the performance of the proposed interpolation technique we compared the CS reconstruction results with that of the state-of-the-art. We compute the CPU time, peak signal-to-noise ratio (PSNR) and mean structural similarity index (MSSIM) for different MR images.

Results and discussions:

From experimental results, we observe that the CPU time required for the proposed interpolation is approximately 0.5 sec whereas the CPU time required for iCS-interpolation is approximately 11 sec for interpolation of nine adjacent slices. From this observation we conclude that the proposed interpolation technique is twenty times faster than the iCS-interpolation. Generally in clinical practice 100-300 2D slices are acquired for 3D reconstruction. Therefore, in clinical MRI the proposed interpolation would be highly significant.

For fair comparisons, we also combine the proposed interpolation scheme with the NCG algorithm as in the iCS [5]. The proposed interpolation technique with the NCG gives better PSNR and MSSIM values than the NCG and the FCSA methods alone. But the PSNR and the MSSIM values of the proposed method with the NCG are quite similar with that of the iCS method whereas the proposed interpolation with the FCSA gives better PSNR and MSSIM values than the iCS and other methods without using interpolation. Results are shown in Tables 6.1 and 6.2. The proposed interpolation technique with the FCSA shows average improvement more than 1dB in PSNR than the iCS method. On the other hand, for the NCG

and the FCSA methods alone, improvements are respectively, 3 dB and 2.5dB. Similarly, proposed interpolation technique with the FCSA shows an average improvement of 0.02 in MSSIM than the iCS method whereas they are respectively 0.05 and 0.03 for the NCG and the FCSA methods alone.

Table 6.1: Comparison of PSNR (in dB) of CS reconstructed knee slices using different techniques

Slice	NCG	FCSA	iCS	Prop. NCG	Prop. FCSA
1	30.06	30.84	32.84	**32.77**	**33.68**
3	30.39	31.07	31.76	**31.96**	**33.19**
4	30.62	31.26	33.32	**33.48**	**33.98**
6	30.37	31.18	32.96	**32.88**	**33.59**
7	28.57	29.44	30.92	**31.01**	**31.92**
9	30.14	30.95	31.98	**32.12**	**33.07**

Table 6.2: Comparison of MSSIM of CS reconstructed knee slices using different techniques

Slice	NCG	FCSA	iCS	Prop. NCG	Prop. FCSA
1	0.8059	0.8122	0.8266	**0.8334**	**0.8415**
3	0.8019	0.8105	0.8227	**0.8357**	**0.8432**
4	0.8205	0.8276	0.8786	**0.8761**	**0.8848**
6	0.8146	0.8208	0.8774	**0.8779**	**0.8852**
7	0.7631	0.7773	0.8031	**0.8092**	**0.8203**
9	0.7963	0.8041	0.8249	**0.8286**	**0.8411**

CS reconstructed BrainWeb and *in vivo* images of brain and knee are shown in Figs. 6.4, 6.5 and 6.6, respectively. From reconstructed images, it is seen that the proposed technique gives better reconstruction result in terms of contrast and preservation of edges compared to other methods. The proposed method also gives less visual aliasing artifacts.

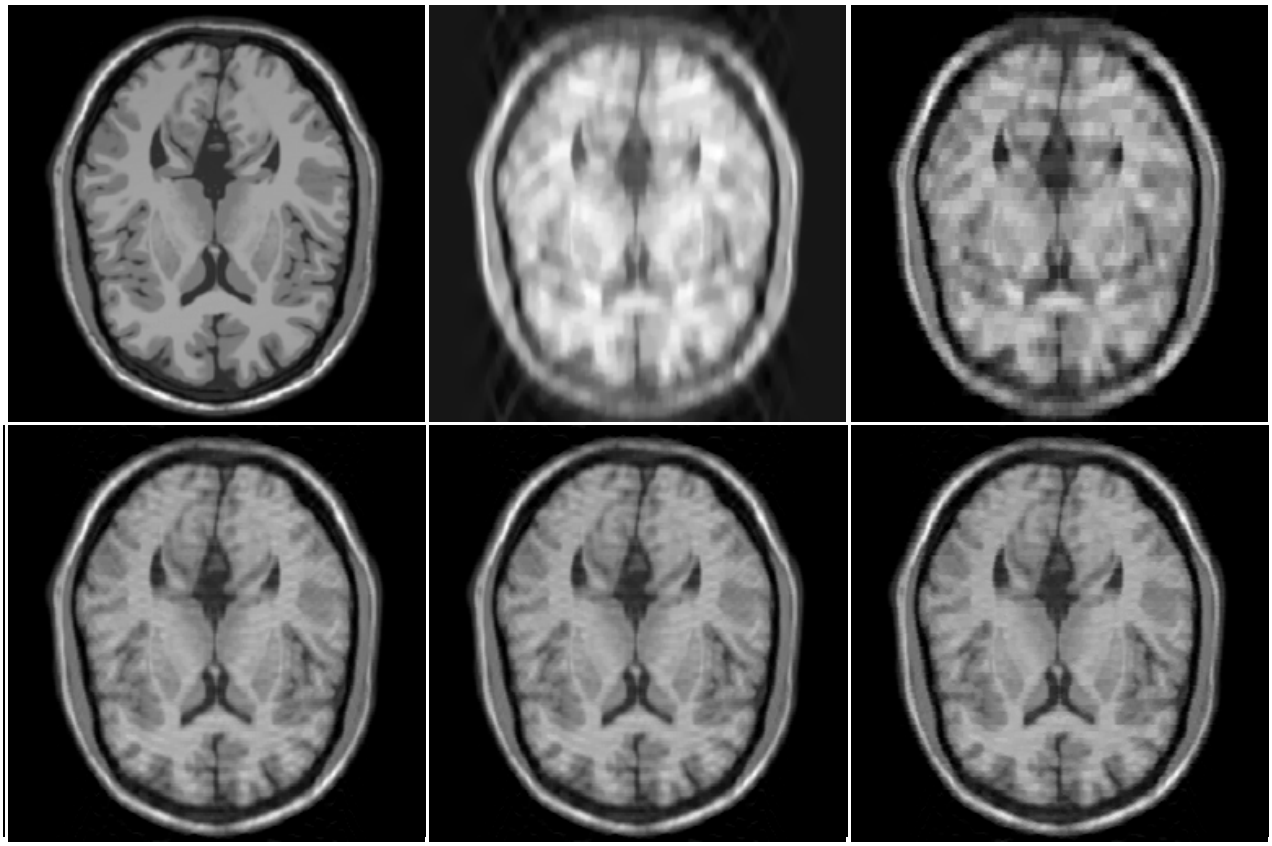

Fig. 6.4: Comparison of reconstructed slices using different techniques at 9% sampling ratio. First row left to right: Original BrainWeb image, NCG method without interpolation and FCSA method without interpolation. Second row left to right: interpolated compressed sensing method, proposed interpolation technique with the NCG and the FCSA methods, respectively

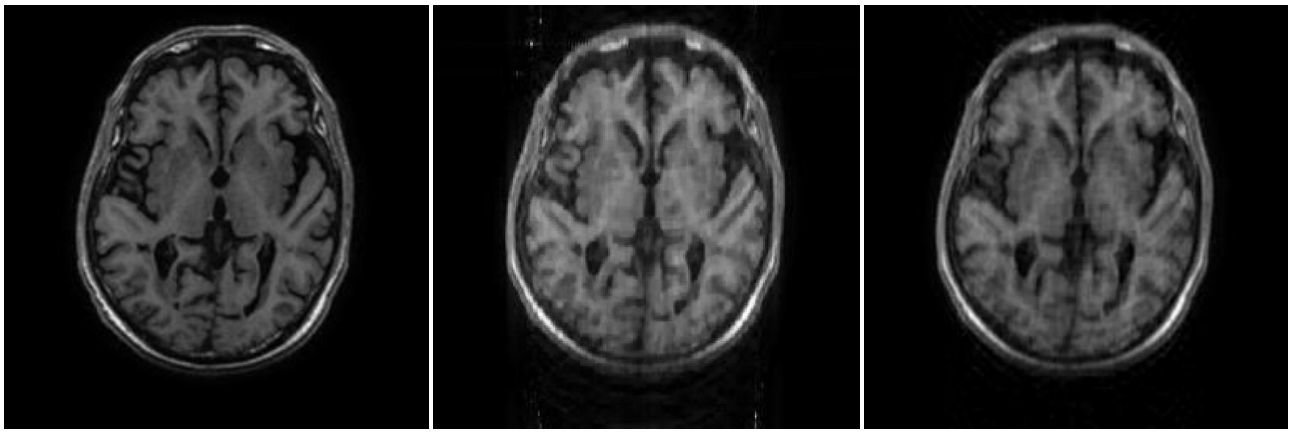

Fig. 6.5: Comparison of reconstructed slices using different techniques at 18% sampling ratio. From left to right: Original *in vivo* brain image, results of the interpolated compressed sensing method, and the proposed method with the FCSA

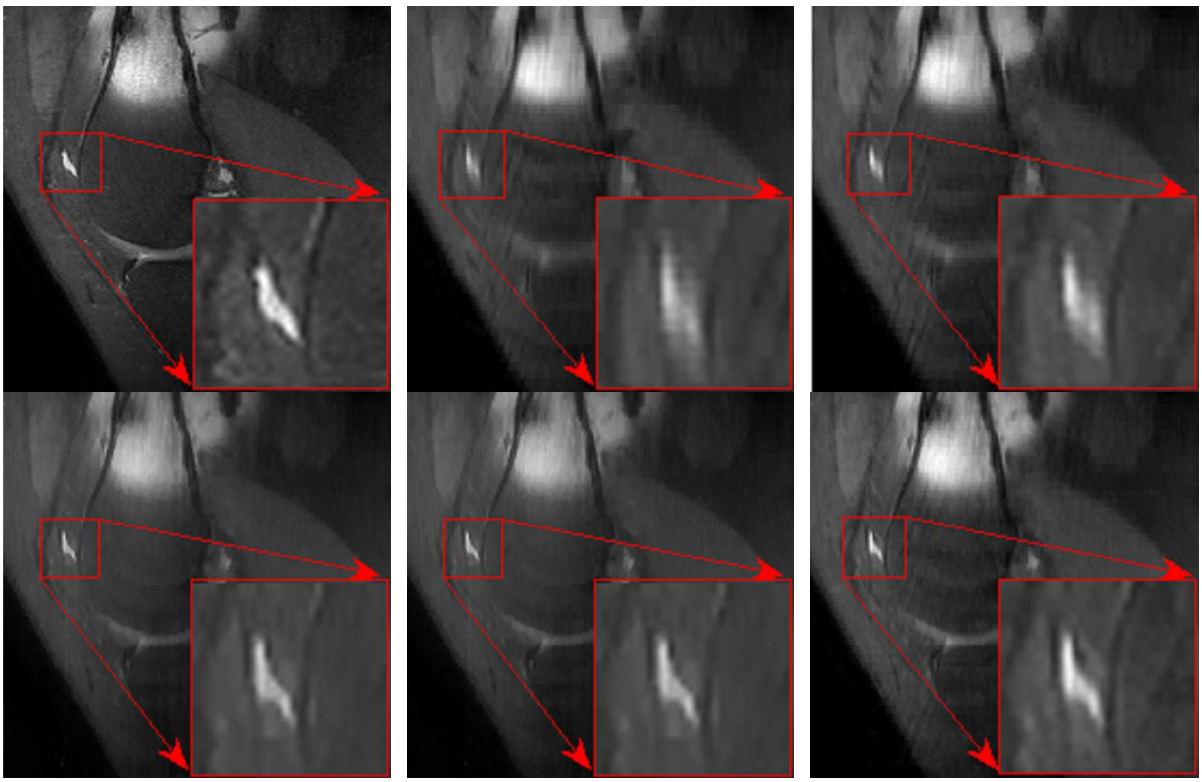

Fig. 6.6: Comparison of reconstructed results using different techniques with a zoomed portion at the bottom rightmost corner. First row left to right: Original knee MR image, and results of the NCG and the FCSA methods without interpolation. Second row left to right: Results of interpolated compressed sensing method, proposed interpolation technique with the NCG and the FCSA methods

6.5. Conclusions

We have proposed a fast interpolation based 2D multi-slice CSMRI reconstruction technique. From the experimental results we observe that the proposed interpolation technique is twenty times faster than the iCS-interpolation. CS reconstructions on both simulated and *in vivo* 2D multi-slice images show that the proposed method with the NCG gives similar or slightly better while the proposed method with the FCSA gives quite superior results compared to the iCS method in terms of better contrast and preservation of edges.

References:

[1] M. Lustig, D. Donoho, and J. M. Pauly, "Sparse MRI: The application of compressed sensing for rapid MR imaging", *Magnetic Resonance in Medicine*, vol. 58, pp. 1182-1195, 2007.

[2] D. Donoho, "Compressed sensing,", *IEEE Transactions on Information Theory*, vol. 52, no. 4, pp. 1289 –1306, 2006.

[3] J. Huang, S. Zhang, and D. N. Metaxas, "Efficient MR image reconstruction for compressed MR imaging", *Medical Image Analysis*, vol. 15, no. 5, pp. 670-679, 2011.

[4] Y. Pang and X. Zhang, "Interpolated compressed sensing MR image reconstruction using neighbouring slice k-space data," *in Proc. of the Proceedings of the 20th Annual Meeting of ISMRM*, Melbourne, Australia, p.2275, 2012.

[5] Y. Pang and X. Zhang, "Interpolated compressed sensing for 2D multiple slice fast MR imaging," *Ed. Jonathan A. Coles. PLoS ONE*, vol. 8, no. 2, pp. 1–5, 2013.

[6] Y. Pang, J. Jiang, and X. Zhang, "Ultrafast fetal MR imaging using interpolated compressed sensing," *in Proc. of the International Society for Magnetic Resonance in Medicine 2014*, p. 2224, 2014.

[7] Y. Pang, B. Yu, and X. Zhang, "Enhancement of the low resolution image quality using randomly sampled data for multi-slice MR imaging," *Quantitative Imaging in Medicine and Surgery*, vol. 4, no. 2, pp. 136–144, 2014.

[8] J. T. Bushberg, A. J. Seibert, E. M. Leidholdt, and J. M. Boone, *The essential physics of medical imaging*, Philadelphia, PA: Lippincott Williams & Wilkins, 3rd Edition, 2012

[9] Rochester Institute of technology, Chester F. Carlson Center for Imaging Science, The Basics of MRI [online]. Available: https://www.cis.rit.edu/htbooks/mri/chap-8/chap-8.htm

[10] D. W. McRobbie, E. A. Moore, M. J. Graves, and M. R. Prince, *MRI from Picture to Proton*, Cambridge University Press, Cambridge, UK, 1st Edition, 2006.

Chapter 7

Conclusions and Future Works

Conclusions of the project are summarized as follows:

1. We have proposed an efficient k-space under-sampling pattern namely the 'variable density under-sampling pattern' to efficiently acquire k-space data in MRI. The reconstructed result using proposed undersampling pattern is compared to other well known undersampling patterns and it has been seen that the proposed under-sampling pattern gives better results compared to other under-sampling patterns in terms of MSE, PSNR, and MSSIM.

2. Proposed a high throughput MR image reconstruction algorithm. The performance of the proposed Algorithm is compared with different L1-minimization algorithms. From the result we observed that the proposed algorithm gives better results in terms of CPU time and quality of reconstructed MR images in terms of PSNR and MSSIM.

3. We have proposed a fast interpolation technique for compressed sensing based 2D multi-slice MR image reconstruction from highly undersampled measurements. Results show that the proposed interpolation technique is more than twenty times faster than the state-of-the-art.

A few important tracks of future works for this project could be as mentioned below:

1. In future, works on enhancing the sparsity of the MR image for better reconstruction may be pursued. For this, structural sparsity of the MR image in transform domain may be considered. Also, inclusion of some weighting scheme for enhancing the sparsity in both the transform domain as well as in the spatial domain may be carried out.
2. To focus on the design of efficient undersampling patterns for 2D multi-slice and 3D MRI data acquisition.
3. To give thrust on compressed sensing based dynamic MR image reconstruction in cine cardiac MRI.
4. To extend the proposed method for the efficient implementation of CS based parallel MRI.

Research outcome:

1. B. Deka, and S. Datta, "High Throughput MR Image Reconstruction Using Compressed Sensing", in *Proceedings of the 2014 Indian Conference on Computer Vision Graphics and Image Processing*, ACM, pp. 89:1-89:6,2014**.**
2. B. Deka, and S. Datta, "A Practical Under-Sampling Pattern for Compressed Sensing MRI" *Advances in Communication and Computing*, Springer India, vol. 347(9), pp. 115-125, 2015.
3. S. Datta and B. Deka "A Fast Interpolation Technique for Compressed Sensing Based Reconstruction of Multi-slice MRI" *Imaging Science Journal,* Taylor & Francis (submitted)
4. S. Datta and B. Deka "An Efficient Interpolated Compressed Sensing Method for 2D Multi-slice MRI" *IEEE Signal Processing Letters* (submitted, Ref. No. SPL-19362-2016)
5. B. Deka and S. Datta **"** Recent Developments of Compressed Sensing based MR Image Reconstruction Algorithms with a new one**"** *Medical Engineering and Physics,* Elsevier (Submitted)

Annexure-2

Important Highlights, Observations, Findings of this Research Work

i. Database Preparation

We have collected different types of real MRI data sets from GNRC Hospital, Guwahati, India. For example, we have collected 2D multi-slice 3D BRAVO T1 HR brain MRI data, 3D TOF- 1SLAB brain MRI data, and 2D single slice Sag T2 TOP L. S. Spine MRI data. Another set of real MRI data representing fully sampled 3D fast spin-echo (FSE) knee MR images are also collected from (http://www.mridata.org). For comparisons with real MRI, 2D multi-slice brain MR images are simulated using the BrainWeb simulator (http://brainweb.bic.mni.mcgill.ca/brainweb) for performing various experiments.

ii. Comparison of Reconstruction Algorithms

Different relevant works on convex optimization are studied for implementation on CSMRI, viz. the Primal-Dual Interior Point Method (PDIPM), the Truncated Newton Interior-Point Method (TNIPM), the Gradient Projection (GP) Method, the Iterative Shrinkage Thresholding Algorithm (ISTA), the Fast Iterative Shrinkage Thresholding Algorithm (FISTA), the Two-Step IST (TWIST), the Sparse Reconstruction by separable Approximation (SpaRSA), the Total Variation (TV) based algorithms, the Projections Over Convex Set (POCS), the Gradient Projection for Sparse Reconstruction (GPSR), the Split Bregman Method, the Alternating Direction Method (ADM), and the Split Augmented Lagrangian Shrinkage Algorithm (SALSA).

From recent studies on CSMRI, it is seen that the TV-L1-L2 model for MR image reconstruction from random undersampled data gives better results. The model is defined as follows:

$$\mathbf{x}^* = \arg\min_{\mathbf{x}} \left\{ \tfrac{1}{2} \left\| \mathbf{F}_u \mathbf{x} - \mathbf{y} \right\|_2^2 + \lambda_1 \left\| \mathbf{\Psi x} \right\|_1 + \lambda_2 \left\| \mathbf{x} \right\|_{TV} \right\}$$

where $\mathbf{x}$ is the MR image, $\mathbf{y}$ is the measured Fourier data and $\mathbf{F}_u$ is the undersampling Fourier operator. Assume that $\mathbf{x}$ has a sparse representation in the wavelet domain ($\mathbf{\Psi}$). Some of the well known TV-L1-L2 model based CS reconstruction algorithms for MR image reconstruction are-

- Total Variation L1 Compressed Sensing (TVCMRI), 2008 [1].
- Reconstruction from Partial Fourier data (RecPF), 2010 [2].
- Fast Composite Splitting Algorithm (FCSA), 2011 [3].

iii. Proposed High Throughput Reconstruction Technique for CS based MRI

We have proposed a novel high throughput MR image reconstruction algorithm based on the TV-L1-L2 model. The experimental results show that the proposed method is quite efficient compared to the state-of-the-art MR image reconstruction techniques in terms of the CPU time and the quality of the reconstructed MR images. The average CPU time required for the proposed method is approximately 2-3 seconds per image for 20% sampling ratio when implemented in a PC equipped with Intel i7 processor with 2 GB RAM.

iv. Proposed variable density undersampling pattern

An incoherent aliasing artifact is an important criterion for CS reconstruction. To increase the incoherency between the k-space and the sparse representation basis, we need to acquire

samples with a random under-sampling pattern. Due to the use of random undersampling pattern, reconstructed images would contain some visible artifacts which would be similar to white noise. This artifact appears in the MR Image due to the leakage of energy resulting from random undersampling and can be minimized during the reconstruction process by thresholding [4].

In MRI, data acquisition process is performed in k-space. Centre region of the k-space contains information about gross structure and contrast of the original MR Image, most of the information required to produce the MR image. Accordingly, the peripheral region contains the spatial resolution information of MR image. Therefore, if the total numbers of samples are limited then we have to acquire more samples from the centre region and relatively less samples from the periphery.

The proposed variable density sampling pattern known as the variable density Poisson disk sampling pattern mainly consists of several Poisson Disks arranged concentrically. The Poisson disk generates random points which have following properties-

1. They are tightly packed together.

2. They maintain a specified minimum distance between two neighbouring points.

In Poisson disk, at first a grid is generated such that every cell contains at most one sampling point. If points are at least distance r from each other, then cell size must be $r/2$. Therefore no two neighbouring points are too close. But points in the Poisson Disk sampling pattern are purely random in nature i.e. they contain the randomness property but also keep a minimum distance between two neighbouring points.

v. Wavelet Tree Property and Interpolated Compressed Sensing for Multi-slice MR Image Reconstruction

It has been observed that sparse signal can be exactly reconstructed from highly undersampled linear measurements. In compressed sensing MRI, we can reconstruct good quality MR image with a small number of measurements because MR images are sparse in transform domain like the wavelet. From recent studies [5], it has been observed that wavelet coefficients follow a quadtree structure for 2D image. In 2D images, wavelet filters are normally applied in both vertical and horizontal directions to produce four subbands, namely, the Low-Low (LL), the Low-High (LH), the High-Low (HL) and the High-High (HH) bands. Then only the LL band is iteratively decomposed to obtain the coarsest approximation band and a series of detail subbands at different resolutions. Since each subband represents a filtered and a subsampled version of the underlying image, coefficients of each subband are related to the original image. In other words we can say that in wavelet domain the children coefficient follows the property of the parent coefficients. By utilizing this structural property of wavelet coefficients the quality of CSMRI reconstruction can be improved further.

3D MRI is the best way to analysis the 3D anatomical structure. But due to the slow imaging process the conventional 3D MRI usually leads to impractical scan time. Due to this reason, 2D multi-slice MRI is used instead. In 2D multi-slice MRI, the anatomical variations in

adjacent slices are vary less as they are highly correlated because a number of slices are acquired within a small volume. Therefore, we can estimate any intermediate slice from neighbouring slices. So, we can undersample adjacent slices non-uniformly and reconstruct good quality MR images by interpolating missing samples in a highly undersampled slice from neighbouring low undersampled slices using simple mathematics.

This interpolation technique significantly reduces amount of total acquired data or measurements which in turn reduces the MRI scan time. We have proposed a fast 2D multi-slice interpolation technique to estimate the relative missing samples of a highly undersampled slice from a neighbouring low undersampled slice. From the experimental results of nine adjacent slices we observe that the proposed interpolation technique is twenty times faster than the state-of-the-art.

References:

1. S. Ma, W. Yin, Y. Zhang, and A. Chakraborty, "An efficient algorithm for compressed MR imaging using total variation and wavelets," *in Proc. of the IEEE Conference on Computer Vision and Pattern Recognition*, pp. 1-8, 2008.
2. J. Yang, Y. Zhang, and W. Yin, "A fast alternating direction method for TVL1-L2 signal reconstruction from partial Fourier data*," IEEE Journal of Selected Topics in Signal Processing*, vol. 4, no. 2, pp.288-297, 2010.
3. J. Huang, S. Zhang, and D. N. Metaxas, "Efficient MR image reconstruction for compressed MR imaging", *Medical Image Analysis*, vol. 15, no. 5, pp. 670-679, 2011.
4. M. Lustig, D. Donoho, and J. M. Pauly, "Sparse MRI: The application of compressed sensing for rapid MR imaging," Magnetic Resonance in Medicine, vol. 58, pp. 1182-1195, 2007.
5. C. Chen and J. Huang, "The benefit of tree sparsity in accelerated MRI," *Medical Image Analysis*, vol. 18, no. 6, pp. 834 - 842*,* 2014.

vi. Publications from the project:

1. B. Deka, and S. Datta, "High Throughput MR Image Reconstruction Using Compressed Sensing", in Proceedings of the 2014 Indian Conference on Computer Vision Graphics and Image Processing, ACM, pp. 89:1-89:6,2014**.**
2. B. Deka, and S. Datta, "A Practical Under-Sampling Pattern for Compressed Sensing MRI" Advances in Communication and Computing, Springer India, vol. 347(9), pp. 115-125, 2015.
3. S. Datta and B. Deka "A Fast Interpolation Technique for Compressed Sensing Based Reconstruction of Multi-slice MRI" Imaging Science Journal, Taylor & Francis (submitted)
4. S. Datta and B. Deka "An Efficient Interpolated Compressed Sensing Method for 2D Multi-slice MRI" IEEE Signal Processing Letters (submitted, Ref. No. SPL-19362-2016)
5. B. Deka and S. Datta **"**Recent Development of Compressed Sensing based MR Image Reconstruction Algorithms- A Review**"** Image and Vision Computing, Elsevier (under preparation)

Annexure - V

UNIVERSITY GRANTS COMMISSION

BAHADUR SHAH ZAFAR MARG

NEW DELHI – 110 002

Utilization certificate

Certified that the grant of **Rs. 10,38,154.00** (Rupees Ten Lakh Thirty Eight Thousand One Hundred Fifty Four only) received from the University Grants Commission under the scheme of support for Major Research Project entitled **Development of Compressed Sensing Based Image Reconstruction Techniques for Medical Imaging Applications** vide UGC letter No. **F. No. 41-603/2012(SR)** dated **16.07.2012 & 01.07.2015** and **Rs. 10,22,532.00** (Rupees Ten Lakh Twenty Two Thousand Five Hundred Thirty Two only) has been fully utilized for the purpose for which it was sanctioned and in accordance with the terms and conditions laid down by the University Grants Commission and that the balance of Rs. 15,622/- (Rupees Fifteen Thousand Six Hundred Twenty Two only) remaining unutilized at the end of the year 2015-2016 has been returned to UGC (vide ~~DD/Cheque No.~~ (UTR TRANS) SBIN816181553254 dated 29.06.2016).

27.05.2016

SIGNATURE OF THE PRINCIPAL INVESTIGATOR

REGISTRAR/PRINCIPAL
Registrar
(Seal)
Tezpur University

STATUTORY AUDITOR
Finance Officer
(Seal)
Tezpur University

Not Applicable
SIGNATURE OF THE CO-INVESTIGATOR

UGC A/c 01571010017339
(CNR B0008627 for Rs. 15622.00)
Dt. 29.06.2016

Certified Copy
Registrar

Annexure - III
(A)

UNIVERSITY GRANTS COMMISSION
BAHADUR SHAH ZAFAR MARG
NEW DELHI – 110 002

STATEMENT OF EXPENDITURE IN RESPECT OF MAJOR RESEARCH PROJECT

1. Name of Principal Investigator : **Dr. Bhabesh Deka**
2. Deptt. of Principal Investigator: **Electronics and Communication Engineering**
   University/College: **Tezpur University**
3. UGC approval Letter No. and Date: **F. No. 41-603/2012(SR) and 16.07.2012**
4. Title of the Research Project: **Development of Compressed Sensing Based Image Reconstruction Techniques for Medical Imaging Applications.**
5. Effective date of starting the project : **01.07.2012**
6. a. Period of Expenditure: **From 01.07.2012 to 31.03.2016**
   b. Details of Expenditure:

S.No.	Item	Amount Approved (Rs.)	Expenditure Incurred (Rs.)
i.	Books & Journals	Nil	Nil
ii.	Equipment	4,00,000.00	3,85,654.00
iii.	Contingency	1,00,000.00	90,310.00
iv.	Field Work/Travel (Give details in the proforma at Annexure-IV).	80,000.00	72,113.00
v.	Hiring Services	50,000.00	37,200.00
vi.	Chemicals & Glassware	Nil	Nil
vii.	Overhead	67,800.00	62,416.00
viii.	Any other items (Please specify)	Nil	Nil

Certified Copy

Registrar

Finance Officer
Tezpur University

c . Staff: Date of Appointment: (a) 05.10.2012 and (b) 02.08.2013-31

S.No	Items	From	To	Amount Approved (Rs.)	Expenditure incurred (Rs.)
1	Honorarium to PI (Retired Teachers) @ Rs. 18,000/-p.m.			Nil	Nil
2	**Project fellow:** i) NET/GATE qualified-Rs. 16,000/- p.m. for initial 2 years and Rs. 18,000/- p.m. for the third year ii) Non-GATE/Non-NET- Rs. 14,000/- p.m. for initial 2 years and Rs. 16,000/- p.m. for the third year	05.10.2012 02.08.2013	31.03.2013 31.05.2015	5,28,000.00	3,74,839.00 @ Rs. 14000 p.m.

Total from 6(b)+6(c)

- Amount approved (Rs.) = **6, 97,800.00 + 5, 28,000.00 = Rs. 12,25,800.00**
- Amount Received (Rs.) = **6,74,800.00 + 3,63,354.00 = Rs. 10,38,154.00**
- Expenditure Incurred (Rs.) = **6,47,693.00 + 3,74,839.00 = Rs. 10,22,532.00**
- Balance Amount (Rs.) = **10,38,154.00 - 10,22,532.00 = Rs. 15,622.00**

1. It is certified that the appointment(s) have been made in accordance with the terms and conditions laid down by the Commission.

2. If as a result of check or audit objection some irregularly is noticed at later date, action will be taken to refund, adjust or regularize the objected amounts.

3 Payment @ revised rates shall be made with arrears on the availability of additional funds

4 It is certified that the grant of **Rs. 10,38,154.00** (Rupees Ten Lakh Thirty Eight Thousand One Hundred Fifty Four only) received from the University Grants Commission under the scheme of support for Major Research Project entitled **Development of Compressed Sensing Based Image Reconstruction Techniques for Medical Imaging Applications** vide UGC letter No. F. **41-603/2012(SR)** dated **16.07.2012 & 01.07.2015** and **Rs. 10,22,532.00** (Rupees Ten Lakh Twenty Two Thousand Five Hundred Thirty Two only) has been fully utilized for the purpose for which it was sanctioned and in accordance with the terms and conditions laid down by the University Grants Commission.

27.05.2016

PRINCIPAL INVESTIGATOR
(SIGNATURE WITH SEAL)
Associate Professor
Department Of Electronics & Comm.Engg.
Tezpur University

Certified Copy

Registrar

REGISTRAR
(SIGNATURE WITH SEAL)
Registrar
Tezpur University

Annexure - III

(B)

UNIVERSITY GRANTS COMMISSION
BAHADUR SHAH ZAFAR MARG
NEW DELHI – 110 002

STATEMENT OF EXPENDITURE IN RESPECT OF MAJOR RESEARCH PROJECT

1. Name of Principal Investigator : **Dr. Bhabesh Deka**
2. Deptt. of Principal Investigator: **Electronics and Communication Engineering**
   University/College: **Tezpur University**
3. UGC approval Letter No. and Date: **F. No. 41-603/2012(SR) and 16.07.2012**
4. Title of the Research Project: **Development of Compressed Sensing Based Image Reconstruction Techniques for Medical Imaging Applications**.
5. Effective date of starting the project : **01.07.2012**
6. a. Period of Expenditure: **From 01.07.2012 to 31.03.2016**
   b. Details of Expenditure:

S. No.	Item	Amount Sanctioned (Rs.)	A. Amount Received (Rs.)					B. Expenditure Incurred (Rs.)					(A-B) (Rs.)
			2012 - 2013	2013 - 2014	2014 - 2015	2015 - 2016	Total (Rs.)	2012 - 2013	2013 - 2014	2014 - 2015	2015 - 2016	Total (Rs.)	
i.	Books & Journals	NIL	NIL	NIL	NIL	NIL	NIL	NIL	NIL	NIL	NIL	NIL	NIL
ii.	Equipment	4,00,000	4,00,000	NIL	NIL	NIL	4,00,000	3,85,654	NIL	NIL	NIL	3,85,654	14,346
iii.	Contingency	1,00,000	50,000	NIL	NIL	40,000	90,000	17,285	59,135	NIL	13,890	90,310	(-) 310
iv.	Field Work/ Travel	80,000	40,000	NIL	NIL	32,000	72,000	22,594	7,000	NIL	42,519	72,113	(-) 113
v.	Hiring Services	50,000	25,000	NIL	NIL	20,000	45,000	10,000	NIL	15,000	12,200	37,200	7,800
vi.	Chemicals & Glassware	NIL	NIL	NIL	NIL	NIL	NIL	NIL	NIL	NIL	NIL	NIL	NIL
vii.	Overhead	67,800	67,800	NIL	NIL	NIL	67,800	62,416	NIL	NIL	NIL	62,416	5,384
viii.	Any other items	NIL	NIL	NIL	NIL	NIL	NIL	NIL	NIL	NIL	NIL	NIL	NIL
Grand Total (Rs.)		6,97,800	5,82,800	NIL	NIL	92,000	6,74,800	4,97,949	66,135	15,000	68,609	6,47,693	27,107

Finance Officer
Tezpur University

Certified Copy

Registrar
Tezpur University

c . Staff: Date of Appointment: (a) 05.10.2012 and (b) 02.08.2013-3

S. No.	Item	Amt Sanctioned (Rs.)	A. Amount Received (Rs.)					B. Expenditure Incurred (Rs.)					(A-B) (Rs.)
			2012 - 2013	2013-2014	2014-2015	2015 - 2016	Total (Rs.)	2012 - 2013	2013 - 2014	2014-2015	2015 - 2016	Total (Rs.)	
i.	Honorarium to PI (Retired Teachers) @ Rs. 18,000/- p.m.	NIL	NIL	NIL	NIL	NIL	NIL	NIL	NIL	NIL	NIL	NIL	NIL
ii.	Project fellow. i) NET/GATE qualified- Rs. 16,000 - p.m for initial 2 years and Rs 18,000/- p.m. for the third year. ii) Non-GATE/Non-NET - Rs. 14,000/- p.m. for initial 2 years and Rs. 16,000 - p.m. for the third year	5,28,000	2,64,000	NIL	NIL	99,354	3,63,354	67,742	1,11,097	98,000	98,000	3,74,839	(-)11,485
Grand Total (Rs.)		5,28,000	2,64,000	NIL	NIL	99,354	3,63,354	67,742	1,11,097	98,000	98,000	3,74,839	(-)11,485

Total from 6(b) +6(c)

- Amount Sanctioned (Rs.) = **6,97,800.00 + 5,28,000.00 = Rs. 12,25,800.00**
- Amount Received (Rs.) = **6,74,800.00 + 3,63,354.00 = Rs. 10,38,154.00**
- Expenditure Incurred (Rs.) = **6,47,693.00 + 3,74,839.00 = Rs. 10,22,532.00**
- Balance Amount (Rs.) = **10,38,154.00 - 10,22,532.00 = Rs. 15,622.00**

1. It is certified that the appointment(s) have been made in accordance with the terms and conditions laid down by the Commission.

2. If as a result of check or audit objection some irregularly is noticed at later date, action will be taken to refund, adjust or regularize the objected amounts.

3. Payment @ revised rates shall be made with arrears on the availability of additional funds.

4. It is certified that the grant of **Rs. 10,38,154.00** (Rupees Ten Lakh Thirty Eight Thousand One Hundred Fifty Four only) received from the University Grants Commission under the scheme of support for Major Research Project entitled **Development of Compressed Sensing Based Image Reconstruction Techniques for Medical Imaging Applications** vide UGC letter No F. **41-603/2012(SR)** dated **16.07.2012 & 01.07.2015** and **Rs. 10,22,532.00** (Rupees Ten Lakh Twenty Two Thousand Five Hundred Thirty Two only) has been fully utilized for the purpose for which it was sanctioned and in accordance with the terms and conditions laid down by the University Grants Commission.

29.05.2016

PRINCIPAL INVESTIGATOR
(SIGNATURE WITH SEAL)
Associate Professor
Department Of Electronics & Comm.Engg.
Tezpur University

REGISTRAR
(SIGNATURE WITH SEAL)
Registrar
Tezpur University

Certified Copy

Registrar
Tezpur University